UC-25
LBL-19479

Lawrence Berkeley Laboratory
UNIVERSITY OF CALIFORNIA

Materials & Molecular Research Division

RECEIVED
LAWRENCE
BERKELEY LABORATORY

MAY 22 1985

LIBRARY AND
DOCUMENTS SECTION

ITINERANT MAGNETISM AND ITS CHARACTERIZATION
IN HETEROGENEOUS SYSTEMS

R.H. Victora
(Ph.D. Thesis)

April 1985

For Reference

Not to be taken from this room

LBL-19479

Prepared for the U.S. Department of Energy under Contract DE-AC03-76SF00098

DISCLAIMER

This document was prepared as an account of work sponsored by the United States Government. While this document is believed to contain correct information, neither the United States Government nor any agency thereof, nor the Regents of the University of California, nor any of their employees, makes any warranty, express or implied, or assumes any legal responsibility for the accuracy, completeness, or usefulness of any information, apparatus, product, or process disclosed, or represents that its use would not infringe privately owned rights. Reference herein to any specific commercial product, process, or service by its trade name, trademark, manufacturer, or otherwise, does not necessarily constitute or imply its endorsement, recommendation, or favoring by the United States Government or any agency thereof, or the Regents of the University of California. The views and opinions of authors expressed herein do not necessarily state or reflect those of the United States Government or any agency thereof or the Regents of the University of California.

LBL-19479

ITINERANT MAGNETISM AND ITS CHARACTERIZATION IN HETEROGENEOUS SYSTEMS

Randall Harry Victora
Ph.D. Thesis

Lawrence Berkeley Laboratory
University of California
Berkeley, California 94720

April 1985

This work was supported by the U.S. Department of Energy under Contract Number DE-AC03-76SF00098.

are difficult or impossible to treat by first-principle methods, and to test for unusual configurations or symmetry breaking in simple systems. Important conclusions drawn from these calculations include:

1. The unusual shape of the Fe-Co curve on the Slater-Pauling plot, a subject of theoretical debate since the 1930s, is primarily caused by magnetic saturation in the Co-rich alloy and a weak electron-electron interaction in the Fe-rich alloy. The explanation of Pauling, i.e., only 2.4 magnetizable d electrons per spin, is an incomplete representation of the true reasons behind this anomalous Fe-Co curve.

2. A Co monolayer on a Cu(111) surface possesses a new kind of two-atom state which may be described as "spatially modulated". This state has a total energy only slightly above the ferromagnetic ground-state energy.

3. A Cr monolayer on the Fe (100) surface is ferromagnetic with a spin polarization of 3.63 electrons. This spin polarization is considerably larger than any other known transition-metal system and suggests new directions for the creation of highly magnetic surfaces.

The thesis concludes with a set of derived qualitative rules that describe the systematics of itinerant magnetism in heterogeneous systems.

L.M. FALICOV
APRIL 16, 1985

ITINERANT MAGNETISM AND ITS CHARACTERIZATION IN HETEROGENEOUS SYSTEMS

Randall Harry Victora

Abstract

This thesis describes calculations for the magnetic and electronic properties of a variety of systems that display itinerant magnetism. An early chapter considers the exact solution of a Hubbard Hamiltonian within the context of periodic boundary conditions; remaining calculations treat various heterogeneous transition-metal systems by means of a realistic tight-binding scheme, with single site, full orbital interactions treated self consistently.

The latter method is shown to be consistently reliable: In each case where comparison with experiment or with state-of-the-art calculations could be made, there is agreement in the integrated properties, such as spin polarization, to within a few percent. Comparison of calculated density of states with photoemission data, although complicated by various many-body processes, again shows excellent agreement.

This relatively inexpensive computational method is used to calculate the properties of complex systems which

ACKNOWLEDGMENTS

I am most grateful to my thesis adviser, Professor L.M. Falicov, for his guidance and insight throughout the course of this work. His participation has helped make my doctoral research both productive and enjoyable.

I would like to thank Drs. J. Tersoff, M.O. Robbins, J. Oliva, and A.R. Williams for valuable discussions. I would like to thank Drs. L.E. Klebanoff, R.M. White, R. Miranda, and Y. Petroff for sharing unpublished experimental data with me. I would also like to acknowledge the use of computer programs by Drs. J. Tersoff and S. Ishida as a basis for some of my own programs.

I would like to thank the AT&T Bell Laboratories Ph.D. fellowship program under whose sponsorship part of this work was completed. I would also like to thank the staff of the Laboratoire pour l'Utilisation du Rayonnement Electromagnétique, associé à l'Université de Paris-Sud, Orsay, France, for providing hospitality during six months of my research.

Finally, I would like to acknowledge the ideas, suggestions, and technical assistance provided by my fellow members of the condensed matter theory group at Berkeley. These conversations have often assisted me greatly.

TABLE OF CONTENTS

		PAGE
I.	Introduction	1
	A. Overview of Itinerant Magnetism	1
	B. Models of Itinerant Magnetism	4
	1. Stoner Model	4
	2. Hubbard Model	5
	3. Parametrized General Hamiltonians	6
	4. Density Functional Theory	6
	C. Itinerant Magnetism in Heterogeneous Systems	7
	References	9
	Figure Caption	10
	Figure	11
II.	Exact Solution of the Hubbard Model for a Four-Center Tetrahedral Cluster	12
	A. Introduction	12
	B. Calculation and Results	14
	References	19
	Tables	20
	Figure Captions	30
	Figures	31
III.	Calculational Technique Used for Heterogeneous Systems	36
	A. The Hamiltonian	36

B. Method of Implementation 39
C. Error Analysis of the Hamiltonian 43
Appendix 46
References 47
Table 49
IV. The Magnetic States of Cobalt Overlayers on Copper (111) 50
A. Introduction 50
B. Results 53
1. Clean Cu(111) Surface 53
2. Co on Cu(111) : One-Atom Surface Cell 54
3. Co on Cu(111) : Two-Atom Surface Cell 57
C. Conclusions 59
References 62
Tables 64
Figure Captions 66
Figures 69
V. Magnetization of Iron-Cobalt Disordered Alloys 78
A. Introduction 78
B. Results 81
C. Conclusions 83
References 85
Figure Captions 87
Figures 88

VI. Surface Electronic Structure of Ferromagnetic Iron and the Ferromagnetic Ordered Iron-Cobalt Alloy 90
A. Introduction 90
B. Results 92
1. Fe Surfaces 92
2. Bulk FeCo 94
3. FeCo Surfaces 96
4. Fe Segregated Surface 98
C. Conclusions 98
References 100
Table 102
Figure Captions 103
Figures 104
VII. Electronic Structure of Chromium Surfaces and Chromium Monolayers on Iron 110
A. Introduction 110
B. Results 112
1. Cr(100) Surface 112
2. Cr(110) Surface 120
3. Cr Monolayers on Fe 122
C. Conclusions 124
References 127
Tables 129
Figure Captions 132
Figures 136
VIII. Conclusion 148
Table 152

I. INTRODUCTION

In 1269 A.D., Peregrinus examined the magnetic field lines of lodestone in the earliest known treatise of experimental physics. In 1928, Heisenberg and Dirac independently provided a modern theory of ferromagnetism in one of the first applications of quantum mechanics. Today, numerous researchers throughout the world continue to place great emphasis on the understanding of magnetism and, in particular, its very important subset: itinerant magnetism. The first chapter of this contribution introduces the reader to the concept of itinerant magnetism, appropriate models for describing it, and its importance in heterogeneous systems.

A. Overview of Itinerant Magnetism

There are three contributions to the energy of an electron in a solid: the kinetic energy, the potential energy arising from the attractive electron-nucleus interaction, and the potential energy arising from the repulsive electron-electron interaction. Quantum mechanics plays an instrumental role in determining the value of these energies. In particular, the required antisymmetry of the many-body wavefunction produces the Pauli exclusion principle, which requires that electronic states be at most singly occupied. Consequently, electrons adopting the same spin direction are forced to occupy different spatial states and thus may lower the repulsive electron-electon

interaction between them. This is the origin of magnetism.

It is clear that for magnetism to occur the decrease in potential energy from reducing the electron-electron interaction must exceed the increase in energy from forcing the electrons to occupy higher level one-particle states. This criterion is met by five of the 3-d transition metals: nickel (Ni), cobalt (Co), iron (Fe), manganese (Mn) and chromium (Cr). These metals are said to exhibit itinerant magnetism[2] because their magnetization derives from the 3-d electrons which are itinerant, i.e., are able to easily hop from atom to atom. Their itinerancy is quantitatively specified by their paramagnetic d-bandwidth[3] of 0.3-0.5 Ry. This may be contrasted to the other large group of magnetic elements, the rare earth metals, in which the magnetic f-electrons exhibit bandwidths of less than 0.1 Ry and the exchange mechanism is said to be indirect, not itinerant.

The five magnetic transition metals are contiguous on the periodic table with atomic number Z ranging from 24 (Cr) to 28 (Ni). The atomic configurations[4] are $(1s)^2(2s)^2(2p)^6(3s)^2(3p)^6(3d)^{Z-20}(4s)^2$, except for Cr, which is $(3d)^5(4s)^1$. The spins of the atomic ground state range from 3 (Cr) to 1 (Ni), i.e., the maximum spin quantum mechanically allowable given the available number of holes. When these atoms form a solid, there is of course

considerable hydridization which obscures the distinction between the 4s and 3d electrons. Nonetheless, it is qualitatively clear (see Figure 1) that a transition metal bandstructure consists of two parts: a free electron-like band to which the 4s electrons contribute and a much narrower set (0.3-0.5 Ry) of five bands which have mostly d-orbital character. This narrower band approximately bisects the free electron-like band and is itself partly cut by the Fermi level. This band is the source of magnetism in the 3d transition metals.

Iron, cobalt and nickel are ferromagnets: their magnetizations[5] are of equal magnitude and direction on each atom. The magnetization[6] decreases from iron ($2.22\mu_\beta$), to cobalt ($1.71\mu_\beta$), to nickel ($0.61\mu_\beta$) in rough correspondence to the number of available d-holes. This is similar behavior to that discussed earlier in the atomic limit.

Chromium and manganese, on the other hand, have complicated spin arrangements in which individual atoms exhibit local moments which cancel the local moments of neighboring atoms. Neither element exhibits a macroscopic spin imbalance. In particular, Cr has an antiferromagnetic ground state modulated by an incommensurable spin density wave (SDW). The SDW is in one of the (100) directions with a wavelength of approximately 21 lattice spacings.[7] The magnetization at the maximum is 0.59 Bohr magnetions.[8]

The magnetic structure of Mn is also very complicated and will not be treated explicitly in this work.

B. Models of Itinerant Magnetism

It is quite clear from the preceeding discussion that itinerant magnetism is a very complicated phenomenon. Accurate theoretical description encounters the intrinsic difficulty that both the strong electron-electron interaction and the band nature of the d electrons must be properly included. Although each of the two characteristics can be treated separately to great accuracy, the combined problem demands a full treatment of electron correlation in an infinite system, i.e. a many-body problem without any as yet discovered small parameters. This problem, of course, is insoluble, but fortunately many properties of these transition metal systems can be accurately treated within the context of simplified models. Four of the most important models are described below.

(1) Stoner Model

In 1933, Stoner proposed a mean field model,

$$H = \sum_{\vec{K}\sigma} \varepsilon_{\vec{K}} \hat{n}_{\vec{K}} + I \sum_{\vec{K},\vec{K}'\sigma} \hat{n}_{\vec{K}'\sigma} < \hat{n}_{\vec{K}\bar{\sigma}} > \qquad (1)$$

where $\hat{n}_{\vec{K}\sigma}$ is the number operator for the state of wave-vectpr $\vec{K}$ and spin σ , I is a phenomenological exchange parameter, and $\varepsilon_{\vec{K}}$ is the one-particle energy of state $\vec{K}$. Strong points of this model include the ability

to allow a realistic band structure and the basic simplicity of the description which permits easy understanding of some phenomena. On the other hand, the model makes the rigid band approximation, in which the only effect of exchange is to split the two spin subbands rigidly relative to each other. This is unrealistic for most systems. Furthermore, many body effects beyond the mean-field approximation are completely ignored. The Stoner model will be used in this thesis for the qualitative discussion of some results.

(2) The Hubbard Model

In 1963, Hubbard[10] proposed a model Hamiltonian which placed the appropriate twin emphasis on the on-site Coulomb repulsion and the banding of the d states. The Hamiltonian contains a parameter U for the intrasite Coulomb repulsion and a parameter t_{ij} for the intersite hopping: it is written,

$$H = \sum_{ij\sigma} t_{ij} \, c^{+}_{i\sigma} \, c_{j\sigma} + U \sum_{i} c^{+}_{i\sigma} c^{+}_{i\bar{\sigma}} \, c_{i\bar{\sigma}} \, c_{i\sigma} \quad (2)$$

where $c^{+}_{i\sigma}$ creates the state on atom i with spin σ. The single band nature of this Hamiltonian prohibits realistic treatment of actual physical systems. However, the extreme simplicity does provide a testing ground for various many-body schemes[11] which may suggest directions for the treatment of correlations in more realistic Hamiltonians. The solutions for an fcc Hubbard Hamiltonian with periodic boundary conditions will be found in

Chapter II of this thesis.

(3) Parametrized General Hamiltonians

This class of Hamiltonian, typically written in the tight-binding representation, may include most or all of the features of the true Hamiltonian, including realistic d and conduction electron band structure and an accurate electron-electron interaction. The parameters establishing the coefficients in the Hamiltonian are typically taken from experiment or other calculations. Hamiltonians of this form have been used in the study of correlation[12] in d-band metals and in the study of surfaces.[13] A major advantage of this scheme is realistic results with relative ease, while a major disadvantage is the difficulty of procuring accurate parameters. As in all realistic schemes, correlation effects are still difficult to correctly estimate. Much of this thesis uses a particular version of this Hamiltonian and thus further discussion of it will be deferred to Chapter III.

(4) Density Functional Theory

This scheme uses an assumed electron-electron interaction, usually taken in the local density approximation,[14] to minimize the energy of the constituent electrons. The one electron eigenvalues are typically interpreted as the quasiparticle excitation energies which compose the band structure. This is the only theory that is currently able to start with the atomic number of an element and ultimately produce a crystal structure, electronic

structure, and magnetization which can reasonably be compared to experimental results. Unfortunately, the true form of the electron-electron interaction within the density functional is not known and this can yield, in the case of transition metals, inaccurate results[15] for lattice constants and magnetizations. Also, the method becomes quite expensive for large systems. Nonetheless, it must be emphasized that this method is state-of-the-art, and this thesis shall compare to density functional results whenever possible.

C. Itinerant Magnetism in Heterogeneous Systems

In recent years, there has been considerable technological interest in the electronic and magnetic properties of transition metal alloys, surfaces, and overlayers. This interest stems from the importance of such processes as thin film magnetic recording and surface passivation, in which a reactive substrate is covered by a non-reactive overlayer. Another very important process is catalysis, in which the catalyst often consists of small clusters of a reactive transition metal atop an inert substrate. Alloying is of obvious use in producing materials with the most desired properties of several constituent elements. New techniques such as molecular beam epitaxy promise the creation of whole new classes of materials with properties tailored to particular uses.

The study of heterogeneous systems is also useful for providing information about basic properties of magnetism.

Alloys, for example, may be viewed as "elements" intermediate between the actual elements, and thus may yield additional data points for discussions of trends in the periodic table. Thin magnetic overlayers provide representations of two-dimensional magnetic systems, a topic of great fundamental interest, particularly in statistical mechanics. The sensitivity of the d-electrons to local environment may be probed by the absence of neighboring atoms at a surface or the presence of dissimilar neighbors as found in an alloy. This provides information on magnetic healing lengths and the importance of the d-electron itineracy to the magnetic moment.

In the following pages, many of the issues raised in the previous two paragraphs will be examined. The bulk of this thesis consists of results of calculations for the zero temperature electronic and magnetic properties of a large variety of heterogeneous transition metal systems. We use the Slater-Koster parametrized tight-binding scheme in which the one- and two-center integrals are fitted to the bulk band structure. The exchange interaction is treated self-consistently in a single-site approximation. The method is shown to be accurate and comparisons to experiment and other calculations are made. Finally, the ability of this method to systematically calculate the properties of a large variety of systems shall be exploited to develop some general rules about magnetism in heterogeneous systems.

References

1. D.C. Mattis, The Theory of Magnetism I (Springer-Verlag, Berlin, 1981), Chapter 1.

2. Itinerant magnetism is discussed extensively by C. Herring, in Exchange Interactions among Itinerant Electrons, Vol. IV of Magnetism, edited by G.T. Rado and H. Suhl (Academic, New York, 1966).

3. Calculated bands are shown in V.L. Moruzzi, J.F. Janak, and A.R. Williams, Calculated Electronic Properties of Metals (Pergamon, New York, 1978). Photoemission bandwidths are often somewhat narrower.

4. C.E. Moore, Atomic Energy Levels, Vol. II (National Bureau of Standards, Washington, 1952).

5. Magnetizations reflect a g-factor times a spin projection and consequently correspond to roughly twice a spin value.

6. C. Kittel, Introduction to Solid State Physics, 5th ed. (Wiley, New York, 1976).

7. S.A. Werner, A.S. Arrott, and H. Kendrick, Phys. Rev. 155, 528 (1967).

8. G. Shirane and W.J. Takei, J. Phys. Soc. Japan Suppl. 17 BIII, 35 (1962).

9. E.C. Stoner, Phil. Mag. 15, 1018 (1933).

10. J. Hubbard, Proc. Roy. Soc. A276, 238 (1963).

11. See, for example, J. Bernasconi, Phys. Kondens. Materie 14, 225 (1972), and references therein.

12. A.M. Oles and G. Stollhof, Phys. Rev. B 29, 314 (1984).

13. See, for example, D.G. Dempsey, L. Kleinman, and E. Caruthers, Phys. Rev. B12, 2932 (1975).

14. A.R. Williams and U. von Barth, "Applications of Density Functional Theory to Atoms, Molecules, and Solids", edited by S. Lundquist and N.H. March (Plenum, New York, 1983).

15. V.L. Moruzzi, J.F. Janak, and A.R. Williams, Calculated Electronic Properties of Metals (Pergamon, New York, 1978).

Figure Caption

Figure 1 Bandstructure of bcc ferromagnetic Fe as calculated using the technique described in Chapter III. Majority spins correspond to dashed lines; minority spins correspond to solid lines. The bands between + 0.15 Ry and - 0.45 Ry have a large exchange splitting and mostly d-like character. The low energy band at Γ and the high energy bands near H and P have a free electron-like shape and very little exchange splitting.

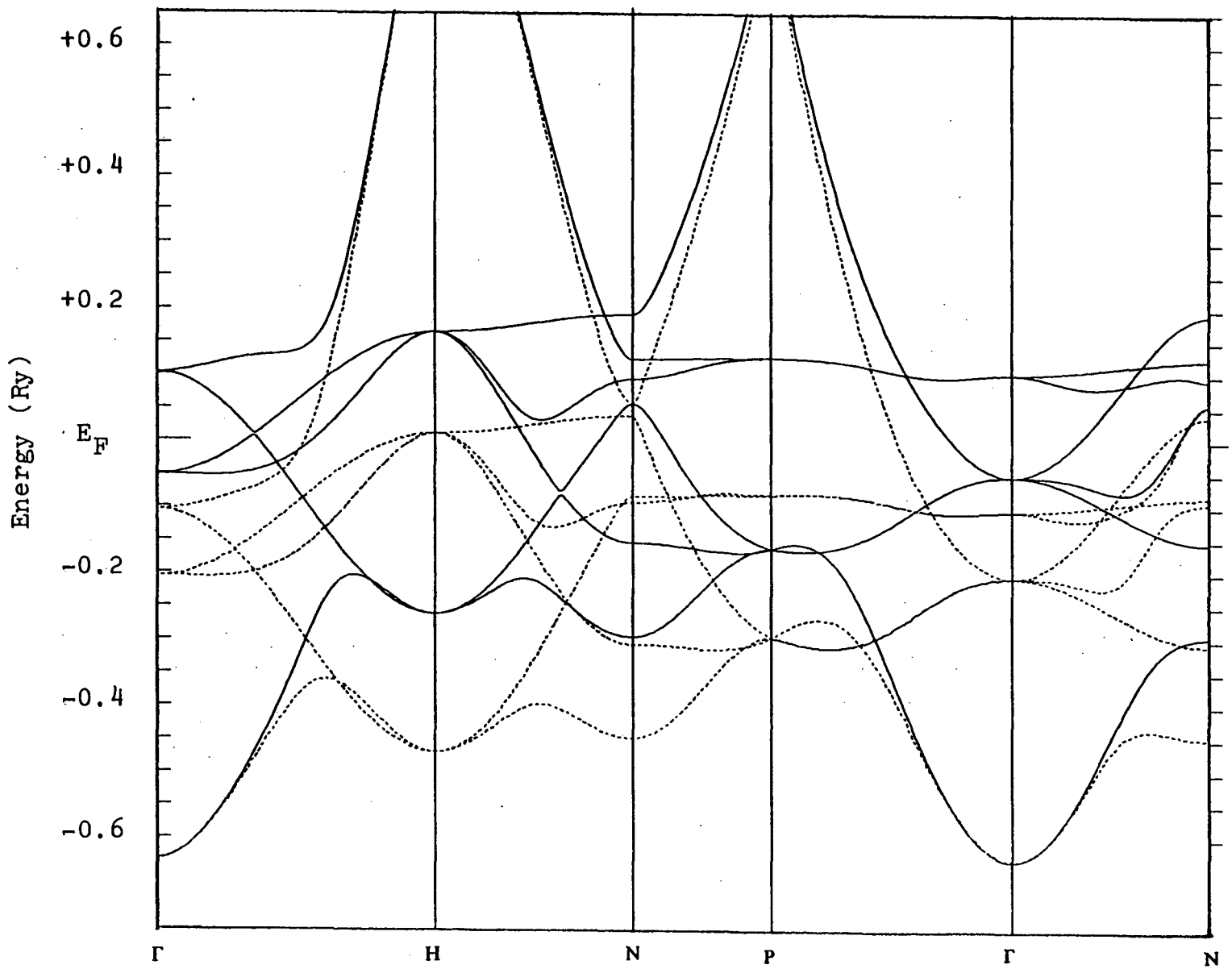

Figure 1

II. EXACT SOLUTION OF THE HUBBARD MODEL FOR A FOUR-CENTER TETRAHEDRAL CLUSTER

A. Introduction

Hubbard's model has become, since its introduction[1] in 1963, the most popular example of a system of interacting electrons with short-range interactions. It has been used in the literature to study a great variety of many-body effects in metals, of which ferromagnetism, antiferromagnetism, metal-insulator transitions, spin-density waves, and charge-density waves are the most common examples.[1-6]

The model has been applied to a variety of lattices, one, two, and three dimensional,[2,3,7] and occasionally to small clusters.[8] Exact solutions are available in very few instances[7,8] and general theorems[9] have been proved for some cases. With all this activity, however, exact solutions are not possible for most systems, and some of the approximations found in the literature remain, at best, appealing conjectures or blind tries.[10,11]

The object of this chapter is to solve exactly a very simple system, simple enough to allow an exact solution, but with enough complexity to shed light into the physics of real systems. We have chosen the case of a four-atom cluster of tetrahedral symmetry, given by the Hamiltonian

$$H = (-t)\sum_{i,j,\sigma} c^{\dagger}_{i\sigma} c_{j\sigma} + U\sum_{i} c^{\dagger}_{i\uparrow} c_{i\uparrow} c^{\dagger}_{i\downarrow} c_{i\downarrow}, \tag{1.1}$$

where $c_{i\sigma}$ ($c^{\dagger}_{i\sigma}$) is the annihilation (creation) operator for an electron of spin σ, located at the site i of the tetrahedral cluster (i,j = 1,2,3,4). For the sake of simplicity we consider only the case of non-negative t, $t \geq 0$, which corresponds to attractive nuclear potentials (s orbitals lower in energy than p orbitals). U is chosen to be positive, which corresponds to the normal repulsive electron-electron interaction found in magnetic transition metals.

Several aspects of this model deserve discussion from the start.

(1) It is identical to the Hamiltonian of the infinite face-centered-cubic lattice if the Brillouin-zone sampling is restricted to four reciprocal-lattice points, the zone center Γ, and the three square-face-center points X.

(2) Since the four one-electron orbitals which diagonalize the first term in (1.1) are one s-like orbital, of energy $\varepsilon_s = -3t$, and three p-like orbitals, of energy $\varepsilon_p = t$, there is a marked electron-hole asymmetry in the one-electron spectrum. This asymmetry is characteristic of odd-numbered rings (triangular rings in this case), and typical of the closed-packed faced-centered-cubic and hexagonal lattices. The asymmetry brings new features into the spectrum and carries with it a more interesting, less symmetric, half-filled band.

(3) It is also possible to think of this system as an atom for which only the $s^n p^m$ configurations ($0 \leq n \leq 2$, $0 \leq m \leq 6$)

are possible and with $\varepsilon_s < \varepsilon_p$. Under these conditions the usual techniques of atomic physics, Hund's rule in particular,[12,13] can be applied, and their results compared with the exact solution. As we find out, agreement and exceptions are both encountered.

(4) The presence or absence of magnetic solutions for the ground states are both instructive and in some instances surprising. The main conclusion to extract from these calculations is that Hubbard's model exhibits a richness of structure in its solutions which defies easy global generalizations. In its variety it permits the mimicking, albeit poorly, of many electronic and magnetic phases found in real transition metals.

Our problem is greatly simplified by systematic application of group theory. As a result, the most complicated equation to solve for the eigenvalues is a cubic equation, i.e., the complete problem can be solved analytically. Our procedures and solutions are given in Sec. B.

B. Calculation and Results

Since there are eight spin orbitals in the system, and each one can be either empty or occupied by an electron, we have altogether $2^8 = 256$ possible eigenstates of (1.1). Since the number N of electrons is conserved, and $0 \leq N \leq 8$, for a given N there are $[8!/N!(8-N)!]$ eigenstates.

These eigenstates can be classified according to their spin and their spatial symmetries. Since the spin degree of freedom is conserved by (1.1), the states can be

labeled as spin singlets, doublets, triplets, quartets, and quintets. The symmetry of the spatial part of the Hamiltonian is defined by its point group, which in this case is the full tetrahedral group T_d, of 24 elements. The character table of this group is given in Table I. Also included in Table I are the atomiclike symmetries of the various representations of T_d.

An analysis of the levels and energies in the two extreme limits is presented in Tables II and III. Table II is for the noninteracting limit (finite t, vanishing U), in which the energy levels depend only on the configuration $\underline{s}^n\underline{p}^m$. The 256 states divide into 21 configurations which encompass the 56 distinct levels of the full tetrahedral symmetry. Table III is for the strongly interacting limit (finite U, vanishing t). There the 256 states and 56 levels coalesce into 15 energy levels. From either table it can be seen that N-number, spin, and space symmetries reduce the problem to a completely analytic one, with at most a (3x3) secular equation to solve for a given energy level.

If our system consisting of repulsive interactions is considered as a "structured" atom, it should be possible to apply to it Hund's empirical rule,[12,13] which states that for a given N the ground-state level is determined by (1) selecting the lowest-energy configuration, (2) selecting the largest spin-multiplicity out of the levels in that

configuration, and (3) selecting from those the term of the largest angular momentum L, if (2) leaves more than one level.

An examination of Table II yields the results shown in the first three columns of Table IV. It can be seen that N = 4,5, and 6 are predicted by Hund's rule to yield magnetic states, i.e., ground states with spin multiplicities other than singlets or Kramers doublets.

The group-theory factorization and the calculation of the matrix elements of (1.1) yield the 37 secular equations given in Table V. These equations reduce, as expected, to the results of Tables II and III in the respective limits.

The results for finite t and U are shown in Table IV and Figs. 1-5. Table IV gives the symmetry of the exact ground state. Column 4 is to be compared with the predictions of Hund's rules, column 3. The figures show the excitation energy of various states from the ground state. The energies, in units of 4t+U, are plotted as a function of the parameter [U/(4t+U)]. At the right edge of the figures is the noninteracting limit U=0 (Table II), and at the left edge, the extreme atomic limit is t=0 (Table III).

The results are very rich in structure and information, and exhibit several surprising features, in addition to many expected results.

(1) Hund's rule works for N = 0,1,2,3,5,7, and 8. For N = 4 the rule is violated (the ground state is a singlet

$^1\Gamma_3$ instead of a triplet $^3\Gamma_5$). For N = 6 the predicted $^3\Gamma_5$ is the ground state, but it is degenerate with a singlet $^1\Gamma_3$.

(2) At least for a small system with four centers, Hubbard's model allows, for some occupations, magnetic ground states (the N = 5 and 6 cases). This feature seems to be a consequence of the degeneracy of the p-like one-electron orbital. Particularly interesting is the N = 5 case in which the ground state consists of 2 filled "s" orbitals and 3 filled "p" orbitals with the spins of the "p" orbitals all pointing in the same direction. Changing the spin of one of the "p" orbitals increases the electron-electron interaction and thus demonstrates the role of the Pauli exclusion principle in producing magnetism.

(3) In one instance (N = 6, U > 0) the ground state is "accidentally" degenerate, with a singlet and a triplet "sticking together" for any value of the parameters. This is in accordance with an old theorem[9] (possibly due to Wigner) which states that, for Hamiltonians such as the Hubbard, the two-electron (or hole) ground state has spin 0 with the possibility of degeneracy with a spin 1 state.

(4) For N = 4,5, and 6 there are very-low-lying excited states of other symmetries for any value of U. This effect is very pronounced in the N = 4 case (compare with N = 6).

(5) If the face-centered-cubic lattice is divided into four interpenetrating simple-cubic sublattices, and restriction is imposed that each atom in each sublattice is identical to each other atom in the same sublattice, a Hamiltonian identical to an infinite replica of (1.1) results. This can also be expressed as saying that (1.1) is the Hamiltonian of a face-centered-cubic lattice in which the wave functions are restricted to have the symmetries of the one Γ and the three X points of the Brillouin zone (i.e., a face-centered-cubic-lattice Hubbard Hamiltonian with Brillouin-zone sampling restricted to Γ and X). Under these conditions--which are not as farfetched as they initially seem to be--a half-filled band with a repulsive U would produce[14] a correlated ground state of full translational symmetry (Γ point of the Brillouin zone), doubly degenerate and with no net spin. An occupation of 1.25e/atom would produce a ferromagnetic state.

In conclusion, we find that our simple four-center Hubbard model, with two spin states per site and an arbitrary number of electrons, exhibits in the ground states a complexity of structure which defies easy generalizations. Itinerant magnetism, at least within the context of this model, is clearly difficult to predict and subject to many considerations.

References

1. J. Hubbard, Proc. R. Soc. London, Ser. A 276, 238 (1963); 227, 237 (1964); 281, 401 (1964); 285, 542 (1965); 296, 82 (1966); 296, 100 (1967).

2. D.R. Penn, Phys. Rev. 142, 350 (1966).

3. D. Denley and L.M. Falicov, Phys. Rev. B 17, 1289 (1978).

4. D. Adler, in Solid State Physics, edited by H. Ehrenreich, F. Seitz, and D. Turnbull (Academic, New York, 1968), Vol. 21, p. 1.

5. Proceedings of the International Conference on Metal-Nonmetal Transitions, San Francisco, 1968 [Rev. Mod. Phys. 40, 673 (1968)].

6. N.F. Mott and Z. Zinamon, Rep. Prog. Phys. 33, 881 (1970).

7. E.H. Lieb and F.Y. Wu, Phys. Rev. Lett. 20, 1445 (1968).

8. L.M. Falicov and R.A. Harris, J. Chem. Phys. 51, 3153 (1969); D.J. Newman, K.S. Chan, and B. Ng, J. Phys. Chem. Sol. 45, 643 (1984).

9. E. Lieb and D. Mattis, Phys. Rev. 125, 164 (1962).

10. J. Bernasconi, Phys. Kondens. Mater. 14, 225 (1972) and references therein.

11. A.B. Harris and R.V. Lange, Phys. Rev. 157, 295 (1967).

12. F. Hund, Linienspektren und periodisches System der Elemente (Springer, Berlin, 1927), p. 124.

13. E.U. Condon and G.H. Shortley, The Theory of Atomic Spectra (Cambridge University Press, Cambridge, England, 1957), p. 209.

14. Under the conditions of a face-centered-cubic lattice with restricted Γ and X sampling, there is a correspondence between the point-group symmetries of T_d in the cluster and the space-group symmetry of the cubic lattice with Γ_1, Γ_2, and Γ_3 of T_d corresponding to the Γ point of the Brillouin zone, and Γ_4 and Γ_5 of T_d corresponding to the X point.

TABLE 1

Character table of T_d

	1	3	8	6	6	
	E	C_2	C_3	σ	S_4	Atomic symmetries
Γ_1	1	1	1	1	1	s_g
Γ_2	1	1	1	-1	-1	s_u
Γ_3	2	2	-1	0	0	$d_g d_u$
Γ_4	3	-1	0	1	-1	$p_u d_g$
Γ_5	3	-1	0	-1	1	$p_g d_u$

TABLE 2

Configurations, Symmetries and Eigenvalues in the Non-Interacting Limit U=0

N	States	Levels	Configuration	Energy	Symmetries
0	1	1	---	0	${}^1\Gamma_1$
1	2	1	s^1	-3t	${}^2\Gamma_1$
1	6	1	p^1	t	${}^2\Gamma_4$
2	1	1	s^2	-6t	${}^1\Gamma_1$
2	12	2	s^1p^1	-2t	${}^1\Gamma_4$ ${}^3\Gamma_4$
2	15	4	p^2	2t	${}^1\Gamma_1$ ${}^1\Gamma_3$ ${}^1\Gamma_4$ ${}^3\Gamma_5$
3	6	1	s^2p^1	-5t	${}^2\Gamma_4$
3	30	5	s^1p^2	-t	${}^2\Gamma_1$ ${}^2\Gamma_3$ ${}^2\Gamma_4$ ${}^2\Gamma_5$ ${}^4\Gamma_5$
3	20	4	p^3	3t	${}^2\Gamma_3$ ${}^2\Gamma_4$ ${}^2\Gamma_5$ ${}^4\Gamma_2$
4	15	4	s^2p^2	-4t	${}^1\Gamma_1$ ${}^1\Gamma_3$ ${}^1\Gamma_4$ ${}^3\Gamma_5$
4	40	8	s^1p^3	0	${}^1\Gamma_3$ ${}^1\Gamma_4$ ${}^1\Gamma_5$ ${}^3\Gamma_2$ ${}^3\Gamma_3$
					${}^3\Gamma_4$ ${}^3\Gamma_5$ ${}^5\Gamma_2$
4	15	4	p^4	4t	${}^1\Gamma_1$ ${}^1\Gamma_3$ ${}^1\Gamma_4$ ${}^3\Gamma_5$
5	20	4	s^2p^3	-3t	${}^2\Gamma_3$ ${}^2\Gamma_4$ ${}^2\Gamma_5$ ${}^4\Gamma_2$

TABLE 2 (continued)

N	States	Levels	Configuration	Energy	Symmetries
5	30	5	s^1p^4	t	${}^2\Gamma_1$ ${}^2\Gamma_3$ ${}^2\Gamma_4$ ${}^2\Gamma_5$ ${}^4\Gamma_5$
5	6	1	p^5	5t	${}^2\Gamma_4$
6	15	4	s^2p^4	-2t	${}^1\Gamma_1$ ${}^1\Gamma_3$ ${}^1\Gamma_4$ ${}^3\Gamma_5$
6	12	2	s^1p^5	2t	${}^1\Gamma_4$ ${}^3\Gamma_4$
6	1	1	p^6	6t	${}^1\Gamma_1$
7	6	1	s^2p^5	-t	${}^2\Gamma_4$
7	2	1	s^1p^6	3t	${}^2\Gamma_1$
8	1	1	s^2p^6	0	${}^1\Gamma_1$

TABLE 3

Symmetries and Eigenvalues in the Strongly Interacting Limit t=0

N	States	Levels	Energy	Symmetries
0	1	1	0	${}^{1}\Gamma_{1}$
1	8	2	0	${}^{2}\Gamma_{1}$ ${}^{2}\Gamma_{4}$
2	24	5	0	${}^{1}\Gamma_{1}$ ${}^{1}\Gamma_{3}$ ${}^{1}\Gamma_{4}$ ${}^{3}\Gamma_{4}$ ${}^{3}\Gamma_{5}$
2	4	2	U	${}^{1}\Gamma_{1}$ ${}^{1}\Gamma_{4}$
3	32	5	0	${}^{2}\Gamma_{3}$ ${}^{2}\Gamma_{4}$ ${}^{2}\Gamma_{5}$ ${}^{4}\Gamma_{2}$ ${}^{4}\Gamma_{5}$
3	24	5	U	${}^{2}\Gamma_{1}$ ${}^{2}\Gamma_{3}$ ${}^{2}\Gamma_{4}$ ${}^{2}\Gamma_{4}$ ${}^{2}\Gamma_{5}$
4	16	3	0	${}^{1}\Gamma_{3}$ ${}^{3}\Gamma_{5}$ ${}^{5}\Gamma_{2}$
4	48	10	U	${}^{1}\Gamma_{1}$ ${}^{1}\Gamma_{3}$ ${}^{1}\Gamma_{4}$ ${}^{1}\Gamma_{4}$ ${}^{1}\Gamma_{5}$ ${}^{3}\Gamma_{2}$ ${}^{3}\Gamma_{3}$ ${}^{3}\Gamma_{4}$ ${}^{3}\Gamma_{5}$ ${}^{3}\Gamma_{5}$
4	6	3	2U	${}^{1}\Gamma_{1}$ ${}^{1}\Gamma_{3}$ ${}^{1}\Gamma_{4}$
5	32	5	U	${}^{2}\Gamma_{3}$ ${}^{2}\Gamma_{4}$ ${}^{2}\Gamma_{5}$ ${}^{4}\Gamma_{2}$ ${}^{4}\Gamma_{5}$
5	24	5	2U	${}^{2}\Gamma_{1}$ ${}^{2}\Gamma_{3}$ ${}^{2}\Gamma_{4}$ ${}^{2}\Gamma_{4}$ ${}^{2}\Gamma_{5}$

TABLE 3 (continued)

N	States	Levels	Energy	Symmetries
6	24	5	2U	${}^1\Gamma_1$ ${}^1\Gamma_3$ ${}^1\Gamma_4$ ${}^3\Gamma_4$ ${}^3\Gamma_5$
6	4	2	3U	${}^1\Gamma_1$ ${}^1\Gamma_4$
7	8	2	3U	${}^2\Gamma_1$ ${}^2\Gamma_4$
8	1	1	4U	${}^1\Gamma_1$

TABLE 4

Symmetry of the Ground States

N	Configuration	Hund's Rule Symmetry	Symmetry U>0	Symmetry U<0
0	---	${}^1\Gamma_1$	${}^1\Gamma_1$	${}^1\Gamma_1$
1	s^1	${}^2\Gamma_1$	${}^2\Gamma_1$	${}^2\Gamma_1$
2	s^2	${}^1\Gamma_1$	${}^1\Gamma_1$	${}^1\Gamma_1$
3	s^2p^1	${}^2\Gamma_4$	${}^2\Gamma_4$	${}^2\Gamma_4$
4	s^2p^2	${}^3\Gamma_5$	${}^1\Gamma_3$	${}^1\Gamma_1$
5	s^2p^3	${}^4\Gamma_2$	${}^4\Gamma_2$	${}^2\Gamma_3$
6	s^2p^4	${}^3\Gamma_5$	${}^1\Gamma_3 \oplus {}^3\Gamma_5$	${}^1\Gamma_1$
7	s^2p^5	${}^2\Gamma_4$	${}^2\Gamma_4$	${}^2\Gamma_4$
8	s^2p^6	${}^1\Gamma_1$	${}^1\Gamma_1$	${}^1\Gamma_1$

TABLE 5

Energy Equations for the 56 Eigenvalues

N=0	${}^{1}\Gamma_1$	$E=0$
N=1	${}^{2}\Gamma_1$	$E+3t=0$
	${}^{2}\Gamma_4$	$E-t=0$
N=2	${}^{1}\Gamma_1$	$E^2+(4t-U)E-(12t^2+4tU)=0$
	${}^{1}\Gamma_3$	$E-2t=0$
	${}^{1}\Gamma_4$	$E^2-UE-4t^2=0$
	${}^{3}\Gamma_4$	$E+2t=0$
	${}^{3}\Gamma_5$	$E-2t=0$
N=3	${}^{2}\Gamma_1$	$E+t-U=0$
	${}^{2}\Gamma_3$	$E^2-(2t+U)E-3t^2=0$
	${}^{2}\Gamma_4$	$E^3+(3t-2U)E^2-(13t^2+5tU-U^2)E-(15t^3-9t^2U-2tU^2)=0$

TABLE 5 (continued)

	${}^{2}\Gamma_5$	$E^2-(2t+U)E-(3t^2-2tU)=0$
	${}^{4}\Gamma_2$	$E-3t=0$
	${}^{4}\Gamma_5$	$E+t=0$
N=4	${}^{1}\Gamma_1$	$E^2-3UE-(16t^2-2U^2)=0$
	${}^{1}\Gamma_3$	$E^3-3UE^2-(16t^2-2U^2)E+24t^2U=0$
	${}^{1}\Gamma_4$	$E^3-4UE^2-(16t^2-5U^2)E+(24t^2U-2U^3)=0$
	${}^{1}\Gamma_5$	$E-U=0$
	${}^{3}\Gamma_2$	$E-U=0$
	${}^{3}\Gamma_3$	$E-U=0$
	${}^{3}\Gamma_4$	$E-U=0$
	${}^{3}\Gamma_5$	$E^3-2UE-(16t^2-U^2)E+8t^2U=0$
	${}^{5}\Gamma_2$	$E=0$

TABLE 5 (continued)

N=5	$^2\Gamma_1$	$E-t-2U=0$
	$^2\Gamma_3$	$E^2+(2t-3U)E-(3t^2+2tU-2U^2)=0$
	$^2\Gamma_4$	$E^3-(3t+5U)E^2-(13t^2-11tU-8U^2)E$ $+(15t^3+22t^2U-10tU^2-4U^3)=0$
	$^2\Gamma_5$	$E^2+(2t-3U)E-(3t^2+4tU-2U^2)=0$
	$^4\Gamma_2$	$E+3t-U=0$
	$^4\Gamma_5$	$E-t-U=0$
N=6	$^1\Gamma_1$	$E^2-(4t+5U)E-(12t^2-12tU-6U^2)=0$
	$^1\Gamma_3$	$E+2t-2U=0$
	$^1\Gamma_4$	$E^2-5UE-(4t^2-6U^2)=0$
	$^3\Gamma_4$	$E-2t-2U=0$
	$^3\Gamma_5$	$E+2t-2U=0$

TABLE 5 (continued)

N=7	$^2\Gamma_1$	E-3t-3U=0
	$^2\Gamma_4$	E+t-3U=0
N=8	$^1\Gamma_1$	E-4U=0

Figure Captions

Figure 1 Energies, as measured from the ground state, for $N = 2$. The abscissas correspond to the quantity $U/(4t + U)$. The ordinates are the excitation energies from the ground state in units of $4t + U$. The symmetries of ground and excited states are indicated.

Figure 2 Energies, as measured from the ground state, for $N = 3$. See caption of Figure 1.

Figure 3 Energies, as measured from the ground state, for $N = 4$. See caption of Figure 1.

Figure 4 Energies, as measured from the ground state, for $N = 5$. See caption of Figure 1.

Figure 5 Energies, as measured from the ground state, for $N = 6$. See caption of Figure 1.

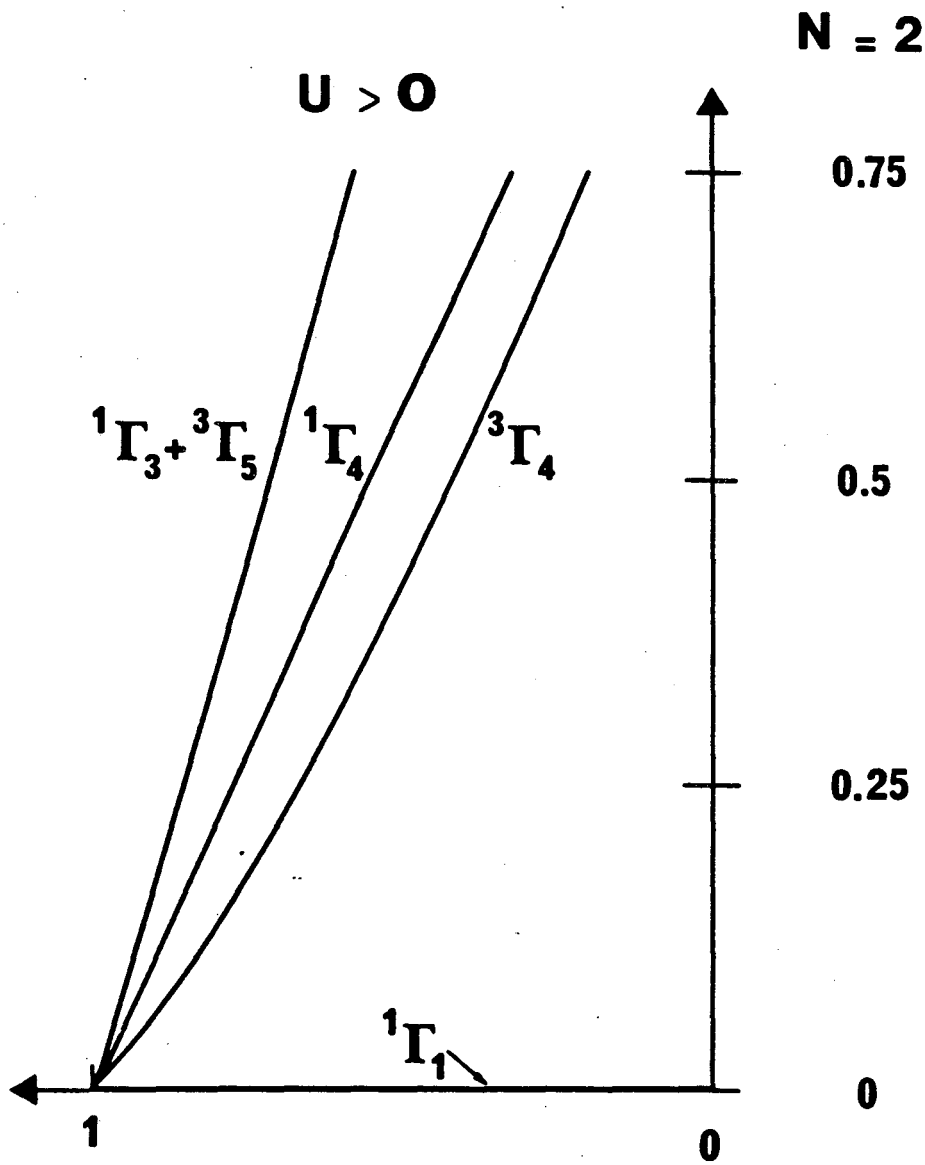
N = 2
U > O
0.75
0.5
0.25
0
$^1\Gamma_3 + {}^3\Gamma_5$
$^1\Gamma_4$
$^3\Gamma_4$
$^1\Gamma_1$
1
0

Figure 1

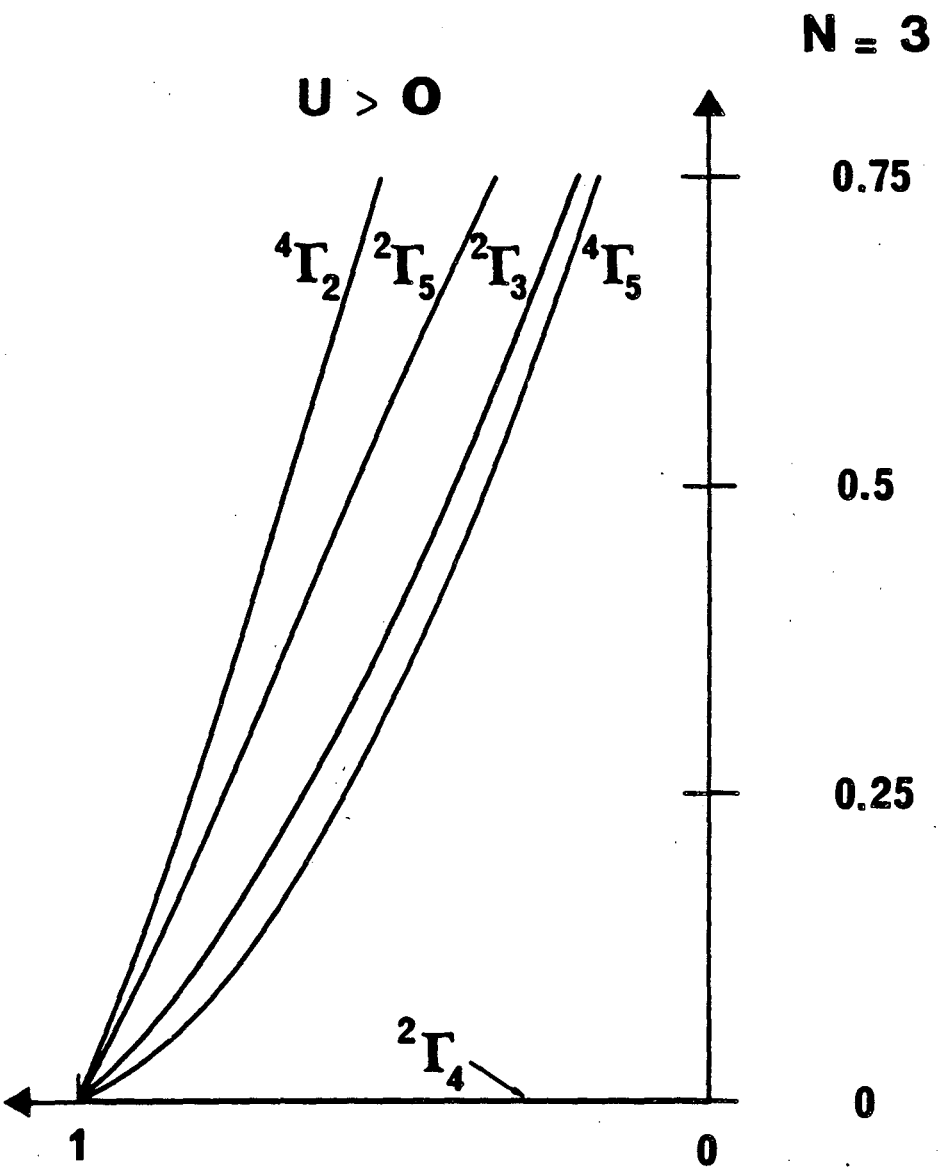
N = 3
U > O
0.75
0.5
0.25
0
$^4\Gamma_2$
$^2\Gamma_5$
$^2\Gamma_3$
$^4\Gamma_5$
$^2\Gamma_4$
1
0

Figure 2

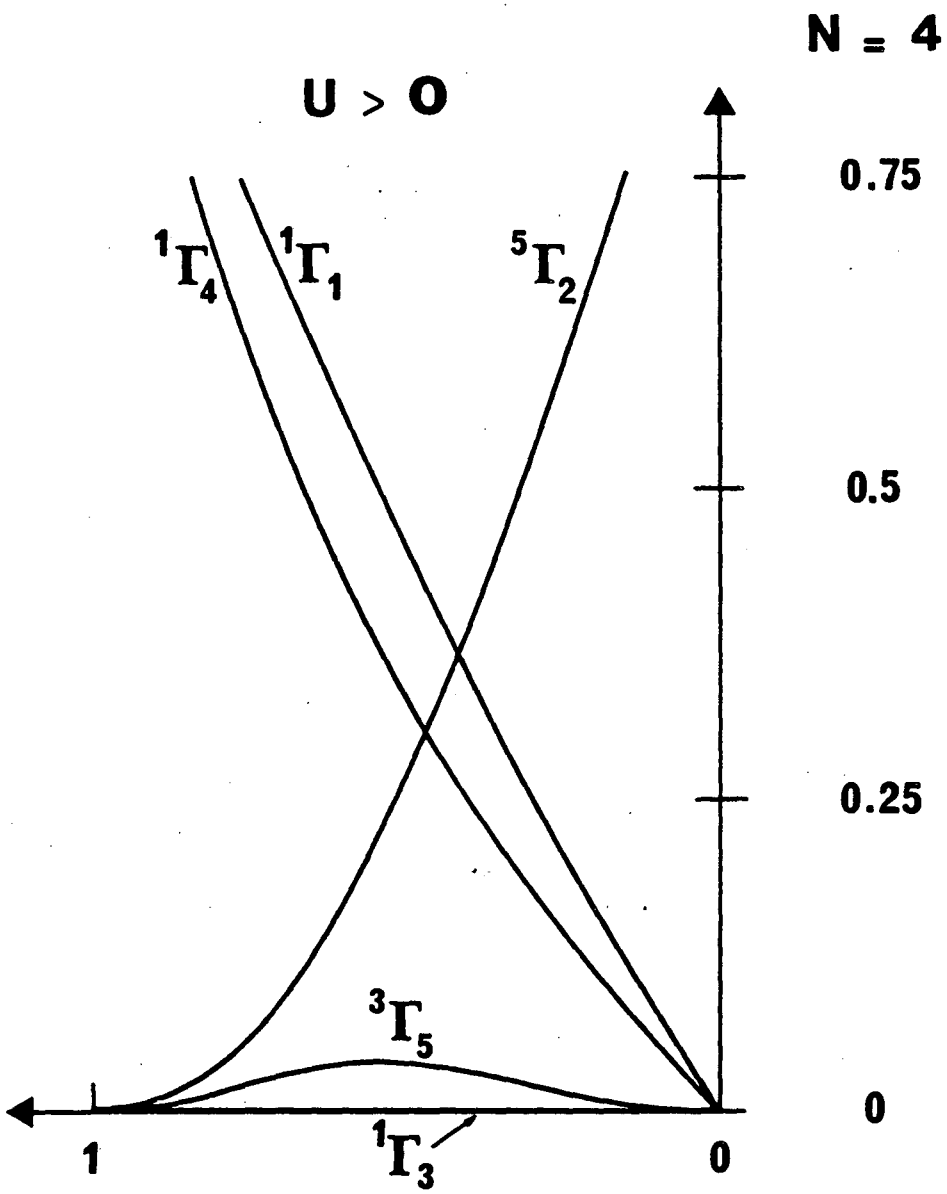
N = 4
U > O
0.75
0.5
0.25
0
$^1\Gamma_4$
$^1\Gamma_1$
$^5\Gamma_2$
$^3\Gamma_5$
$^1\Gamma_3$
1
0

Figure 3

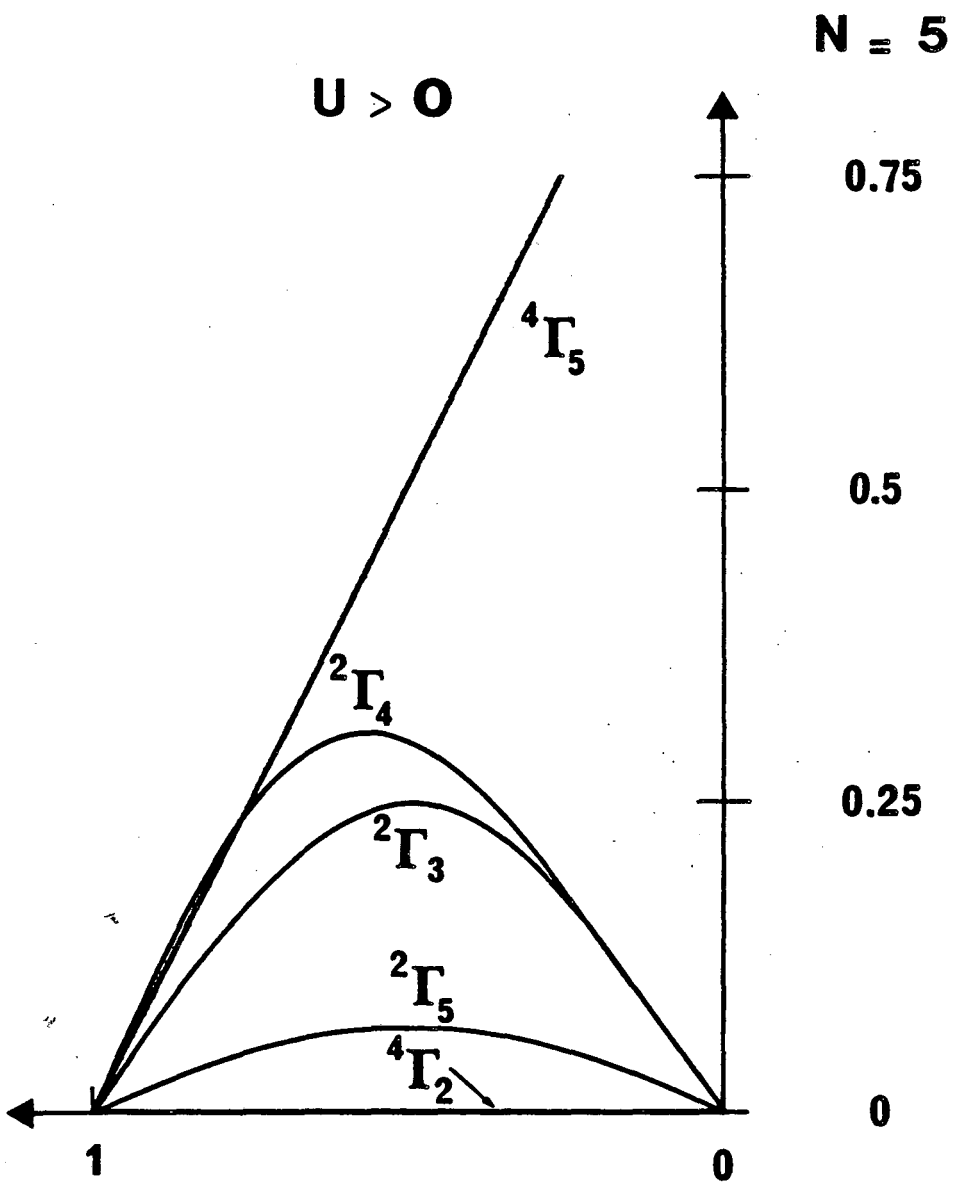
N = 5
U > O
0.75
0.5
0.25
0
$^4\Gamma_5$
$^2\Gamma_4$
$^2\Gamma_3$
$^2\Gamma_5$
$^4\Gamma_2$
1
0

Figure 4

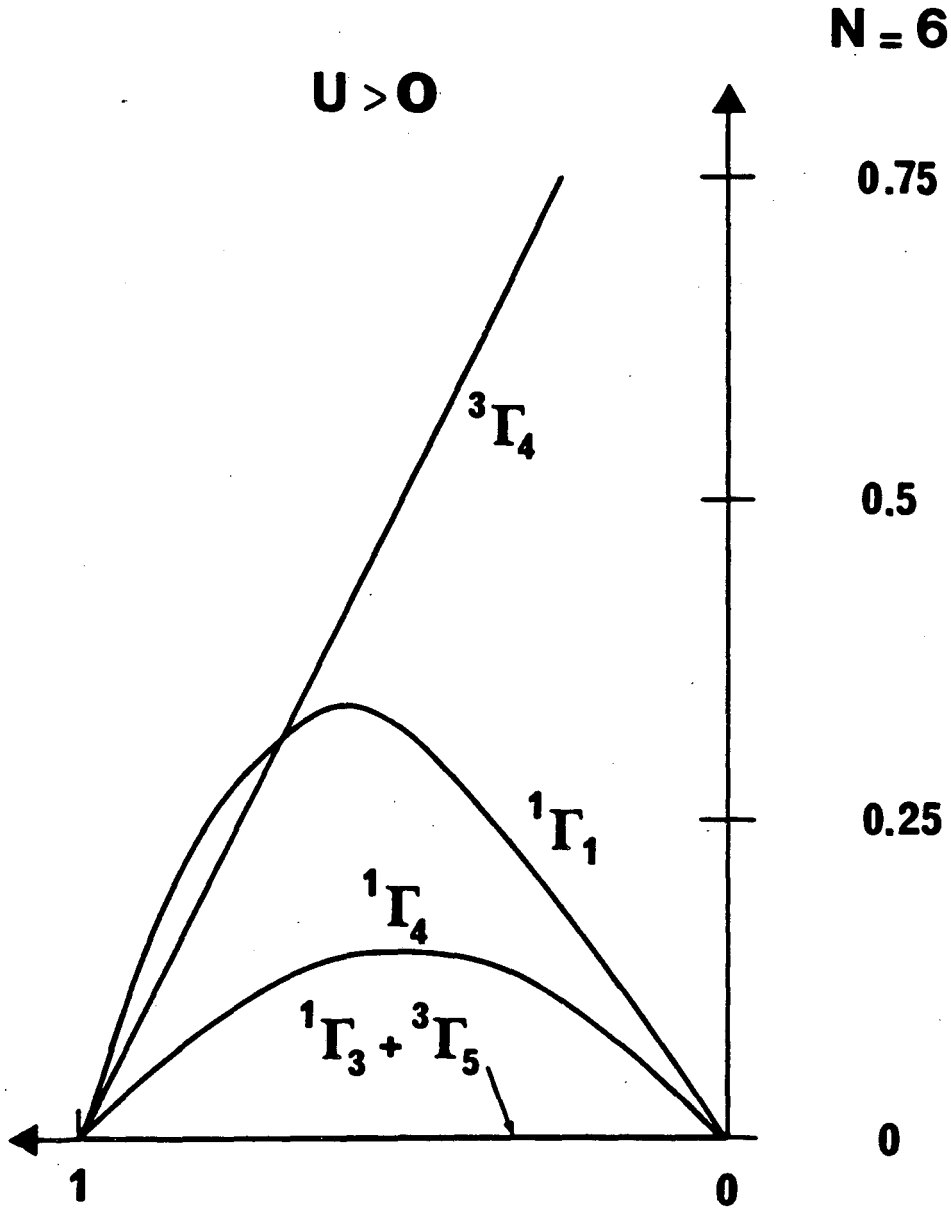
N = 6
U > O
0.75
0.5
0.25
0
$^3\Gamma_4$
$^1\Gamma_1$
$^1\Gamma_4$
$^1\Gamma_3 + {}^3\Gamma_5$
1
0

Figure 5

III. CALCULATIONAL TECHNIQUE USED FOR HETEROGENEOUS SYSTEMS

This chapter describes the calculational techniques used for evaluating the properties of the various heterogeneous systems discussed in this thesis. The Hamiltonian is described in Section A, while Section B outlines the method of implementation and the accompanying numerical accuracy. Section C examines the possible errors introduced by the major approximations. Several calculational details relevant for a single material will be discussed only in the chapter describing that material.

A. The Hamiltonian

The Hamiltonian is taken to be the sum of a one-electron term H_o and an electron-electron interaction term H_{e-e}. For H_o the parametrized tight-binding scheme of Slater and Koster is chosen.[1] The Hamiltonian H_o is written in terms of one- and two-center integrals, which are treated as parameters chosen to fit the bulk band structure. (See Table I.) In several of the elements (Co and Cr), there is a marked discrepancy between the calculated and the experimentally measured bandwidth (photoemission experiments). For Cr, Fe, and Co, we have chosen the calculated paramagnetic band structures of Moruzzi *et al.*[2,3] (see Appendix), with the belief that discrepancies with photoemission data are caused by additional many body effects, as has been argued for Ni. We include *s*, *p*, and *d* orbitals, with

interactions up to second nearest neighbors. For the matrix elements between dissimilar neighbors, the geometric average of the two bulk elements is chosen. In one of the systems, Co overlayed on Cu, the Co-Co element has the opposite sign of the Cu-Cu element for three of the second-nearest neighbor matrix elements. In this case, the arithmetic mean is used. The various sets of intersite matrix elements are similar, so the results are insensitive to the precise scheme for choosing matrix elements between dissimilar neighbors.

For the electron-electron interaction we use a single-site approximation which has been extensively discussed.

$$H_{e-e} = \sum_{i,\sigma,\sigma'} \sum_{\alpha,\beta,\gamma,\delta} U_{\alpha\beta\gamma\delta} c^{\dagger}_{i\alpha\sigma} c^{\dagger}_{i\beta\sigma'} c_{i\gamma\sigma'} c_{i\delta\sigma} , \qquad (1)$$

where $c^{\dagger}_{i\alpha\sigma}$ creates an orbital of symmetry α and spin σ at site $\underline{i}$.

We treat H_{e-e} in the Hartree-Fock approach; we can, with some approximations, reduce H_{e-e} to a simple form for the on-site potential shifts,

$$\begin{aligned} \Delta E_{d\nu\sigma} &= -\tfrac{1}{2}(U - J)\langle m_{d\nu\sigma}\rangle - \tfrac{1}{2}J\langle m_{d\sigma}\rangle \\ &\quad + \tfrac{1}{2}(U - 2U' + J)\langle n_{d\nu} - n^0_{d\nu}\rangle \\ &\quad + V_{sd}\langle n_s - n^0_s\rangle + V_{dd}\langle n_d - n^0_d\rangle , \\ \Delta E_{s\sigma} &= V_{ss}\langle n_s - n^0_s\rangle + V_{sd}\langle n_d - n^0_d\rangle . \end{aligned} \qquad (2)$$

Here, $\Delta E_{d\nu\sigma}$ is the on-site potential shift for a d orbital of symmetry ν and spin σ, measured relative to the value for the pure paramagnetic metal. By $m_{d\nu\sigma}$ we denote the spin polarization $(n_{d\nu\sigma}-n_{d\nu\bar{\sigma}})$ in the d orbital of symmetry ν at a given site, and $m_{d\sigma} \equiv \sum_{\nu} m_{d\nu\sigma}$. The total d occupancy at the site is denoted by $n_d \equiv \sum_{\nu,\sigma} n_{d\nu\sigma}$, and the value for the respective pure metal is n_d^0. (See Table I.) Quantities for s and p orbitals are similarly defined. In (2), s refers to the entire sp complex.

We define U as the on-site direct Coulomb integral between d orbitals of the same symmetry (rescaled by correlation effects; see below), U' is the integral between d orbitals of different symmetry, and J is the exchange integral. We define $V_{dd} \equiv U'-\frac{1}{2}J$, which gives the effective (repulsive) interaction between d electrons, aside from magnetic effects. We similarly define an effective interaction V_{ss} among sp electrons, and V_{sd} between sp and d electrons. We neglect the on-site exchange integrals other than those between d orbitals. Atomic symmetry[5] demands that $U = U'+2J$. The ratio U:J is taken to be 5:1 as suggested by Herring.[6] The absolute magnitude of U is scaled to give the correct bulk magnetization, $\mu=1.72\mu_\beta$ for Co, $\mu = 2.22\mu_\beta$ for Fe, and $\mu = 0.67\mu_\beta$ for simple[7] anti-ferromagnetic Cr. (See Table I.) We use Auger-electron spectroscopy data[8] to set V_{dd} for Fe and Co. We also use the Fe value for Cr which should cause only negligible error since there is virtually no charge rearrangement between

paramagnetic and antiferromagnetic Cr, even when $V_{dd} = 0$. The ratios of V_{sd} and V_{dd} are taken to be the ratios of the atomic values.[9]

It is difficult within the tight-binding approximation to treat charge transfer accurately at the surface. To avoid this problem and still treat charge transfer and potential shifts at the surface in a simple way, we impose upon our potential the constraint

$$\Delta n_{sp} = \Delta n_d = 0 \tag{3}$$

That is, the average on-site potentials of the d orbitals and the s and p orbitals are fixed by the requirement that the total occupancies of the sp and d complexes at any site should not differ from the bulk values. More fully-self-consistent calculations[10-12] suggest that the d band gains or loses no more than 0.1 electrons at the surface. By neglecting this, we may expect to alter the calculated surface magnetization by less than $0.1\mu_B$ per atom, an acceptable level of error.

B. Method of Implementation

The Hamiltonian described in Section A may be viewed as a one-electron theory. This means that the problem of an infinite number of atoms in a homogeneous crystal is easily solved by the transformation to reciprocal space via Bloch's theorem. The problem of an ordered alloy is of equally easy solution, albeit with a larger unit cell. The situation is less clear for an infinite surface. Bloch's

theorem may still be applied parallel to the surface, but the perpendicular direction lacks translational symmetry and thus must be treated in real space. Two techniques for treating this problem are the finite slab method, which imagines the crystal to be characterized by two surfaces separated by a small number of "bulk" atoms, and the Green's function transfer matrix method, which acknowledges the semi-infinite nature of the problem but requires that the distant bulk atoms be ignorant of the surface. Either technique allows accurate solution of most problems: choice depends on consideration of cost and simplicity.

Our fcc surface calculations use the Green's function transfer matrix method. In principle, the Green's function $\overleftrightarrow{G}$ is obtained by solving Dyson's equation:

$$\overleftrightarrow{I} = (E\overleftrightarrow{I}-\overleftrightarrow{H})\,\overleftrightarrow{G}, \qquad (4)$$

where $\overleftrightarrow{H}$ is the one particle Hamiltonian and E is an energy. The solution is made practical by assuming that atoms more than a few layers down (three layers for pure Cu surface or a monolayer Co on Cu, four layers for a di-layer Co on Cu) exhibit bulk behavior and thus may be treated by a transfer matrix connecting different parts of the Green's function. Only the top two or three layers are treated self-consistently with respect to surface effects. A more complete explanation of the method may be found in Ref. 13.

A density of states D(E) is obtained from the Green's function through the formula:

$$D(E) = -\frac{1}{\pi} \mathrm{Im} \sum_{\vec{k}} \mathrm{Tr}\, \overleftrightarrow{G}(\vec{k}, E), \tag{5}$$

where Tr indicates the trace of the matrix $\overleftrightarrow{G}$. Integrated properties such as spin polarization and total occupancies are obtained from an integration path consisting of 48 points chosen along a complex contour with the aid of the method of Gaussian quadratures.[14] This provides an estimated accuracy of 0.01 electrons. For calculations, involving a two-atom unit surface cell, reasons of economy demanded a slightly less accurate 24-point integration.

Our bcc surface calculations use the finite slab method. Typically a seven layer slab is found sufficient to produce bulk-like behavior in the middle of the slab and surface behavior that is independent of further widening of the slab. However, in certain cases a 9-layer slab [Cr overlayer on Fe(100)] or even an 11-layer slab [Cr(100) surface] is necessary to provide convergent behavior at the surface. In some cases the middle atom does not reach truly bulk-like characteristics, but it is found that this has no effect on the surface atom. Nonetheless, it is clear that for these cases [Cr(100) surface, Fe(100) surface] some interior atoms are strongly affected by both surfaces, and consequently are not representative of true interior atoms.

Convergence in reciprocal space is provided by sampling $\vec{K}$ vectors in the irreducible Brillouin zone. For

bulk calculations, approximately 350 $\vec{K}$ points in the irreducible 1/48th wedge of the Brillouin zone are used. This should ensure excellent (approximately 0.001 electron) convergence.

Surface calculations present more expense and consequently fewer $\vec{K}$ vectors are employed. We use 15 points in the (100) bcc irreducible Brillouin zone, 24 points in the two-atom (110) bcc irreducible Brillouin zone, and 12 points in the two-atom (111) fcc irreducible Brillouin zone. Tests with special $\vec{K}$ vector sampling schemes suggest that the accuracy is approximately 0.01 electrons.

Several of the systems display more than one self-consistent state. We calculated the total energy of each such state using the well-known formula:[15]

$$E = \sum_{n,\vec{K}} \left[\varepsilon_{\vec{K}} - \tfrac{1}{2} \sum_{n',\vec{K}'} H_{e-e} \right]$$

where $\varepsilon_{\vec{K}}$ is the one-particle removal energy and the sums are performed over the occupied states. The nonintuitive term involving H_{e-e} corrects for the double counting of the electron-electron interaction.

Potentials are converged sufficiently that they contribute no error to the accuracy of our scheme. Overall numerical accuracy is quite high, better than 0.01 electrons and 0.001 Ry for most systems. Only the two-atom unit cell fcc surface calculations have the possibility

of a higher error: 0.02 electrons and 0.002 Ry. On the other hand, bulk calculations are typically an order of magnitude more accurate. It is not expected that numerical inaccuracies in the implementation of our Hamiltonian constitute any problem in the calculations presented in this thesis.

C. Error Analysis of the Hamiltonian

We recapitulate now the crucial approximations in our Hamiltonian, and consider their effects. The use of a tight-binding scheme at surfaces produces several difficulties because it is unable to represent fully the non-spherical spilling of the electronic charge density into the vacuum. The resultant error in the charge transfer is handled in our scheme by the approximation (3), in which the self-consistent change in the potential is approximated by an on-site term, determined by imposing a zero-charge-transfer condition on the sp- and d-projected subbands separately at each site. Comparison with fully self-consistent calculations[10-12] suggests that this is an excellent approximation. Still the uncertainty of up to 0.1 electrons in the local d occupancy corresponds to a possible error of up to one-tenth of a Bohr magneton, which may be measurable for some systems. However, there is no evidence that any available method is accurate to better than $0.1\mu_B$ for inhomogeneous systems. Approximation (3) also neglects the crystal-field splitting of the on-site

potential.

Our tight-binding representation of charge densities also produces inaccuracies in the prediction of some surface features in the spectra. Chapter VII of this thesis provides a detailed comparison with a chromium (100) photoemission experiment which suggests that we accurately predict the existence or absence of surface features and qualitatively predict the dispersion and intensities of those surface features. Errors in binding energy prediction, however, may be as large as 0.05 Ry.

Even within the bulk, the use of a tight-binding Hamiltonian should be analyzed with care. This method provides a good treatment of the d band, but the handling of the sp band is less accurate. Since sp-d hybridization plays an important role here, the tight binding approximation introduces some risk of reduced quantitative accuracy.

Finally, it is important to note that, if many-body effects are important, the one-electron DOS which we calculate may not be the same as the excitation spectrum measured by photoemission. In particular, both bulk Cr and bulk Co exhibit a slightly compressed (approximately 20%) photoionization spectrum[16,17] compared to the calculated DOS.

Ultimately we must base our assessment of overall accuracy upon comparison with reported results of fully self-consistent calculations for simple systems, and with experiment. Such comparisons have been made by a previous

worker[18] and further comparisons will be drawn throughout this thesis. The results suggest that our methods reliably predict the quantitative magnetization of heterogeneous systems. Other important conclusions which we draw either involve comparisons of different systems, in which case our errors should approximately cancel, or involve comparison with photoemission spectra, where our errors can be easily estimated.

Appendix

The fcc Co, bcc Fe, and bcc Cr band structures are taken directly from Ref. 2. The bcc Co and fcc Fe band structures are obtained from the bcc Fe and fcc Co structures by scaling the bandwidths and band centers as suggested in Ref. 3. Unfortunately, the local-density band structures are not given at experimental lattice constants. Consequently, the band structures used in this calculation were evaluated at 3.41, 2.72, 2.72, 2.80, and 3.42 Å for fcc Co, bcc Co, bcc Fe, bcc Cr, and fcc Fe, respectively. Actual lattice constants are 3.54, 2.82, 2.87, and 2.89 Å, where the bcc Co lattice constant is a result of extrapolating the Fe-Co lattice-constant curve and the fcc Fe lattice constant is not listed. Thus theoretical lattice constants are 0.963, 0.964, 0.948, and 0.968 of the experimental lattice constants. This should make no difference since the strength of the electron-electron interaction has been scaled to give the correct magnetization for the bulk elements. Note that bcc Co and fcc Co have nearly identical (0.963 versus 0.964) lattice ratios and consequently, there should be little error in using the same electron-electron interaction strength for both.

References

1. J.C. Slater and G.F. Koster, Phys. Rev. 94, 1498 (1954).

2. V.L. Moruzzi, J.F. Janak, and A.R. Williams, Calculated Electronic Properties of Metals (Pergamon, New York, 1978).

3. V.L. Moruzzi, C.D. Gelatt, Jr. and A.R. Williams, Calculated Electronic Properties of Ordered Alloys, (to be published).

4. C. Herring in Exchange Interactions among Itinerant Electrons, Vol. IV of Magnetism, edited by G.T. Rado and H. Suhl (Academic, New York, 1966), and references therein.

5. A.M. Olés and G. Stollhoff, Phys. Rev. B 29, 314 (1984).

6. C. Herring in Exchange Interactions among Itinerant Electrons, Ref. 4, p. 227.

7. W.C. Koehler, R.M. Moon, A.L. Trego, and A.R. MacKintosh, Phy. Rev. 151, 405 (1966). See Introduction to Chapter VI of this thesis.

8. E. Antonides, E.C. Janse, and G.A. Sawatzky, Phys. Rev. B 15, 1669 (1977).

9. $V_{dd} : V_{sd} : V_{ss}$ is taken as 1 : 0.578 : 0.483 in accordance with arguments presented in J. Tersoff and L.M. Falicov, Phys. Rev. B 24, 754 (1981).

10. H. Krakauer, A.J. Freeman, and E. Wimmer, Phys. Rev. B 28, 610 (1983).

11. S. Ohnishi, A.J. Freeman, and M. Weinert, Phys. Rev. B 28, 6741 (1983).

12. J. Noffke and L. Fritsche, J. Phys. C 14, 89 (1981).

13. J. Tersoff and L.M. Falicov, Phys. Rev. B 24, 754 (1981).

14. Handbook of Mathematical Functions, edited by M. Abramowitz and I. Stegun (National Bureau of Standards, Washington, D. C., 1964).

15. E. Merzbacher, Quantum Mechanics, 2nd ed. (Wiley, New York, 1970) p. 538.

16. G. Gewinner, J.C. Peruchetti, A. Jaégle and R. Pinchaux, Phys. Rev. B 27, 3358 (1983).

17. F.J. Himpsel and D.E. Eastman, Phys. Rev. B 21, 3207 (1980).

18. J. Tersoff and L.M. Falicov, Phys. Rev. B 26, 6186 (1982).

TABLE I

Hamiltonian Parameters

Listed are the 24 Slater-Koster tight-binding matrix elements, the U necessary to produce the correct spin polarization, and the occupancies in the paramagnetic state. A slightly different (wider conduction band) set of fcc Co parameters was used in the Co on Cu calculation. The set listed was used for the Fe-Co calculations and is believed to be more accurate.

	bcc Cr	bccFe	fcc Fe	bcc Co	fcc Co
$(ss)_0$	.594	.514	.600	.507	.560
$(pp)_0$	1.173	1.118	1.384	1.111	1.344
$(dde_g)_0$	+.005	-.068	-.051	-.076	-.092
$(ddt_{2g})_0$	-.016	-.089	-.063	-.094	-.102
$(ss\sigma)_1$	-.10605	-.10605	-.07452	-.10605	-.07452
$(sp\sigma)_1$	-.19326	-.19326	+.14706	-.19326	+.14706
$(sd\sigma)_1$	-.08740	-.08018	+.08777	-.07537	+.08209
$(pp\sigma)_1$	+.26932	+.26932	+.30843	+.26932	+.30843
$(pp\pi)_1$	-.00672	-.00672	-.01129	-.00672	-.01129
$(pd\sigma)_1$	.10807	+.09915	+.11339	+.09320	+.10605
$(pd\pi)_1$	-.02689	-.02467	-.02049	-.02319	-.01917
$(dd\sigma)_1$	-.06735	-.05669	-.05217	-.05009	-.04563
$(dd\pi)_1$	+.04441	+.03738	+.02647	+.03303	+.02315
$(dd\delta)_1$	-.00795	-.00669	-.00290	-.00591	-.00254
$(ss\sigma)_2$	-.05276	-.05276	-.05495	-.05276	-.05495
$(sp\sigma)_2$	-.06725	-.06725	+.08064	-.06725	+.08064
$(sd\sigma)_2$	-.03308	-.03035	.00000	-.02853	.00000
$(pp\sigma)_2$	.17199	+.17199	+.15017	+.17199	+.15017
$(pp\pi)_2$	.03242	+.03242	-.05749	+.03242	-.05749
$(pd\sigma)_2$	.05670	+.05202	.00000	+.04890	.00000
$(pd\pi)_2$	-.00100	-.00092	.00000	-.00086	.00000
$(dd\sigma)_2$	-.04000	-.03367	.00000	-.02975	.00000
$(dd\pi)_2$	.01188	+.01000	.00000	+.00884	.00000
$(dd\delta)_2$	-.00089	-.00075	.00000	-.00066	.00000
U	.167	.220	.220	.296	.296
n^0_{sp}	1.175	1.185	1.154	1.174	1.150
n^0_{t2g}	3.258	4.223	3.954	4.478	4.448
n^0_{eg}	1.567	2.592	2.892	3.348	3.404
n^0_{total}	6.000	8.000	8.000	9.000	9.000

IV. THE MAGNETIC STATES OF COBALT OVERLAYERS ON COPPER (111)

A. Introduction

Recently, there has been renewed interest in the magnetism and related properties of thin magnetic transition-metal layers deposited on nonmagnetic substrates. Experimental evidence shows that two layers of Ni on Cu form a magnetic system,[1,2] but Ni on a Pb-Bi alloy substrate or on an Al substrate is paramagnetic below 2.5-3 atomic layers.[3,4] However, Co and Fe retained their magnetic moment on these same substrates, even when deposited in subatomic layers.[3,4] Theoretical investigation shows that one layer of Ni on Cu(100) is substantially magnetic,[5,6] while the same system on the (111) surface is not.[6] It is also found both theoretically[6,7] and experimentally[1,8] that the surface layer of a magnetic metal is magnetic. In addition, (hypothetical) unsupported monolayer films are theoretically found to have even greater magnetization than bulk.[6,9] This suggests that the reduction in magnetism for thin films on nonmagnetic substrates is caused by the substrate and not by the free surface. In fact, it is believed[6] that the crucial mechanism acting to suppress Ni magnetization at the Ni-Cu interface is hybridization of the Ni *d* band with the Cu *sp* band, which changes the shape of the band edge and reduces the "effective" number of *d*

holes. Both Fe and Co, which have many more holes, should be relatively immune to this effect.

The particular system addressed in this work [Co on Cu (111)] has also been studied previously. Gonzalez et al.[10] and Miranda et al.[11,12] used angle-resolved photoemission spectroscopy to determine a surface density of states for one and two layers of Co deposited on a clean, well-ordered Cu(111) surface. Observations at the surface Brillouin-zone center produced several large peaks, one of which is near the Fermi energy and thus not normally associated with the Cu density of states (DOS). The similarity between this peak and a bulk Do DOS, interpreted as ferromagnetic by Himpsel and Eastman,[13] suggested to them that Co is magnetic with an exchange splitting of 0.7 eV at the $\overline{\Gamma}$ point of the surface Brillouin zone. The system was also examined theoretically[10] with the use of a tight-binding Hamiltonian with a rigid exchange band approximation. The magnetization was constrained to equal the bulk Co magnetization, and local charge neutrality was required. The resultant low exchange splitting (0.7 eV) produced a cobalt DOS with three peaks near the Fermi energy, superposed on a normal Cu background. Several very weak structures near the main experimental Co peak are interpreted as support for the ferromagnetism of this system.

Several related systems have also been examined. Mössbauer spectroscopy shows that two and four layers of Co are magnetic when epitaxially grown on Cu(111)

surfaces.[14] Both theoretical and experimental investigations[10] provide evidence for the ferromagnetism of a Co overlayer on a Cu(100) surface, but this time accompanied by a c(2x2) reconstruction. This is interpreted as being caused by ferromagnetically induced charge-density waves.

In this paper we present results of calculations for the magnetic and electronic properties of thin (one- and two-layer) Co films deposited on the Cu(111) surface. We use the calculational scheme described in Chapter III. The one-atom hexagonal unit surface cell is shown in Fig. 1(a). A single unsupported Co monolayer would have symmetry C_{6v}; however, the presence of the Cu substrate reduces the symmetry to C_{3v}. The hexagonal Brillouin zone with its irreducible $\left(\frac{1}{6}\right)$ wedge is shown in Fig. 1(b). Table 1 lists the character table for the group C_{3v}.

A two-atom rectangular unit surface cell is also shown in Fig. 1(a). This cell permits possible breaking of spatial symmetry such as antiferromagnetism, ferrimagnetism, etc. The presence of two unlike atoms leaves only the symmetry of a single vertical reflection plane. The corresponding rectangular Brillouin zone is half the size of the one-atom hexagonal Brillouin zone [Fig. 1(b)]. Note that it divides into only two irreducible (rectangular) parts.

The search for a self-consistent solution was begun at a variety of starting points and thus a large portion of variational parameter space has been mapped. Nevertheless,

it is entirely possible that, within our ten-dimensional space (five d orbitals, two spin polarizations per atom), we may have missed one or more self-consistent solutions. It is unlikely, however, that the lowest-energy state would be missed by our procedure.

B. Results

In this section we discuss the results of our calculation and compare them with the photoemission experiment of Miranda and co-workers.[10-12] Section 1 discusses our preliminary calculation of the clean Cu(111) surface. Other sections consider the combined Co-on-Cu system employing a one-atom (Sec. 2) and two-atom (Sec. 3) unit surface cell.

(1) Clean Cu(111) Surface

As an aid to the interpretation of the Co-on-Cu(111) experiments, Miranda and co-workers[10,12] first examined the angle-resolved density of states for a clean Cu(111) surface. Of special interest is the off-normal measurement made at the $\bar{K}$ point in which a sharp narrow peak was observed at 0.16 Ry below the Fermi energy. Seeking to understand the nature of this unusual peak before attempting the more complicated Co-on-Cu system, we performed a preliminary calculation for the Cu(111) surface. We compared our results for the total DOS with the calculation of Appelbaum and Hamann[15] and found the maximum disagreement on peak location to be 0.02 Ry. This can be taken as some indication of our accuracy with respect to surface effects.

Figure 2 shows the layer-projected angle-resolved DOS at the $\bar{K}$ point. The symmetry at this point is the same as for the whole surface (C_{3V}), which permits the continued use of the familiar $\Lambda_1, \Lambda_2, \Lambda_3$ labels. The normal selection rule for s-polarized light, i.e., only states of symmetry Λ_3 measured, fails here because the final state is at an angle from the surface normal and thus does not have C_{3V} symmetry. We find that a bulklike peak of symmetry Λ_1 falls very near the experimental peak location, while no other peak is within the error bars stated earlier. Thus the peak is clearly identified and comparisons can be made with the Co-Cu system.

(2) Co-on-Cu(111): One-Atom Surface Cell

Bulk Co is believed[16] to possess a spin polarization of 1.56. The effect of the free surface is to make the surface Co more like a free atom and hence substantially raise the spin polarization. On the other hand, the coupling of the Co atoms to the Cu substrate may be expected to produce a large decrease in the polarization. Our calculations show that for one layer Co on the Cu(111) surface, the spin polarization of the Co atom equals 1.63. However, our approximation (3) may exaggerate this polarization by approximately 0.1 which suggests that the actual spin polarization is essentially unchanged from the bulk. This is in interesting contrast to the case of Ni on the Cu(111) surface in which the Ni magnetization is greatly suppressed. Of course, there is no contradiction present since previous

calculations[6] have shown that small changes in substrate orientation or material composition can produce large effects. This is attributable to the delicate balance between two competing effects: enhancement by the surface and suppression by the substrate hybridization.

The d orbitals of the Co layer can be classified uniquely by specifying their bulk and surface symmetries. This facilitates detailed examination of the distribution of magnetization among orbitals (Table II). One notes that the orbital of symmetry Λ_1 has significantly less spin polarization and exchange splitting than the orbitals of symmetry Λ_3. This is presumably due to its geometric orientation perpendicular to the (111) plane, which means that it points directly into the Cu substrate. In addition, its symmetry is the same as most of the Cu sp electrons, which facilitates hybridization. One interesting conclusion to be drawn from Table II is that rigid-band exchange splitting is only approximately obeyed in this Co-on-Cu(111) system. This contrasts to the bulk system, where our calculations found only negligible (less than 1%) exchange-splitting difference between orbitals.

We also performed our calculations for two layers of Co-on-Cu(111). The top and second layers have spin polarizations of 1.65 and 1.58, respectively. The spin polarization is distributed much more evenly between orbitals although, relative to the Λ_3 states, the Λ_1 orbital has a slightly enhanced (~0.06) value in the surface layer and a

slightly suppressed (~0.05) value in the second layer. The Cu atoms have negligible spin polarization (~0.01) independent of the number of Co overlayers.

Figure 3 shows the calculated one-electron DOS for one and two layers of Co-on-Cu. As in all angle-integrated DOS plots in this paper, the curves are smoothed with a Lorentzian of halfwidth 0.006 Ry at half maximum. One notes that the majority Co peaks have approximately the same energy as the Cu peaks. This leads to significant distortion of the Cu minority peaks where they hybridize with the Co.

Comparison with the experiment of Miranda and coworkers[10-12] is facilitated by Figs. 4 and 5. The agreement between experiment and theory for the most significant peaks of one layer Co-on-Cu is excellent. At the $\bar{\Gamma}$ point, the three largest peaks coincide to within 0.01 Ry, while at the $\bar{K}$ point the two largest calculated peaks of Λ_1 symmetry match the experimental results to the same accuracy. The reduced contribution of the Λ_3 states also occurred in the clean Cu(111) surface as discussed earlier, and is presumably caused by a small photoemission dipole matrix element.

The results from two layers of Co-on-Cu show much poorer agreement, essentially because our calculation shows the Co minority peaks shifting as the number of Co layers increases from one to two. The experiment shows no such shift. We find the discrepancy difficult to explain.

Calculations of Ni on Cu show considerable differences between one and two layers of the magnetic material on the substrate. However, direct comparison is difficult because the Ni spin polarization is affected in these systems more substantially than the Co magnetization is in ours. In any case, experiment should observe band narrowing in the surface layer as is the case with the clean Cu(111) surface.

Another qualitative difficulty in comparison with the experiment of Miranda and co-workers is their observation of dispersion in the single Co layer as they change the energy of their photons. We, of course, find nondispersive peaks and are puzzled by their result.

(3) Co-on-Cu(111): Two-Atom Surface Cell

Through the employment of the two-atom rectangular unit surface cell discussed previously, we have found three locally stable configurations for the system consisting of one layer of Co-on-Cu(111). The simplest of these is the ferromagnetic arrangement discussed in Sec. 2. In this state both of the atoms in the unit cell possess equal polarizations and are identical in all respects.

We also examine an antiferromagnetic state in which the spin polarizations of the two atoms in the unit cell have equal magnitude (1.51) per atom) but opposite orientation. Those states which possess a positive reflection symmetry are found to have the lowest spin polarization, presumably due to their hybridization with the Cu s states. The total energy of this configuration is found to be

considerably higher (0.15 Ry per surface atom) than that of the ferromagnetic system, which implies that it is not the ground state.

Our third configuration is a new kind of state which we call "spatially modulated." This state possesses an approximately equal polarization of 1.60 on each atom of the unit cell, but it is distributed differently between the orbitals. The first three orbitals, which form the t_{2g} representation in the bulk, have equal polarization on both atoms, but the last two orbitals, the "e_g orbitals," switch the polarization between them as one moves from one atom to the other. This redistribution in space leads to the expression "spatially modulated." It is not to be confused with ferrimagnetic states which possess opposite and unequal spins on the two atoms of the unit cell. The total energy of the spatially modulated state is calculated to be 0.03 Ry per surface atom above the ferromagnetic state. Distinctions of this small magnitude are probably not within the accuracy of our approximations. Consequently, we conclude that either the ferromagnetic or spatially modulated state could be the ground state.

Figure 6 illustrates the spatial distribution of magnetization. The plots were calculated by multiplying the spin polarization by the correct spherical harmonic and an atomic radial function. Most trivially, the figures exhibit the C_{3v} symmetry of the ferromagnetic configuration (one reflection line is vertical, the other two at 120° to

it) and the single vertical reflection line of the other two configurations. The wavelike modulation of the spin polarization in the antiferromagnetic case is also clearly visible. More interesting is the asymmetric accumulation of magnetization density above the middle Co atom in the spatially modulated state, leading to the concept of a small wave of periodicity equal to two atoms, superposed on a more constant background.

Figures 7 and 8 show the total DOS for the two-atom configurations. An interesting point is that, although the spatial distribution of magnetization is quite different between the ferromagnetic and spatially modulated states, the total DOS for both spatially modulated atoms and the ferromagnetic atom are remarkably similar. Figure 9 shows the angle-resolved DOS at the $\bar{\Gamma}$ point for the spatially modulated state. Note that the symmetry breaking produces additional small peaks which may be difficult to resolve experimentally.

C. Conclusions

One and two layers of Co on a Cu(111) surface are magnetized with a spin polarization essentially equal to the bulk value. The rigid-band model is only approximately obeyed. The ferromagnetic state has the lowest total energy, but, within our margin of error, a spatially modulated state could be the ground state instead. The ferromagnetic, spatially modulated, and antiferromagnetic states all have approximately equal spin polarizations.

Agreement between our theory and the experiment of Miranda and co-workers is considerable, but discrepancies do exist. The quantitative correspondence between theoretical and experimental peak locations for one layer Co-on-Cu is excellent. The photoemission spectra at the $\overline{K}$ point for both this system and for the clean Cu(111) surface can be consistently explained by theoretical states which transform according to Λ_1, the identity representation. More disappointing is the experimentally observed absence of the theoretically predicted shift in peak locations as an additional layer of Co is added. The experimentally observed displacement in Co peak location with photon energy is also puzzling, since monolayer states can have no dispersion.

Analysis of our results suggests some additional points of interest: (a) The closeness in energy between two considerably different states--ferromagnetic and spatially modulated states--indicates the presence of low-energy excitations and the likelihood of easily accessible phase transitions in the magnetic configuration of the monolayer; (b) the quantitative values of the magnetic moment in the various phases--ferromagnetic, antiferromagnetic, and spatially modulated--indicated that Co monolayers, which are itinerant magnetic systems, should behave in all respects as fairly weakly coupled localized moments of almost constant value; (c) as a consequence of (a) and (b) a fairly low Curie temperature should be expected for these systems,

but there also should be persistence of the localized magnetic moment in the paramagnetic high-temperature phase.

Finally, in order to improve the comparison between our theory and photoemission experimental data, it is necessary to include in the theory the several proposed many-body effects[17-20] (relaxation, exciton formation, Hund rules, Auger processes) inherent in the photoemission process of highly correlated transition-metal atoms. These effects lead to band narrowing, resonant photoemission, and formation of tails and satellites.

References

1. C. Rau, Comments Solid State Phys. 9, 177 (1980).

2. D.T. Pierce and H.C. Siegmann, Phys. Rev. B 9, 4035 (1974).

3. G. Bergmann, Phys. Rev. Lett. 41, 264 (1978); Phys. Today 32 (8), 25 (1979).

4. R. Merservey, P.M. Tedrow, and V.R. Kalvey, Solid State Commun. 36, 969 (1980).

5. D.S. Wang, A.J. Freeman, and H. Krakauer, Phys. Rev. B 26, 1340 (1982).

6. J. Tersoff and L.M. Falicov, Phys. Rev. B 26, 6186 (1982).

7. C.S. Wang and A.J. Freeman, Phys. Rev. B 21, 4585 (1980).

8. C. Rau and S. Eichner, Phys. Rev. Lett. 47, 939 (1981).

9. J. Noffke and L. Fritsche, J. Phys. C 14, 89 (1981).

10. L. González, R. Miranda, M. Salmerón, J.A. Vergés, and F. Ynduráin, Phys. Rev. B 24, 3245 (1981).

11. R. Miranda, F. Ynduráin, D. Chandesris, J. Lecante, and Y. Petroff, Phys. Rev. B 25, 527 (1982).

12. R. Miranda, F. Ynduráin, D. Chandesris, J. Lecante, and Y. Petroff, Surf. Sci. 117, 319 (1982).

13. F.J. Himpsel and D.E. Eastman, Phys. Rev. B 21, 3207 (1980).

14. U. Gradmann, K. Ullrich, J. Pebler, and K. Schmidt, J. Magn. Magn. Mater. 5, 339 (1977).

15. J.A. Appelbaum and D.R. Hamann, Solid State Commun. 27, 881 (1978).

16. F. Batallan, I. Rosenman, and C.B. Summers, Phys. Rev. B 11, 545 (1975). The measured bulk magnetization of $1.72\mu_B$ is believed to reflect a spin imbalance of

$$n\uparrow - n\downarrow = 1.56 \text{ electrons per atom}$$

with a g factor of approximately 2.2.

17. D.A. Shirley, in Photoemission in Solids: I General Principles, edited by M. Cardona and L. Ley (Springer, Berlin 1978), p. 165.

18. L.A. Feldkamp and L.C. Davis, Phys. Rev. Lett. 43, 151 (1979).

19. L.C. Davis and L.A. Feldkamp, Solid State Commun. 34, 141 (1980).

20. A. Liebsch, Phys. Rev. Lett. 43, 1431 (1979); Phys. Rev. B 23, 5203 (1981).

TABLE I. Character table for point group C_{3v}.

	E	$2C_3$	$3\sigma_v$
Λ_1	1	1	1
Λ_2	1	1	-1
Λ_3	2	-1	0

TABLE II. Spin polarization and splitting by orbital for one layer Co on Cu(111).

Bulk Symmetry	t_{2g}		e_g
Degeneracy	3		2
Surface Symmetry	Λ_1	Λ_3	Λ_3
Degeneracy	1	2	2
Radial Wavefunction	xy+yz+zx	2xy-yz-zx; yz-zx .	$2z^2-x^2-y^2$; x^2-y^2 .
Spin Polarization	0.14	0.36	0.41
Splitting at Zone Center*	0.210Ry	0.246Ry	0.234Ry

*Mixing occurs between all Λ_3 states and between the d-orbital of symmetry Λ_1 and the sp orbitals. Those peaks which contain the most contribution from a particular column are used to generate the splitting value.

FIGURE CAPTIONS

Figure 1 (a) The one- and two-atom surface unit cells used in the calculations. Open and full circles represent the Co surface-layer atoms. Crossed circles are the Cu atoms in the adjacent layer. Dashed lines denote reflection planes. (b) Surface Brillouin Zones for the unit cells of (a). Symmetry points are indicated. The hatching shows the irreducible parts of the rectangular and hexagonal cells.

Figure 2 Projected density of states for an ideal Cu(111) surface at the $\bar{K}$ point of the surface Brillouin Zone. (a) Surface layer; (b) second layer; (c) third layer (not selfconsistent). Curves include a Lorentzian broadening of halfwidth 0.022Ry at half maximum. The peaks are labeled according to symmetry.

Figure 3 Projected total density of states for the ferromagnetic state of a one- and two-atom Co layer on Cu(111). (a1) Co monolayer: Co projection. (a2) Co monolayer: Cu interface-layer projection. (b1) Co di-layer: Co surface-layer projection. (b2) Co di-layer: Co interface-layer projection. (b3) Co di-layer: Cu interface-layer projection. Full lines are minority states; dashed lines are majority states.

Figure 4 Projected density of states at the $\bar{\Gamma}$ point for the ferromagnetic state of a one- and two-atom Co layer on

Cu(111). (a1) Co monolayer: Co projection. (a2) Co monolayer: Cu interface-layer projection. (b1) Co di-layer: Co surface-layer projection. (b2) Co di-layer: Co interface-layer projection. (b3) Co di-layer: Cu interface-layer projection. Full lines are minority states; dashed lines are majority states. Curves include a Lorentzian broadening of halfwidth 0.022Ry at half maximum. The peaks are labeled according to symmetry. Some Λ_1 peaks are greatly obscured by the much larger Λ_3 peaks.

Figure 5 Projected density of states at the $\overline{K}$ point for the ferromagnetic state of a one- and two-atom Co layer on Cu(111). See description of Fig. 4.

Figure 6 Real-space magnetization density of a Co monolayer on Cu(111): the Co surface layer for (a) ferromagnetic state; (b) spatially modulated state; (c) antiferromagnetic state. Spin-up density contours are plotted in full lines; spin-down density contours in dashed lines. All graphs are projections on the Co(111) plane of the magnetization of the "vacuum" half-space.

Figure 7 Projected total density of states for the antiferromagnetic state of a Co monolayer on Cu(111) in the double

cell of Fig. 1. The projection is on one of the Co atoms at the surface. (The other atom is identical if spin-up and spin-down labels are interchanged.)

Figure 8 Projected total density of states for the spatially modulated state of a Co monolayer on Cu(111) in the double cell of Fig. 1. (a) Projection on one of the Co atoms. (b) Projection on the other Co atom.

Figure 9 Projected density of states at the $\bar{\Gamma}$ point of the surface Brillouin Zone for the spatially modulated state of a Co monolayer on Cu(111) in the double cell of Fig. 1. (a) and (b) Projections on the two Co atoms. (c) and (d) Projections on the two interface Cu atoms. Curves include a Lorentzian broadening of halfwidth 0.022Ry at half maximum.

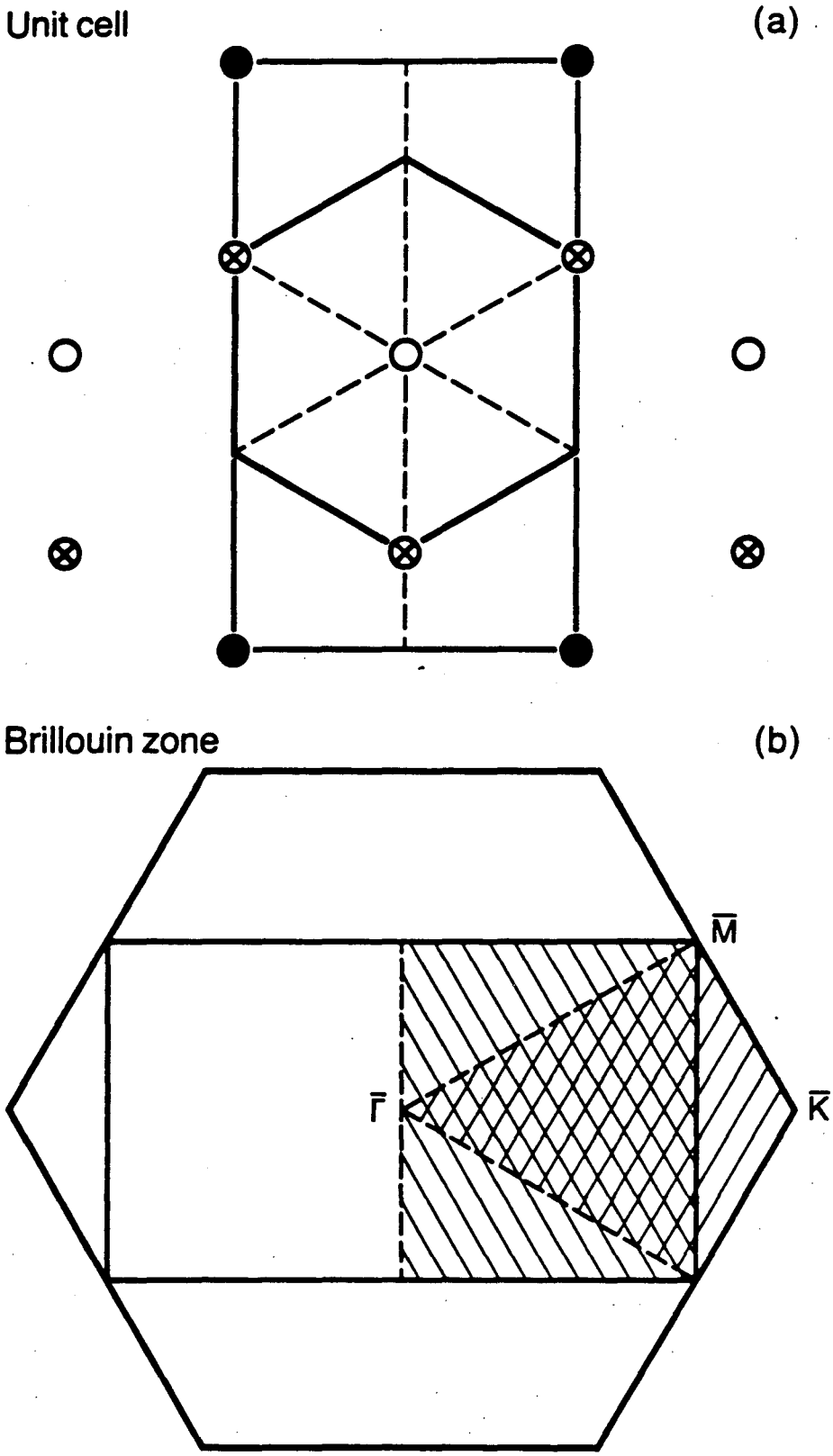

Figure 1

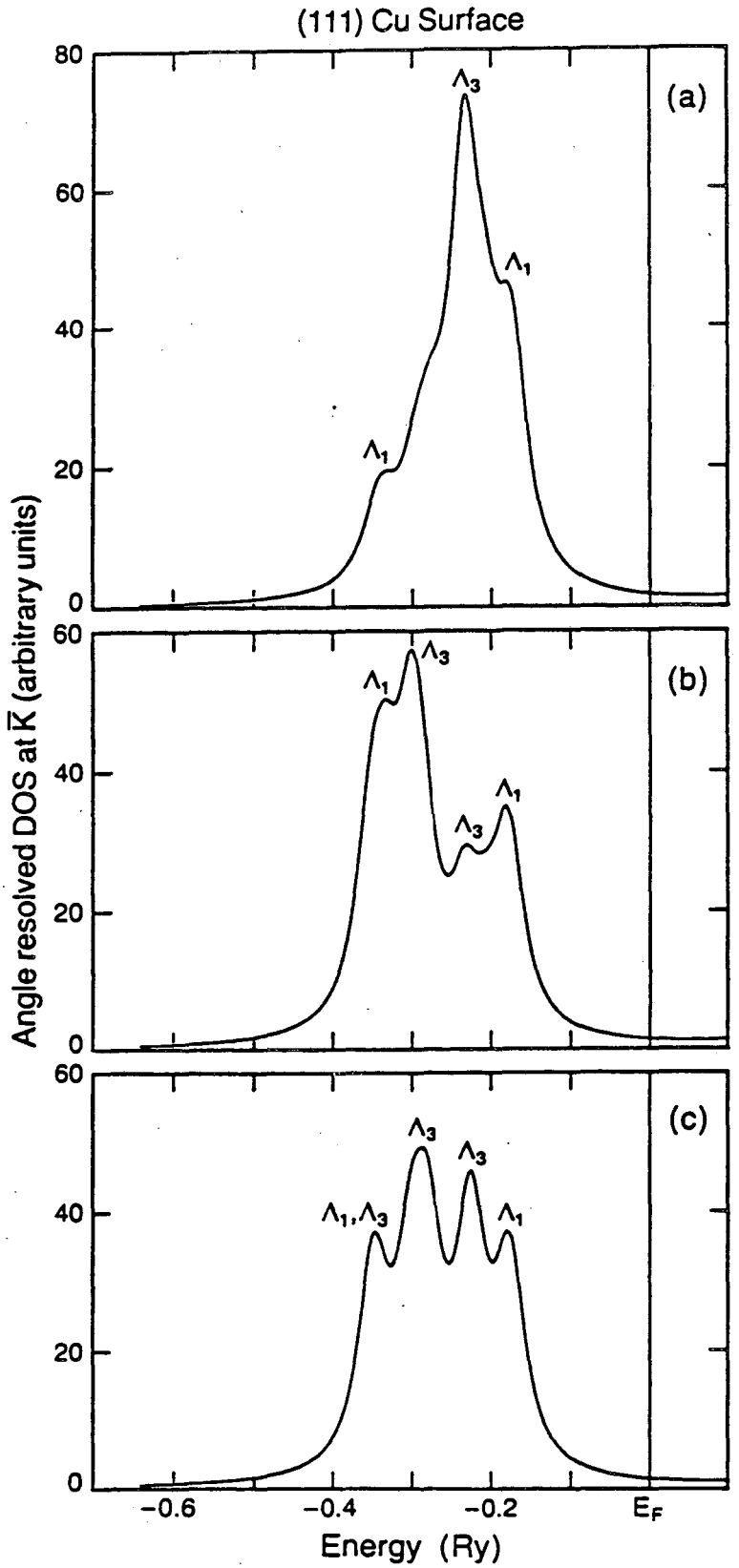
(111) Cu Surface
Angle resolved DOS at $\bar{K}$ (arbitrary units)
(a)
(b)
(c)
Λ_3
Λ_1
Λ_1,Λ_3
80
60
40
20
0
−0.6
−0.4
−0.2
E_F
Energy (Ry)

Figure 2

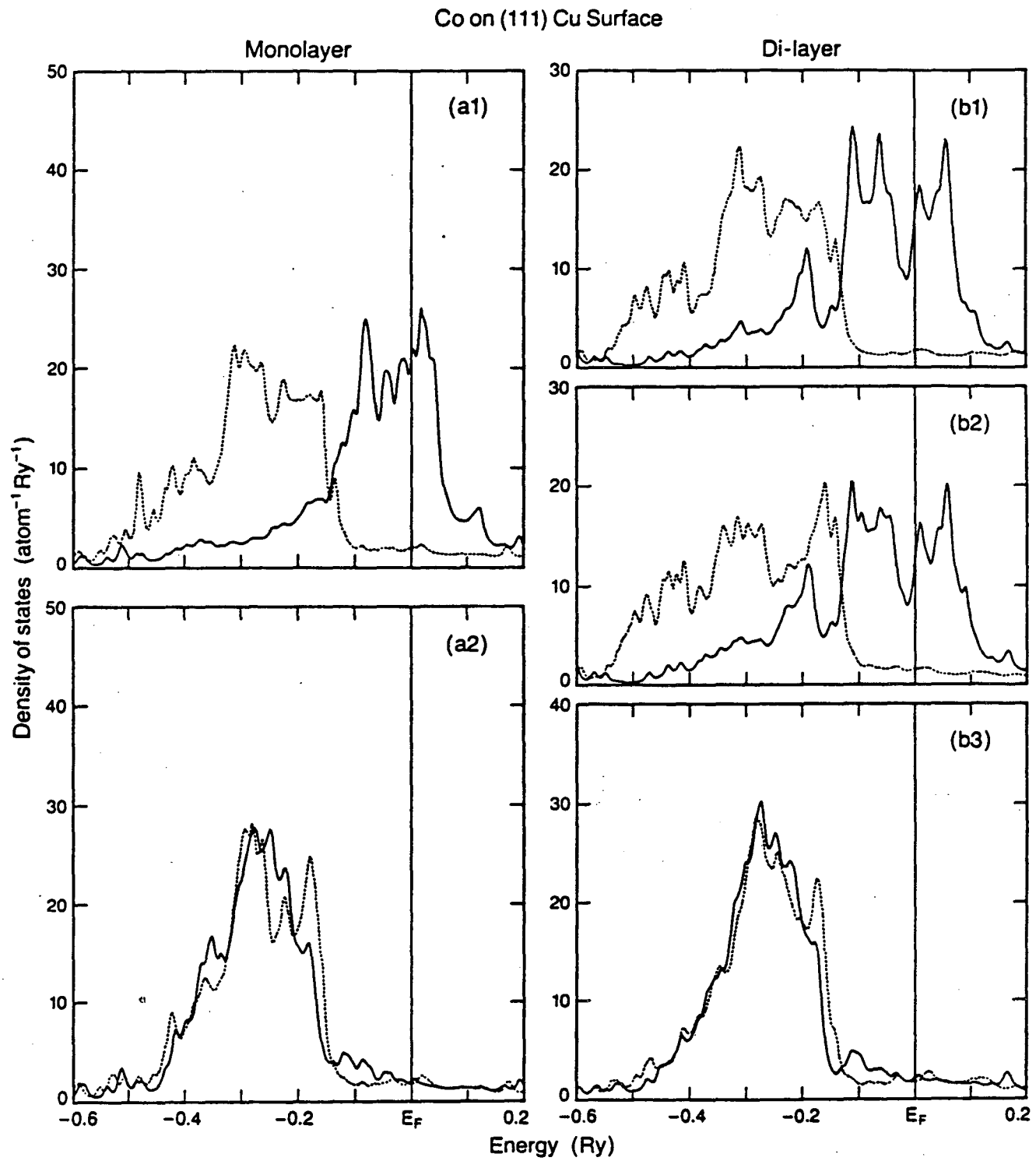
Co on (111) Cu Surface
Monolayer
Di-layer
(a1)
(a2)
(b1)
(b2)
(b3)
Density of states (atom⁻¹ Ry⁻¹)
Energy (Ry)
E_F
-0.6
-0.4
-0.2
0.2

Figure 3

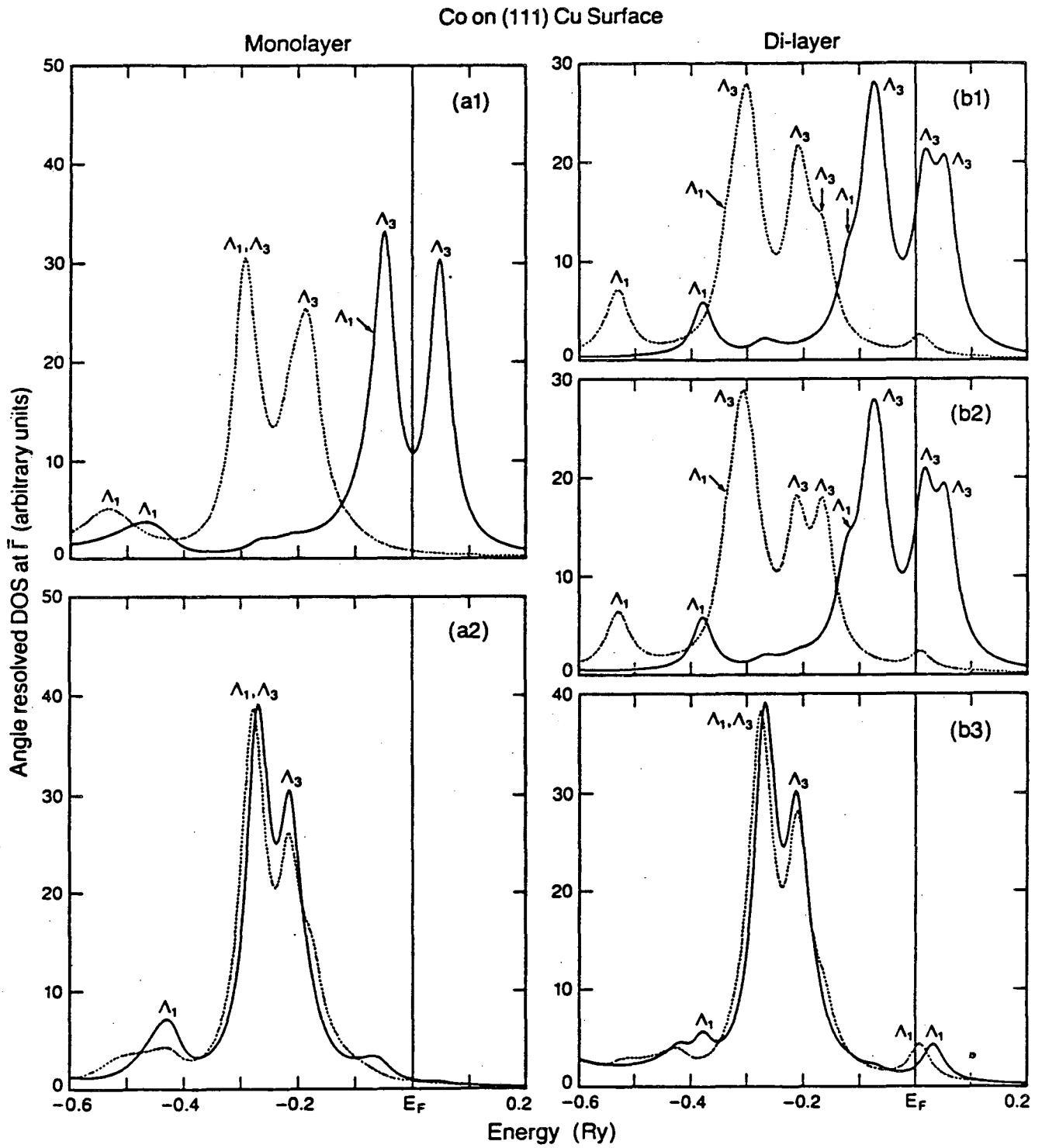
Co on (111) Cu Surface
Monolayer
Di-layer
(a1)
(a2)
(b1)
(b2)
(b3)
Angle resolved DOS at $\bar{\Gamma}$ (arbitrary units)
Energy (Ry)
E_F
Λ_1
Λ_3
Λ_1,Λ_3

Figure 4

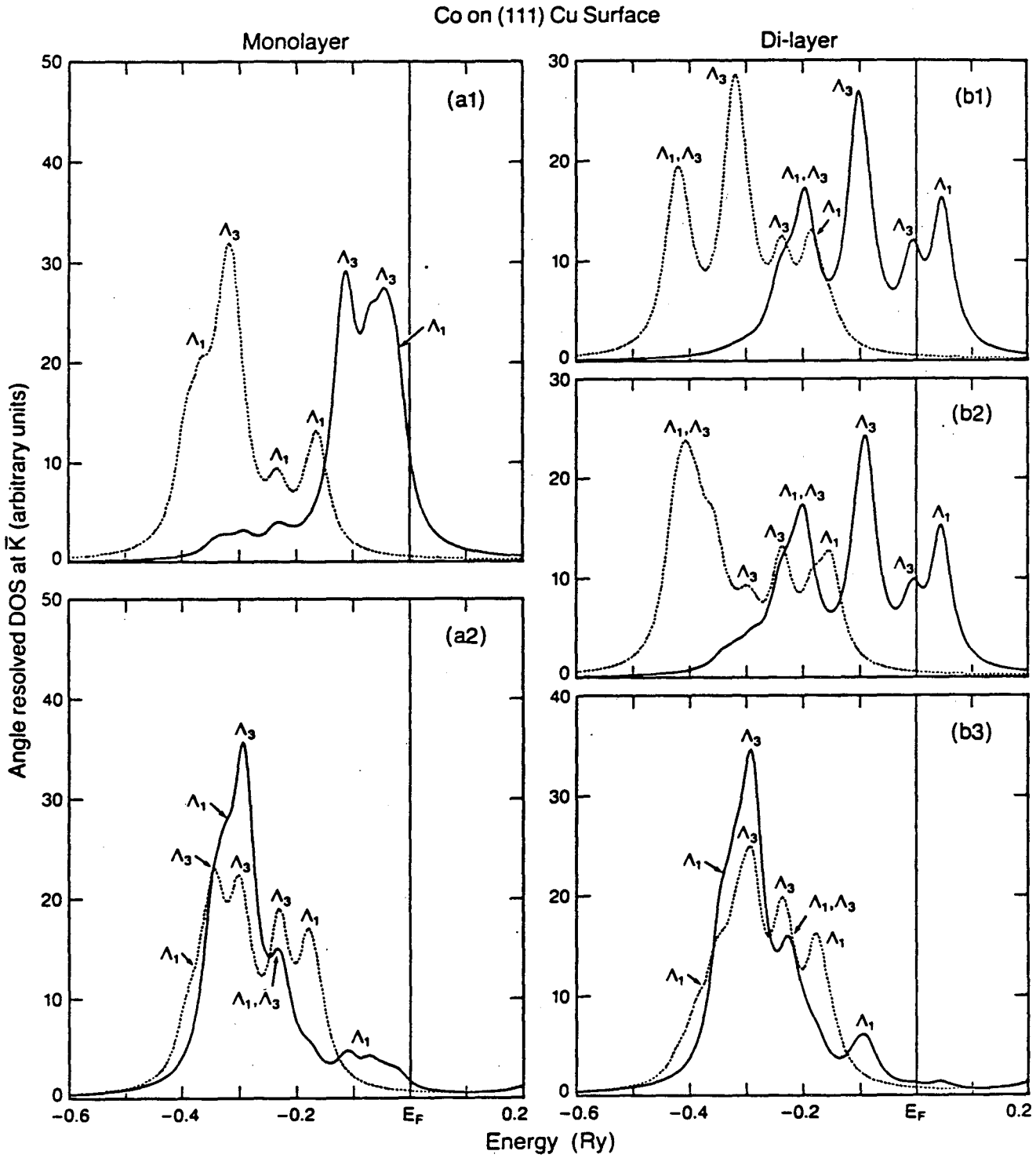
Co on (111) Cu Surface
Monolayer
Di-layer
(a1)
(a2)
(b1)
(b2)
(b3)
Angle resolved DOS at K̄ (arbitrary units)
Energy (Ry)
E_F
Λ1
Λ3
Λ1,Λ3

Figure 5

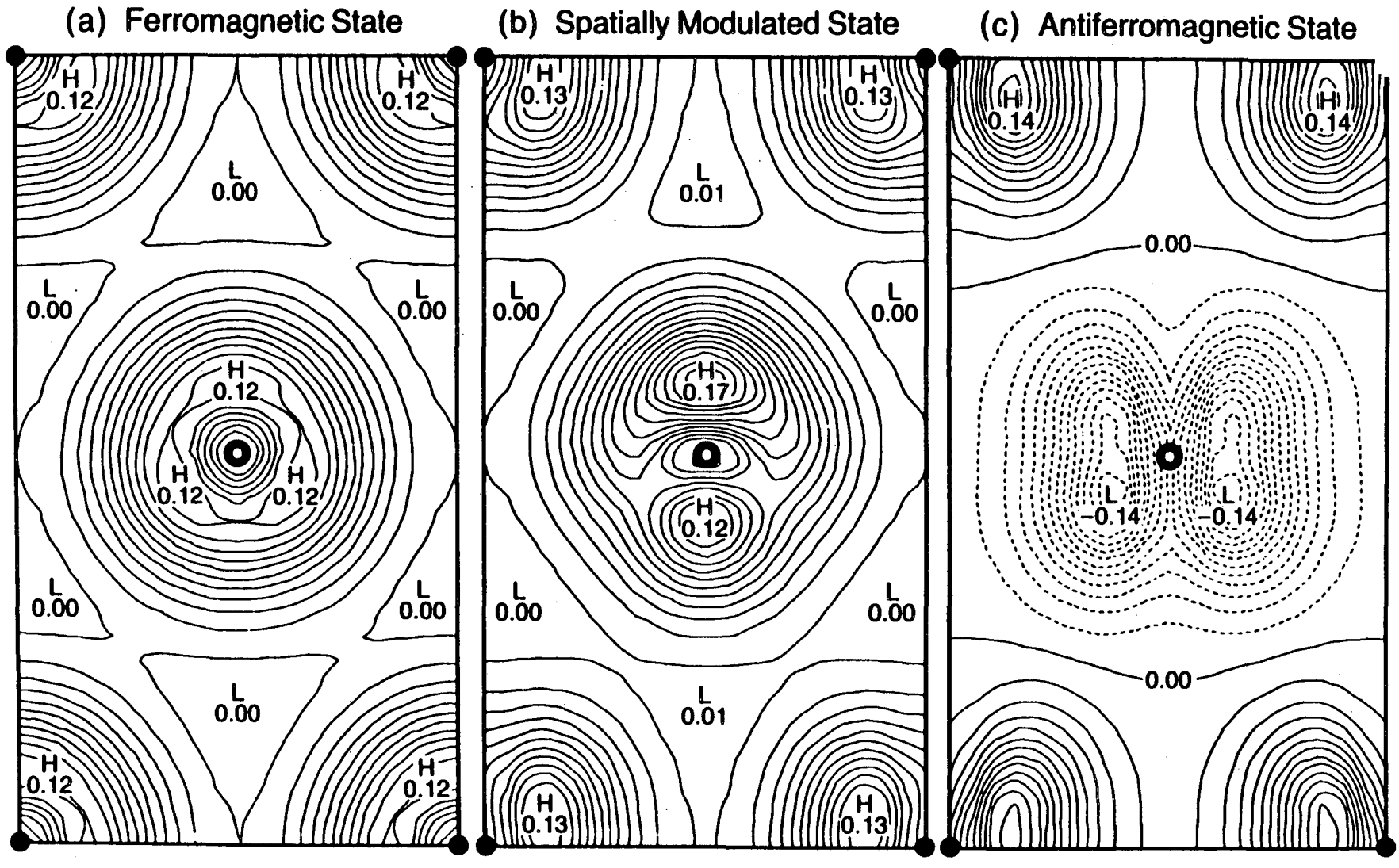
(a) Ferromagnetic State
(b) Spatially Modulated State
(c) Antiferromagnetic State
H 0.12
L 0.00
H 0.13
L 0.01
H 0.17
H 0.14
L −0.14
0.00

Figure 6

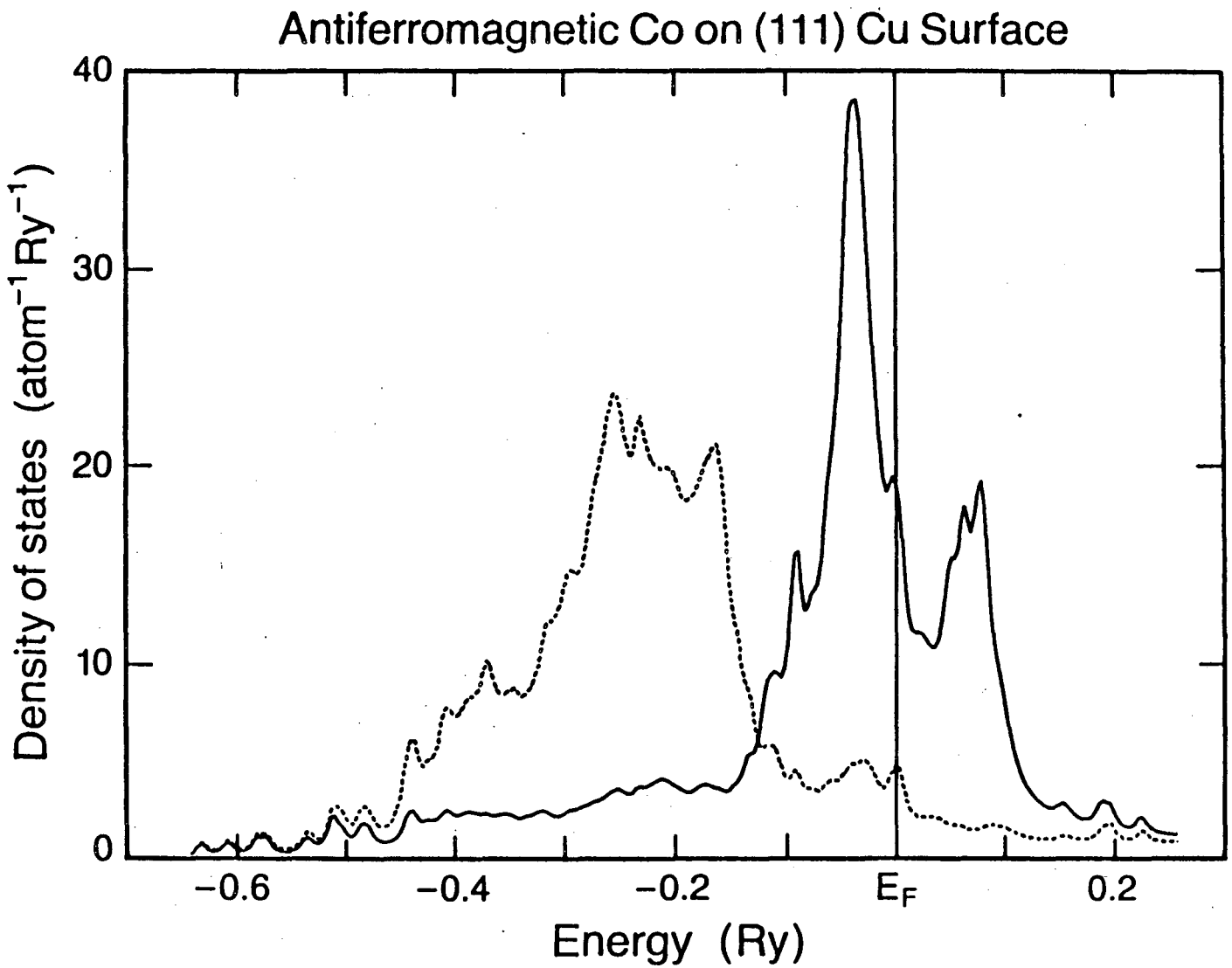
Antiferromagnetic Co on (111) Cu Surface
Density of states (atom^{-1}Ry^{-1})
40
30
20
10
0
−0.6
−0.4
−0.2
E_F
0.2
Energy (Ry)

Figure 7

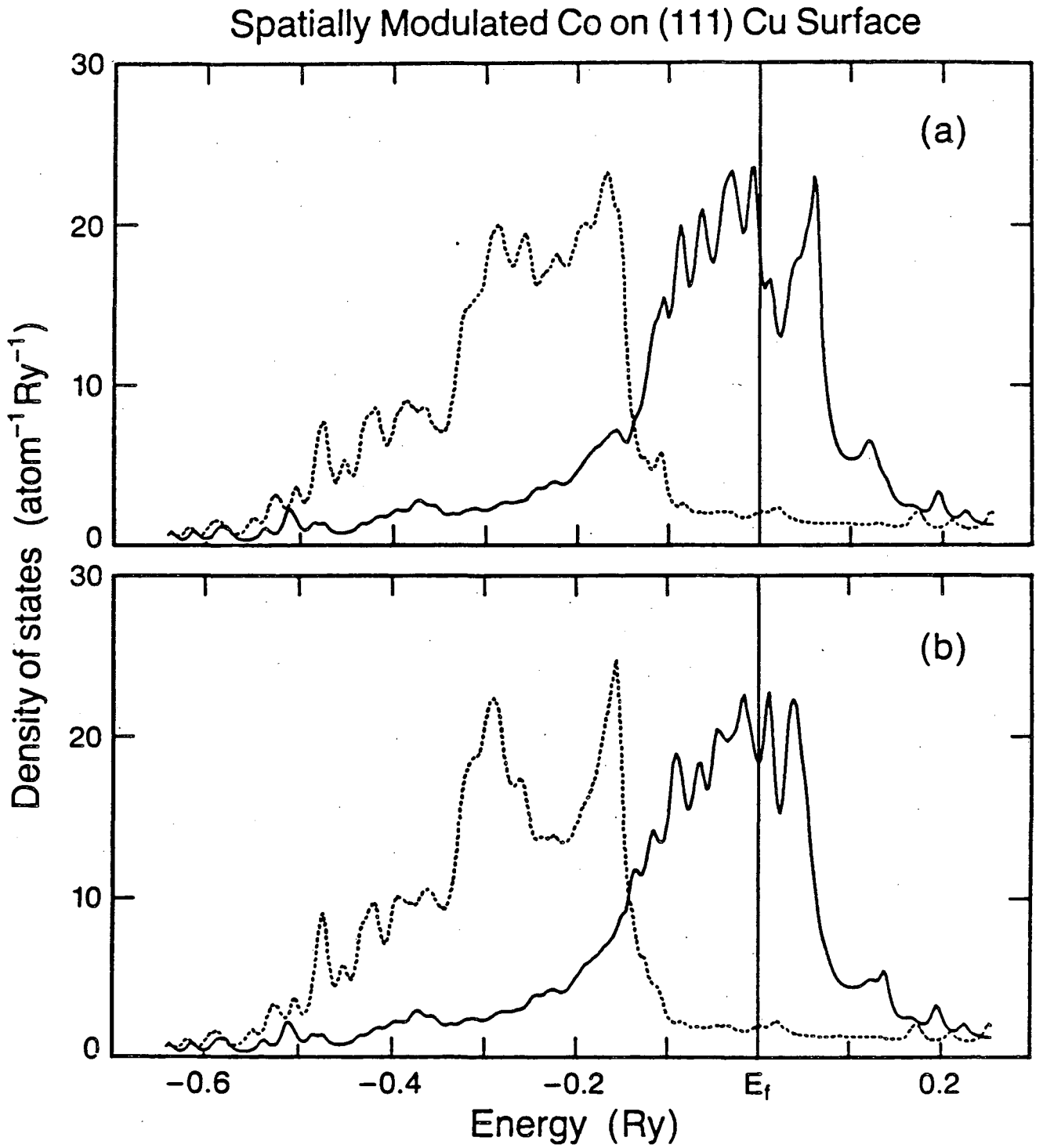
Spatially Modulated Co on (111) Cu Surface
(a)
(b)
Density of states (atom^{-1} Ry^{-1})
30
20
10
0
30
20
10
0
−0.6
−0.4
−0.2
E_f
0.2
Energy (Ry)

Figure 8

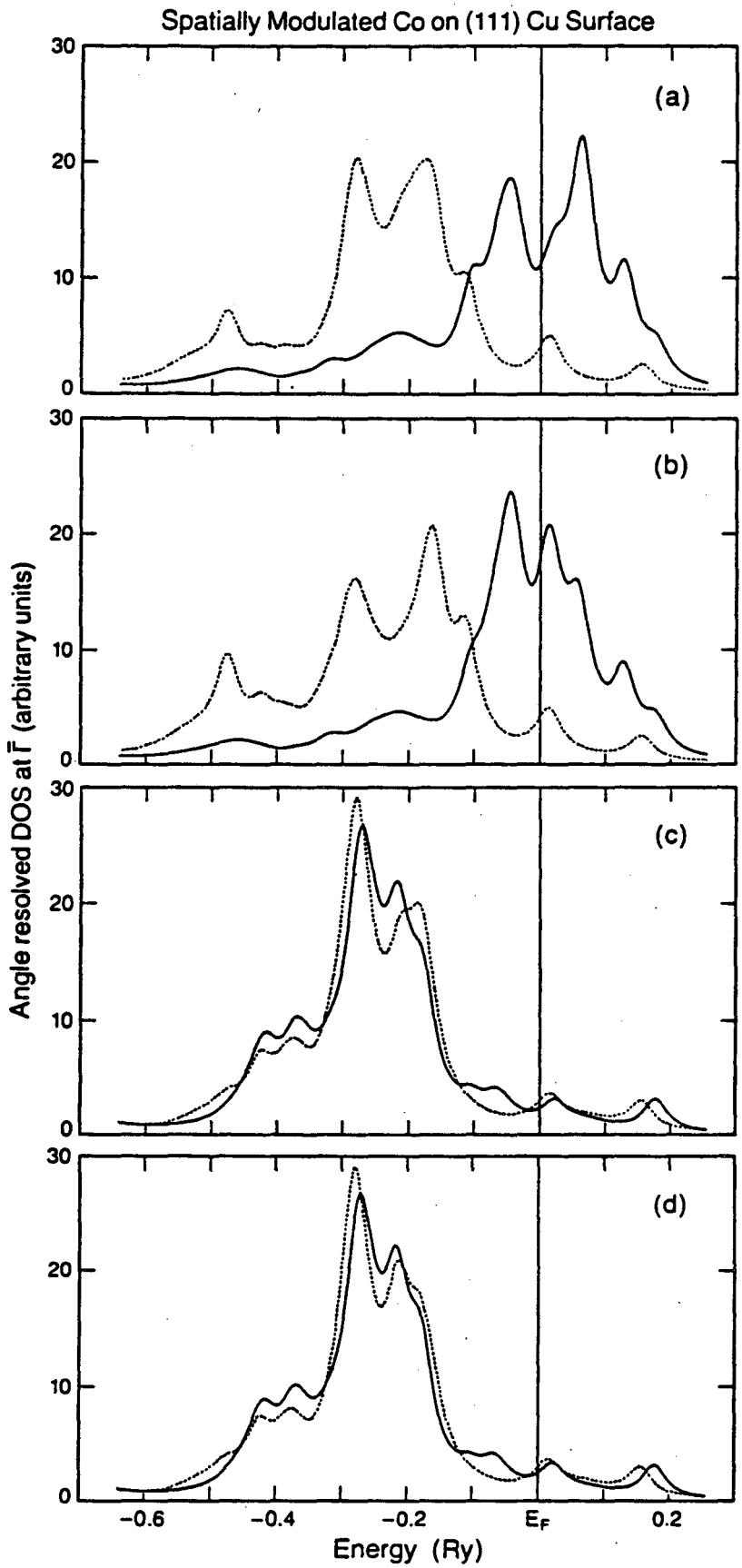
Spatially Modulated Co on (111) Cu Surface
(a)
(b)
(c)
(d)
Angle resolved DOS at $\bar{\Gamma}$ (arbitrary units)
30
20
10
0
−0.6
−0.4
−0.2
E_F
0.2
Energy (Ry)

Figure 9

V. MAGNETIZATION OF IRON-COBALT DISORDERED ALLOYS

A. Introduction

One of the most famous plots in the solid-state literature is the Slater-Pauling curve.[1] This plot displays magnetization versus the electron-to-atom ratio for a large variety of chemically disordered transition-metal alloys. One of the most interesting features of the curve is the abrupt change in its slope as it passes through its maximum at approximately 26.3 electrons per atom. Several explanations have been proposed for this feature. Pauling[2] argued that the number of unbalanced *d* holes could not exceed approximately 2.4 because the other 2.6 *d* electrons of each spin belong to a lower band which cannot lose electrons until the upper one is completely emptied. A somewhat different point of view is provided by Williams *et al.*[3] who argued that the only two relevant features are magnetic saturation, which occurs on the Co side of the maximum, and ferromagnetic weakness, which occurs on the Fe side of the maximum. It is noted[4] that this ferromagnetic weakness coincides with the pinning of the Fermi level at a valley in the minority-spin density of states. Finally, one might expect that band narrowing and other complicated band-structure effects, such as those which occur in Ni-Cu alloys,[5] may be causing the maximum.

The uppermost and sharpest maximum on the Slater-Pauling curves is formed by the Fe-Co alloy system. Consequently, one expects that a complete understanding of

this alloy would lead to the correct explanation for the Slater-Pauling maxima. Several experimental and theoretical studies have been performed for Fe-Co. Early experimental measurements of the saturation magnetization were made by Weiss and Forrer.[6] Later, after the discovery of an ordered structure near the equiatomic alloy, Bardos[7] remeasured the disordered substance. It is also known[8] that Fe-Co undergoes structural phase transitions with a change in concentration: Iron-cobalt is bcc for 25% or more iron; it is fcc or hcp for less than 10% iron, and there is a mixed phase in between. Meyer and Asch[9] determined the g factors for the Fe-Co alloys, thus allowing a comparison of the experimentally measured magnetization with the theoretically predicted spin polarization. Neutron-diffraction[10] studies indicate that the vast majority of the anomalous increase in the magnetic moment is due to an increase in the Fe magnetic moment from $2.2\mu_\beta$ to approximately $3.0\mu_\beta$, while the Co magnetic moment remains approximately constant at $1.8\mu_\beta$.

Theoretical results are less numerous. Kaspar and Salahub[11] used the spin-polarized, self-consistent field, $X\alpha$ scattered-wave method to calculate the magnetic and electronic properties of 15-atom Fe-Co clusters. Unfortunately, results of these authors for the spin polarization differed considerably from experimental bulk values, possibly because Fe "feels" the effect of surfaces quite strongly.[12] Schwarz and Salahub[13] used local-spin-density

theory to calculate the properties of the ordered FeCo alloy with fair success: Calculated spin polarization is 4.36 per unit cell versus 4.50±0.02 experimentally. This calculation demonstrates the correct qualitative behavior, i.e., a large anomalous increase in the alloy magnetization relative to the average of the two elements in their pure bulk form. Desjonquères and Lavagna[14] discuss the differences between the ordered and disordered FeCo alloy: However, their magnetization results appear to contradict experiment.[7]

In this chapter we present results of calculations for the magnetic properties of disordered Fe-Co alloys in both the fcc and bcc structures. We use the calculational method described in Chapter III. Disorder is introduced by the use of the virtual-crystal approximation, in which the Hamiltonian of the two constituent elements is averaged to produce a single alloy element. We expect this approximation to be accurate for our particular system because Fe and Co are very similar elements. They are adjacent on the Periodic Table, and their d-band widths are identical[15] to within 15%. Furthermore, their large density of states at the Fermi level means that the one-electron difference between them does not offset their d bands to a very large extent. It is known experimentally that there is only a very small[16] magneto-volume effect (0.25%) and, therefore, the averaging of the lattice constants as required by the virtual-crystal approximation should produce only the

slightest of errors. Consequently, it is expected that the combination of our standard Hamiltonian with the virtual crystal approximation will produce accurate results.

B. Results

Calculated results for the spin polarization of the disordered Fe-Co alloy are shown in Fig. 1. Also plotted are the experimental spin polarizations obtained from magnetization and g factors. The agreement is excellent with a standard-deviation difference of less than 0.02 electrons. This difference is within the experimental error (1%) found in determining the g factors. Our ability to reproduce accurately this anomalous curve strongly suggests that our calculation includes all of the important physical processes and thus we should be able to understand the physical reasons which cause this unusual shape.

First, one notes that band narrowing, band mismatches, and other band-structure effects of heterogeneous systems cannot be responsible for the shape of the curve because the virtual-crystal approximation does not include them, and yet it reproduces the correct magnetization.

Figure 2 provides an explanation for the curve by plotting the Fe-Co results versus an imaginary "element" described by the Co Hamiltonian, but with a decreasing number of electrons as one approaches the Fe side of the plot. This imaginary element differs from the Fe-Co alloy in that it possesses a much stronger electron-electron interaction than that associated with iron.[17] The plot

demonstrates that the effect of this strong interaction is to raise drastically the Fe magnetization and remove the intermediate maximum. On the other hand, it causes little change on the Co side of the curve, suggesting that in this range saturation has been reached, i.e., all possible d holes are already magnetized. A reasonable conclusion is that the anomalous Fe-Co curve is dominated by magnetic saturation except in those regions of low Co content where an electron-electron interaction insufficient to cause saturation is more important.

Figure 2 also demonstrates that Pauling's explanation of the Fe-Co curve is not to be taken literally. Although we do find that for concentrations of Fe greater than 80%, the Fermi level lies in a minority-spin density-of-states valley as Pauling's argument predicts, it is clear from Fig. 2 that if the electron-electron interaction to band-width ratio had not decreased as the Fe concentration increased, then the Fermi level would have been at its normal strong ferromagnetic position above all of the majority states and hence would have arbitrarily cut the minority density of states. This can be restated in the language of Pauling by noting that the spin polarization at the Fe end of the curve, 2.65, requires an emptying of 2.4 "upper-band" states and 0.25 "lower-band" states. In conclusion, it is clear that a decreasing electron-electron interaction to bandwidth ratio is at least as important as any band-splitting effects.

Finally, one notes that Fig. 2 displays a prediction for the spin polarization of bcc Co. This phase of cobalt has been experimentally constructed by Walmsley *et al.*[18,19] They find a magnetization equal to normal hcp cobalt with 10% error bars. Thus, our value for the spin polarization, 1.80, when combined with a g factor of 2.10, would be within the error bars of Walmsley *et al*. However, these authors find their bcc Co to have a much smaller lattice constant than one would expect from either extrapolating the Fe-Co lattice-constant curve or multiplying local-density minimal-energy results by a factor accounting for the usual underestimation of magnetic transition-metal lattice constants. This reduced lattice constant can be expected to increase the bandwidth and thus decrease the magnetization. Thus our calculation almost surely overestimates the spin polarization of the bcc Co found by Walmsley *et al*.

C. Conclusions

We have calculated the spin polarization of the disordered Fe-Co alloy using a model which depends solely on the elemental properties. Agreement with the experimental curve is excellent and its anomalous behavior is fully reproduced. In the Co-rich region, the Fermi level lies above the majority density of states and the magnetization essentially depends on the number of available *d* holes. In the Fe-rich region, a relatively weak electron-electron interaction allows the Fermi level to lie in a valley

separating the minority bcc density of states into an upper and lower band. The intersection of this weakly ferromagnetic region with the saturated region of the Co-rich alloys produces a maximum in the magnetization at approximately 30 at. % Co.

It is likely that our conclusions for the Fe-Co system have application to many other transition-metal alloys. For example, Fe-Ni demonstrates the same sort of maximum at approximately 10 at. % Ni. Other alloys such as Ni-Cr, Ni-V, Co-Cr, and Co-Mn display magnetization curves at right angles to the saturation line. It is possible that this too is the result of a weak electron-electron interaction. However, the testing of these suggestions may need to be performed within an approximation more accurate than the virtual crystal, because of the increasing dissimilarity of the band structures.

References

1. C. Kittel, Introduction to Solid State Physics, 5th ed. (Wiley, New York, 1976), p. 473.

2. L. Pauling, Phys. Rev. 54, 899 (1938).

3. A.R. Williams, V.L. Moruzzi, A.P. Malozemoff, and K. Terakura, IEEE Trans. Magn., MAG-19, 1983 (1983).

4. A.R. Williams (private communication).

5. J. Tersoff and L.M. Falicov, Phys. Rev. B 25, 4937 (1982).

6. P. Weiss and R. Forrer, Ann. Phys. 12, 279 (1929); R. Forrer, J. Phys. Rad. 1, 325 (1930).

7. D.I. Bardos, J. Appl. Phys. 40, 1371 (1969).

8. R.M. Bozorth, Ferromagnetism (Van Norstrand, New York, 1951), p. 15.

9. A.J.P. Meyer and G. Asch, J. Appl. Phys. 32, 330S (1961).

10. M.F. Collins and J.B. Forsyth, Philos. Mag. 8, 401 (1963).

11. J. Kaspar and D.R. Salahub, J. Phys. F 13, 311 (1983).

12. S. Ohnishi, A.J. Freeman, and M. Weinert, J. Magn. Magn. Mater. 31-34, 889 (1983).

13. K. Schwarz and D.R. Salahub, Phys. Rev. B 25, 3427 (1982).

14. M.C. Desjonquères and M. Lavagna, J. Phys. F 9, 1733 (1979).

15. V.L. Moruzzi, C.D. Gelatt, Jr., and A.R. Williams, Calculated Electronic Properties of Ordered Alloys (Pergamon, New York, 1983).

16. W.B. Pearson (quoting W.C. Ellis and E.S. Greiner), in A Handbook of Lattice Spacings and Structures of Metals and Alloys (Pergamon, New York, 1958), p. 505.

17. Iron has an electron-electron interaction to bandwidth ratio that is only two-thirds as large as that of cobalt or nickel.

18. R. Walmsley, J. Thompson, D. Friedman, R.M. White, and T.H. Geballe, IEEE Trans. MAG-19, 1992 (1983).

19. R.M. White (private communication).

FIGURE CAPTIONS

Figure 1 Spin polarization as a function of Co concentration. Open circles are theoretical results, closed circles are experimental results taken from references 5 and 7 with g-factors from reference 9.

Figure 2 Spin polarization as a function of electron concentration using a virtual crystal Hamiltonian (open circles) and a pure Co Hamiltonian (closed circles).

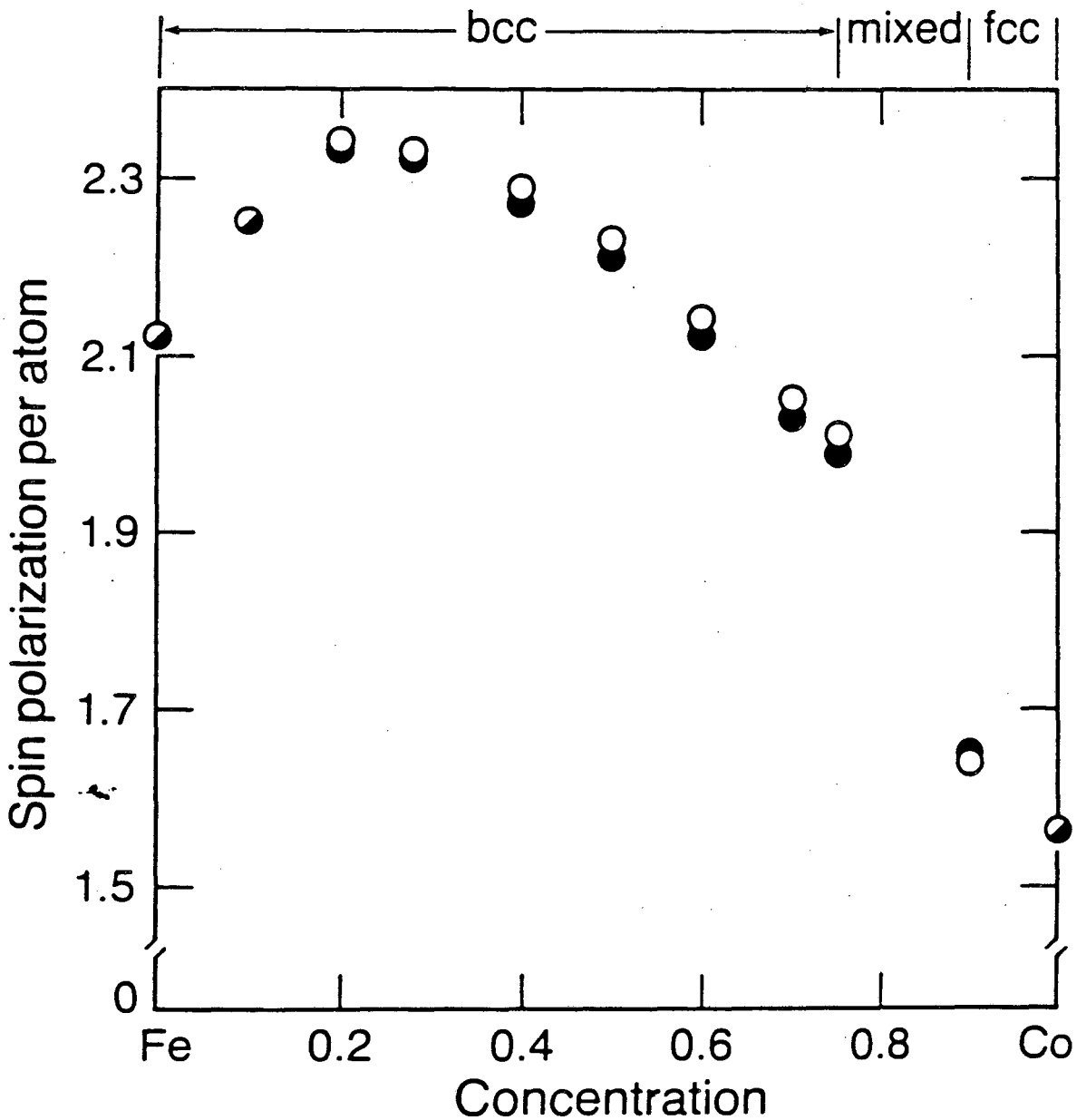
bcc
mixed
fcc
Spin polarization per atom
2.3
2.1
1.9
1.7
1.5
0
Fe
0.2
0.4
0.6
0.8
Co
Concentration

Figure 1

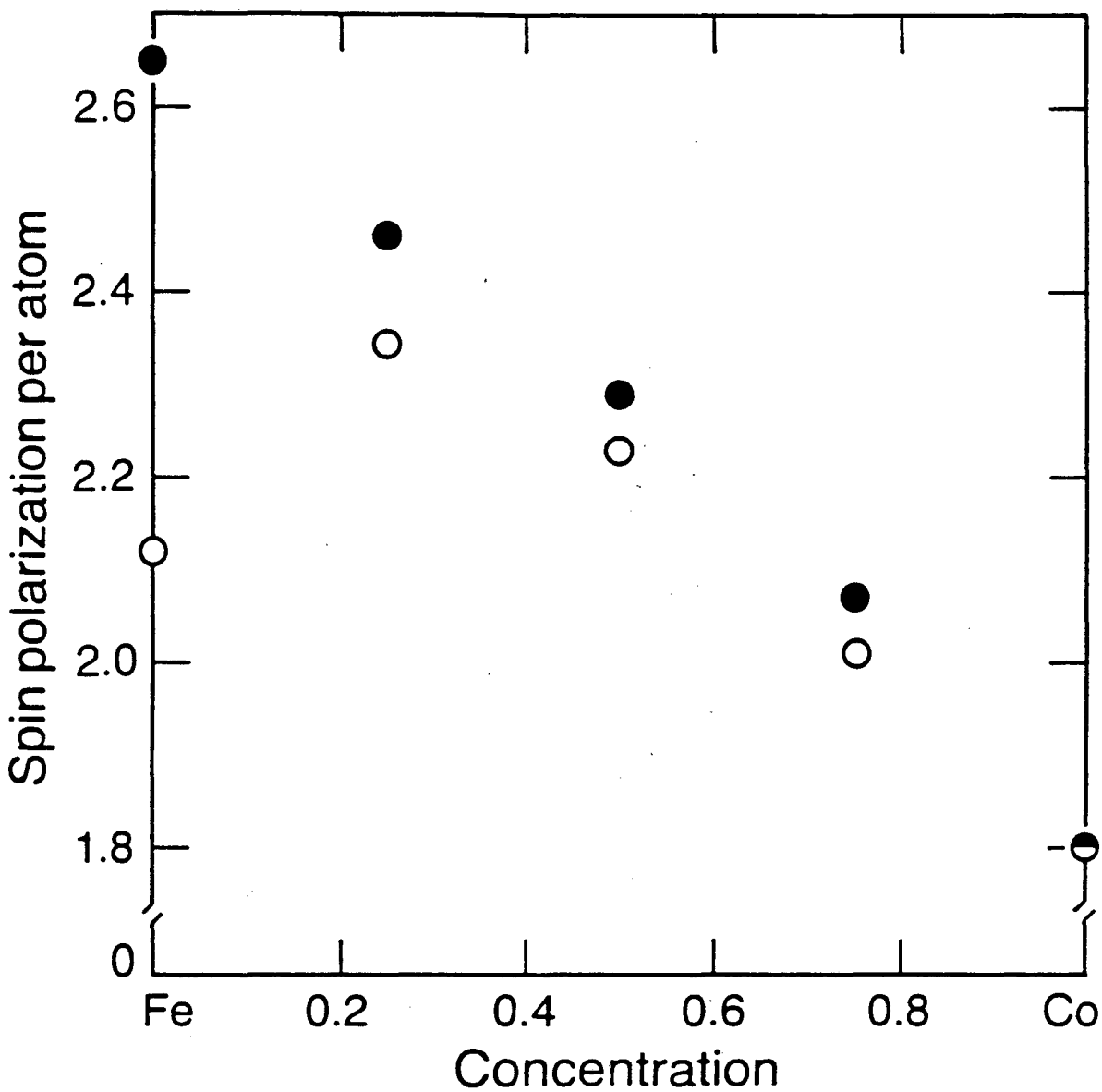
Spin polarization per atom
2.6
2.4
2.2
2.0
1.8
0
Fe
0.2
0.4
0.6
0.8
Co
Concentration

Figure 2

VI. SURFACE ELECTRONIC STRUCTURE OF FERROMAGNETIC IRON AND THE FERROMAGNETIC ORDERED IRON-COBALT ALLOY

A. Introduction

The effort to understand surface behavior must start with an understanding of the bulk material. Iron is an element of great technological importance and its properties have been extensively examined. For our purposes, it is sufficient to note that Fe possesses a g factor[1] of approximately 2.10 and thus a spin polarization of 2.12. This means that Fe is ferromagnetically weak, i.e., not all available d holes contribute to the magnetization. Chapter V shows that this is a direct consequence of a relatively weak electron-electron interaction.

The Fe-Co alloy is also technologically important.[2] This alloy possesses several useful characteristics such as the largest known magnetization per atom and an extremely high Curie temperature. In particular, the ordered FeCo alloy, which consists of Fe and Co atoms arranged at the corner and body-centered positions of simple-cubic lattice, has a magnetization of $2.42\mu_\beta$ per atom.[3] This is $0.45\mu_\beta$ higher than the average of its constituent elements. Neutron-diffraction studies[4] indicate that the vast majority of the anomalous increase in the magnetization is caused by an increase in the Fe magnetic moment from $2.2\mu_\beta$ to approximately $3.0\mu_\beta$, while the Co magnetic moment increases only slightly. Meyer and Asch[5] found the g factor of the equiatomic alloy to be approximately 2.15,

thus suggesting that the spin polarization is 2.25±0.01. Schwarz and Salahub[6] used the local-spin-density technique to calculate the properties of the ordered FeCo alloy and found a spin polarization of 2.18. Chapter V demonstrates that, at least for the disordered equiatomic alloy, the increased magnetization is caused by magnetic saturation made possible by the presence of the strong Co electron-electron interaction.

A wide variety of experimental techniques[7-14] show that the surface layer of a magnetic 3d transition metal is magnetic, while recent theoretical studies demonstrate that the surface magnetization is, in fact, enhanced relative to the bulk value.[15-17] In particular, theory predicts a spin polarization of 2.98 electrons for the Fe(100) surface[17] and approximately 0.70 electrons for the Ni surfaces.[15-16] The experimental evidence of Gradmann *et al.*[14] suggests that the magnetization of the Fe(110) surface is enhanced by approximately 30%. It is found[18] that Fe atoms segregate to the surface of the Fe-Co alloy.

In this paper we present results of calculations for the magnetic and electronic properties of the (100) and (110) surfaces for Fe and the ordered FeCo alloy. We also perform calculations for the Fe segregated (110) surface. We use the calculational scheme described in Chapter III. A necessary input to the FeCo calculations is the energy difference between Fe and Co band centers. This choice of on-site energies has been the focus of debate.[19] We have

experimented with several choices[20,21] of energy difference between the Fe and Co band centers and found that, depending on choice, there exist small charge transfers of less than 0.05 electrons between the Fe and the Co. The direction of the transfer depends on the choice of energy difference. To avoid this ambivalence, we have chosen the energy levels so that there is no charge transfer. This zero-charge transfer requirement is obviously incorrect. However, we find that the total moment per unit cell is independent of small charge transfers. Of course, the distribution of the magnetization between atoms does depend on the location of the available d holes as influenced by charge transfer. Thus, our approximation limits the accuracy of our calculated distribution of magnetization to about 0.05 electrons.

B. Results

In this section we discuss the results of our calculations and compare them with other relevant calculations and experiments. In Sec. 1 we discuss our calculation of the Fe surfaces. In other sections we consider the bulk FeCo (Sec. 2) and its surfaces (Sec. 3). The segregated system is discussed in Sec. 4 and a summary of the spin-polarization results for all systems is given in Table I.

(1) Fe Surfaces

The (100) and (110) surfaces of Fe are shown in Fig. 1. Our calculation gives a surface spin polarization for the (100) surface of 2.90 electrons. The enhanced magnetization

penetrates some distance into the bulk: The second, third, and center layers have spin polarizations of 2.30, 2.24, and 2.18 electrons, respectively. These results are very similar to those of Ohnishi et al.[17] In particular, their surface spin polarization is 2.98 electrons and their calculated DOSs also resemble ours, although 5-10% narrower. This excellent agreement between two different calculational techniques confirms the accuracy of our methods.

The calculated surface DOS of the Fe(110) surface is shown in comparison with bulk iron in Fig. 2. Two features in the surface DOS are immediately apparent: The appearance of a minority surface state near the Fermi energy and the absence at the surface of a small majority peak in the DOS found near the Fermi energy of the bulk. It may also be apparent from the DOS that the magnetization increases at the surface; in fact, the surface spin polarization is 2.55 versus 2.12 in the bulk. This is in agreement with the experimental results of Gradmann et al.[14] The relative magnetizations of bulk Fe and the two surfaces are easily explained by noting that nearest-neighbor interactions dominate the d-band width [matrix elements are proportional[22] to $(\text{distance})^{-5}$ and the first-nearest-neighbor distance is $\frac{1}{2}\sqrt{3}$ smaller than the second-nearest-neighbor (distance)]. The bulk atom in the bcc structure has eight nearest neighbors, an atom on the (110) surface has six, and an atom on the (100) surface has four. Thus the (100) surface has the fewest neighbors, smallest bandwidth, the

same electron-electron interaction as the other geometries, and consequently the highest magnetization. The atom on the (110) surface has an intermediate number of neighbors and consequently will have an intermediate magnetization.

(2) Bulk FeCo

Calculated DOSs for the ordered FeCo alloy are shown in Fig. 3. The majority DOSs have almost identical projections on the Fe and on the Co atoms. The minority DOS has more electrons projected on the Co atom and more holes projected on the Fe atom, which merely corresponds to Fe having fewer electrons than Co. Even in the minority DOS, there are very strong similarities between the two atoms in the location of projected peaks. Clearly, there is considerable hydridization of states between the two atoms; the amount of mixing is quite similar to that found between identical atoms in the pure elemental bulks.

In agreement with experiment, we find a substantially enhanced FeCo magnetization relative to the average of the constituent elements in their pure bulk form. In particular, we find the spin polarization of Fe to equal 2.66 electrons and the spin polarization of Co to equal 1.78 electrons, giving a total of 4.44 electrons per unit cell. Experiment finds a total spin polarization[3] of 4.50 ± 0.02 electrons and individual spin polarization[4] of 2.79 ± 0.1 for Fe and 1.68 ± 0.1 for Co. (In listing the experimental individual spin polarizations, we have assumed that the alloy $\underline{g}$ factor, 2.15, applies to each atom individually.)

These values may be compared to the bulk spin polarizations: 2.12 for Fe and 1.56 for Co. Our calculation finds 93% of the experimental enhancement of the spin polarization (0.77 versus 0.83 experimentally), and we find, in agreement with experiment, that most of the enhancement occurs on the Fe atom.

Explanation for the enhancement is found in ideas proposed in Chapter V for a similar enhancement in the disordered Fe-Co alloy. It was noted that Co is magnetically saturated, i.e., its magnetization is limited by the number of available d holes, while Fe is magnetically weak because of an insufficient electron-electron-interaction to bandwidth ratio. It was found that, for disordered Fe-Co alloys with greater than 30 at. % Co, the electron-electron interaction is sufficient to saturate the magnetic moment. This suggests that the rather large Co electron-electron interaction assists the weaker Fe electron-electron interaction in saturating the moment on the Fe as well as on the Co. It is clear from the considerable hybridization of Fe and Co states as shown in Fig. 3 that such assistance is possible. Additional evidence for the assistance mechanism is provided by the large increase in the Fe exchange splitting relative to pure Fe. One concludes that the strong electron-electron interaction of Co is sufficient to help increase the exchange splitting of the Fe atom, consequently saturating the magnetization without substantially diminishing the Co moment.

The slightly enhanced Co moment is caused by two structural effects. Body-centered-cubic cobalt has been constructed by sandwiching Co layers between Cr layers,[23] and, while the experimental resolution is insufficient to determine which structure of Co has the higher magnetization, a local-density calculation[24] conducted at the experimental lattice constant indicates an enhanced moment for the bcc structure (1.65 versus 1.56). Another contribution to the enhancement comes from the larger lattice constant of FeCo relative to the sandwiched bcc Co. A larger lattice constant means smaller bandwidth and higher magnetization. We find the spin polarization of bcc Co evaluated at the FeCo lattice constant to be 1.80 electrons. This gives a total enhancement relative to fcc Co of 0.24 electrons caused by structural effects. The presence of iron in the FeCo alloy affects this only marginally, making the final spin polarization 1.78.

(3) FeCo Surfaces

The simple-cubic FeCo structure may be cut by the (100) plane, leaving either all Fe atoms at the surface or all Co atoms. The DOS of the Fe surface is shown in Fig. 4(a). This density of states bears a strong resemblance to the DOS at the elemental Fe(100) surface. The spin polarization is 2.95 electrons, which is also very similar to the Fe(100) result of 2.90 electrons. These results suggest that the presence of the (100) surface is the dominant effect and that the precise nature of the second layer is

not too important for the surface Fe layer. This is reasonable since, as previously observed, the effect of Co is to increase the effective electron-electron-interaction to bandwidth ratio at the Fe atom and it is clear from Fe(100) results that a (100) surface can do this much more effectively. Consequently, the presence of Co instead of Fe is somewhat unimportant. The one major difference is that the surface effects are not able to penetrate even one layer deep into the bulk. This is presumably because Co, unlike Fe, has a saturated magnetization. Consequently, spin polarization and related properties are less susceptible to perturbation.

The density of states for the all-Co surface is shown in Fig. 4(b). It has slightly larger exchange splitting and spin polarization than the bulk (2.03 versus 1.78 electrons). Interestingly, there is a very slight (0.1 electron) decrease in the spin polarization of the underlying Fe layer. However, even this effect vanishes at the next Co layer and deeper. Overall, the surface behaves like Ni surfaces[15,16] in that the surface DOS is narrowed and new features appear, but the magnetic saturation allows only small increases in the magnetization.

The (110) surface of FeCo contains both Fe and Co atoms arranged in a two-atom unit surface cell. The surface DOS is shown in Fig. 5. As expected from the nearest-neighbor arguments given in Sec. IIIA, the (110) surface displays behavior intermediate between bulk FeCo

and the (100) FeCo surfaces. The calculated spin polarizations at the surface are 2.75 electrons for Fe and 1.86 electrons for Co. There is very little penetration of surface effects into the bulk.

(4) Fe Segregated Surface

Experimental and theoretical studies indicate that Fe tends to segregate to the surface of the FeCo alloy. To represent this, we have calculated the electronic properties of a Fe(110) overlayer, one atom thick, atop the FeCo alloy. The density of states for the two distinct surface Fe atoms is shown in Fig. 6. The spin polarizations are 2.63 electrons for the Fe atom occupying the Co position and 2.67 electrons for the Fe atom occupying the normal position. Clearly, the two Fe atoms have very similar electronic properties. It is to be noted that their properties are intermediate between the Fe(110) surface and the FeCo(110) surface.

C. Conclusions

The complicated magnetic and electronic properties of FeCo surfaces have been calculated and the results explained through examination of two simpler systems: bulk FeCo and pure-Fe surfaces. The spin polarization of bulk FeCo is calculated to be 4.44 electrons per unit cell, thus capturing more than 90% of the experimental enhancement observed in the alloy relative to the average of the pure elemental magnetization. Most of the increase is found to occur on the Fe atom, where the presence of eight

neighboring Co atoms helps increase the effective electron-electron interaction and saturates the moment. The much smaller magnetic enhancement found on the Co atom is caused by the shift from fcc to bcc structures and possibly a slight swelling in the lattice constant as iron is added.

For both Fe and FeCo, the (100) surface has substantially higher magnetization than the (110) surface, which is in turn more magnetic than the bulk. The effect is particularly vivid in Fe where the spin polarization increases from its bulk value of 2.12 electrons to 2.90 at the (100) surface. These effects may be understood in terms of simple bandwidth arguments, where it is noted that an atom at the (100) surface has only four nearest neighbors, at the (110) surface six nearest neighbors, and in bulk eight. Consequently, the (100) surface has the smallest bandwidth and the largest magnetization. This argument applies to FeCo, as well as Fe, because the nearest-neighbor Co atoms hydridize exceedingly well with their neighboring Fe atoms and consequently produce a larger contribution to the Fe bandwidth than the second-nearest-neighbor Fe atoms. The Fe-overlayered surface on FeCo presents behavior intermediate between the pure Fe(110) surface and the ordinary FeCo(110) surface.

References

1. C. Kittel, Introduction to Solid State Physics, 5th ed. (Wiley, New York, 1976).

2. G. Couderchon and J.F. Tiers, J. Magn. Magn. Mater. 26, 196 (1982).

3. D.I. Bardos, J. Appl. Phys. 40, 1371 (1969).

4. M.F. Collins and J.B. Forsyth, Philos. Mag. 8, 401 (1963).

5. A.J.P. Meyer and G. Asch, J. Appl. Phys. 32, 330S (1961).

6. K. Schwarz and D.R. Salahub, Phys. Rev. B 25, 3427 (1982).

7. C. Rau, Comments Solid State Phys. 9, 177 (1980).

8. E.W. Plummer and W. Eberhardt, Phys. Rev. B 20, 1444 (1979).

9. C. Rau and S. Iechner, Phys. Rev. Lett. 47, 939 (1981).

10. G.P. Felcher, S.D. Bader, R.J. Celotta, D.T. Pierce, and G.C. Wang, in Ordering in Two Dimensions, edited by S.K. Sinha (Elsevier, New York, 1980), p. 107.

11. W. Eib and S.F. Alvarado, Phys. Rev. Lett. 37, 444 (1976).

12. W. Göpel, Surf. Sci. 85, 400 (1979).

13. A.M. Turner, Y.J. Chang, and J.L. Erskine, Phys. Rev. Lett. 48, 348 (1982).

14. U. Gradmann, G. Waller, R. Feder, and E. Tamura, J. Magn. Magn. Mater. 31-34, 883 (1983).

15. J. Tersoff and L.M. Falicov, Phys. Rev. B 26, 6186 (1982).

16. H. Krakauer, A.J. Freeman, and E. Wimmer, Phys. Rev. B 28, 610 (1983).

17. S. Ohnishi, A.J. Freeman, and M. Weinert, Phys. Rev. B 28, 6741 (1983).

18. J.L. Moran-Lopez and H. Wise, Appl. Surf. Sci. 4, 93 (1980).

19. M.O. Robbins and L.M. Falicov, Phys. Rev. B 29, 1333 (1984).

20. M.O. Robbins (private communication).

21. M.C. Desjonquères and M. Lavagna, J. Phys. F 9, 1733 (1979).

22. W.A. Harrison and S. Froyen, Phys. Rev. B 21, 3214 (1980).

23. R. Walmsley, J. Thompson, D. Friedman, R.M. White, and T.H. Geballe, IEEE Trans. Magn. MAG-19, 1992 (1983).

24. D. Bagayoko, Z. Ziegler, and J. Callaway, Phys. Rev. B 27, 7046 (1983).

TABLE I

System	Spin polarization	
	Fe	Co
pure elements	2.12	1.56
FeCo alloy	2.66	1.78
(100) Fe surface	2.90	----
(110) Fe surface	2.55	----
(100) FeCo surfaces	2.95	2.03
(110) FeCo surface	2.75	1.86
(110) Fe overlayer - Co position	2.63	----
- Fe position	2.67	----

FIGURE CAPTIONS

Figure 1 Unit surface cells. Circles represent iron atoms, squares represent cobalt atoms in FeCo surfaces or Fe atoms in pure iron surfaces. Uncrossed atoms are located on the surface, crossed atoms are located on the first layer below the surface.

Figure 2 Projected density of states. (a) Fe (110) surface layer (b) bulk Fe. Solid lines are minority states; dashed lines are majority states.

Figure 3 Projected density of states for bulk FeCo. (a) Fe atom. (b) Co atom. Solid lines are minority states; dashed lines are majority states.

Figure 4 Projected density of states for the two FeCo (100) surfaces. (a) Surface Fe atom. (b) Surface Co atom. Solid lines are minority states; dashed lines are majority states.

Figure 5 Projected density of states for FeCo (110) surface. (a) Surface Fe atom. (b) Surface Co atom. Solid lines are minority states; dashed lines are majority states.

Figure 6 Projected density of states for an Fe overlayer on the FeCo (110) surface. (a) Surface Fe atom at normal position. (b) Surface Fe atom at the "Co" position. Solid lines are minority states; dashed lines are majority states.

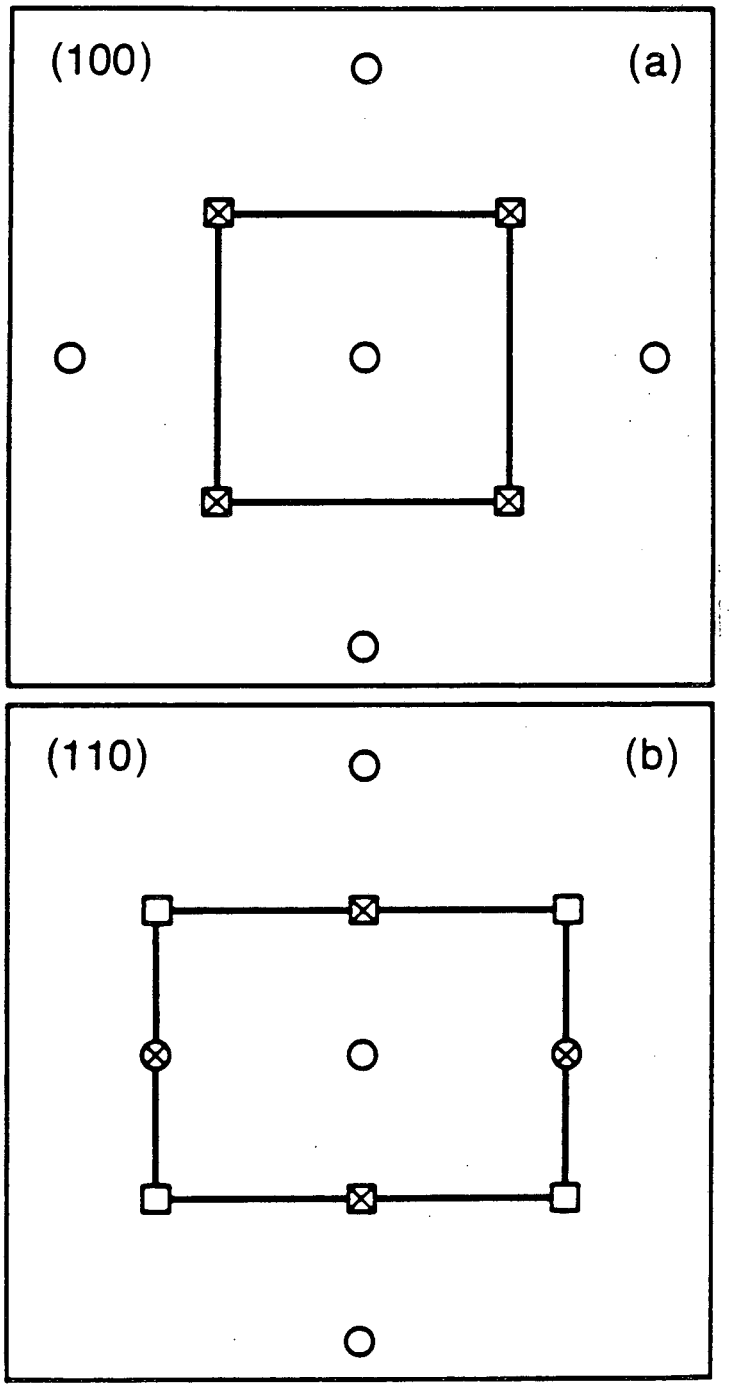

Figure 1

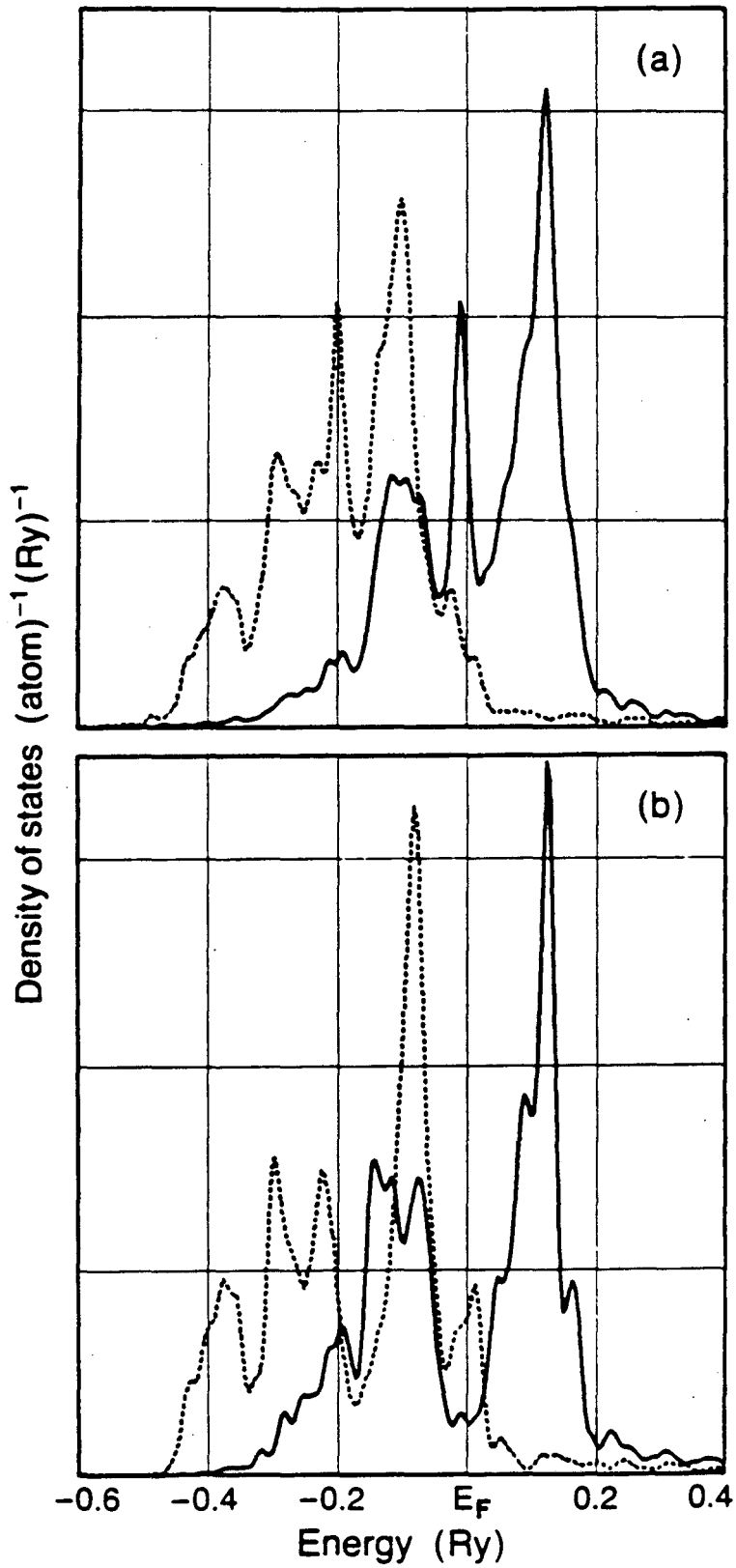

Figure 2

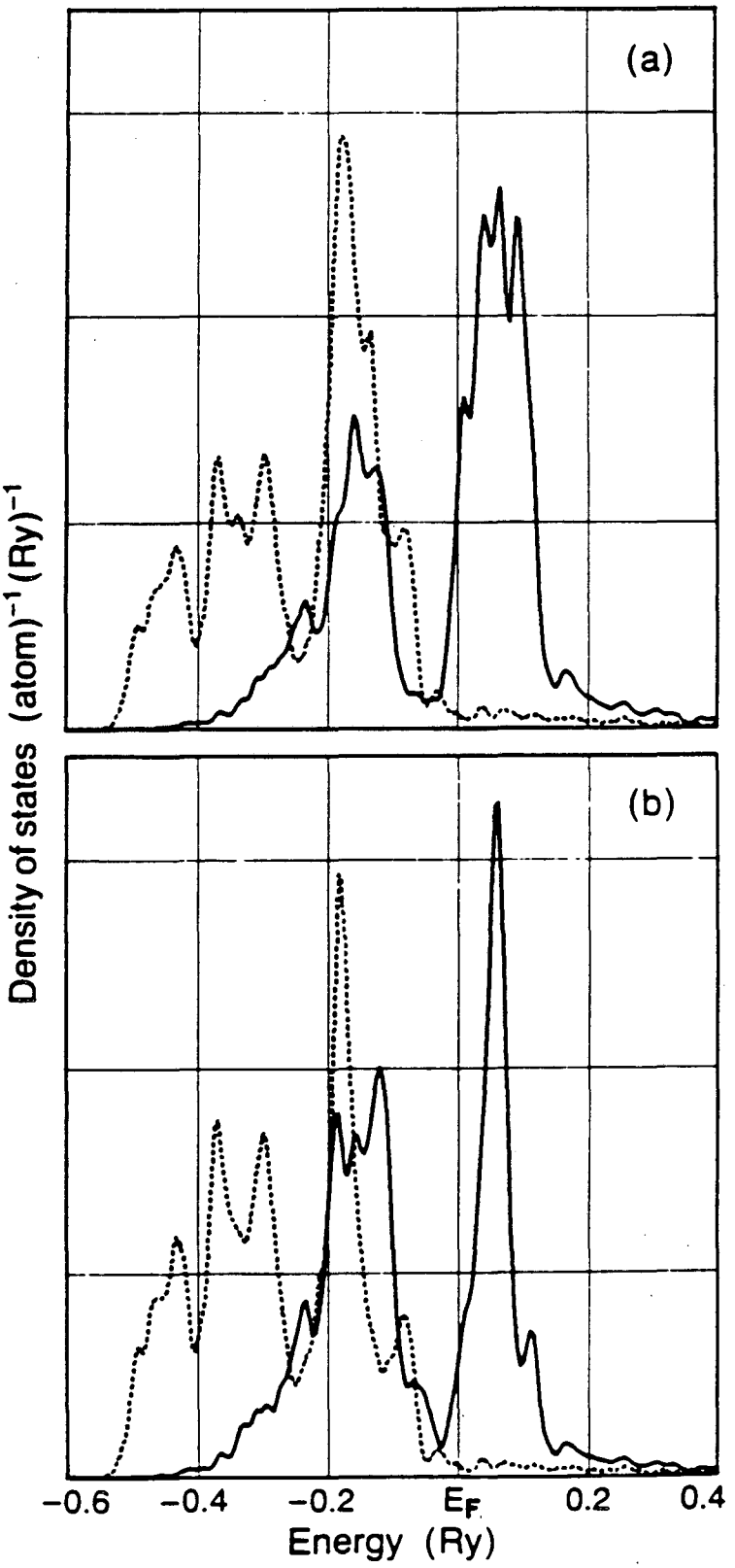

Figure 3

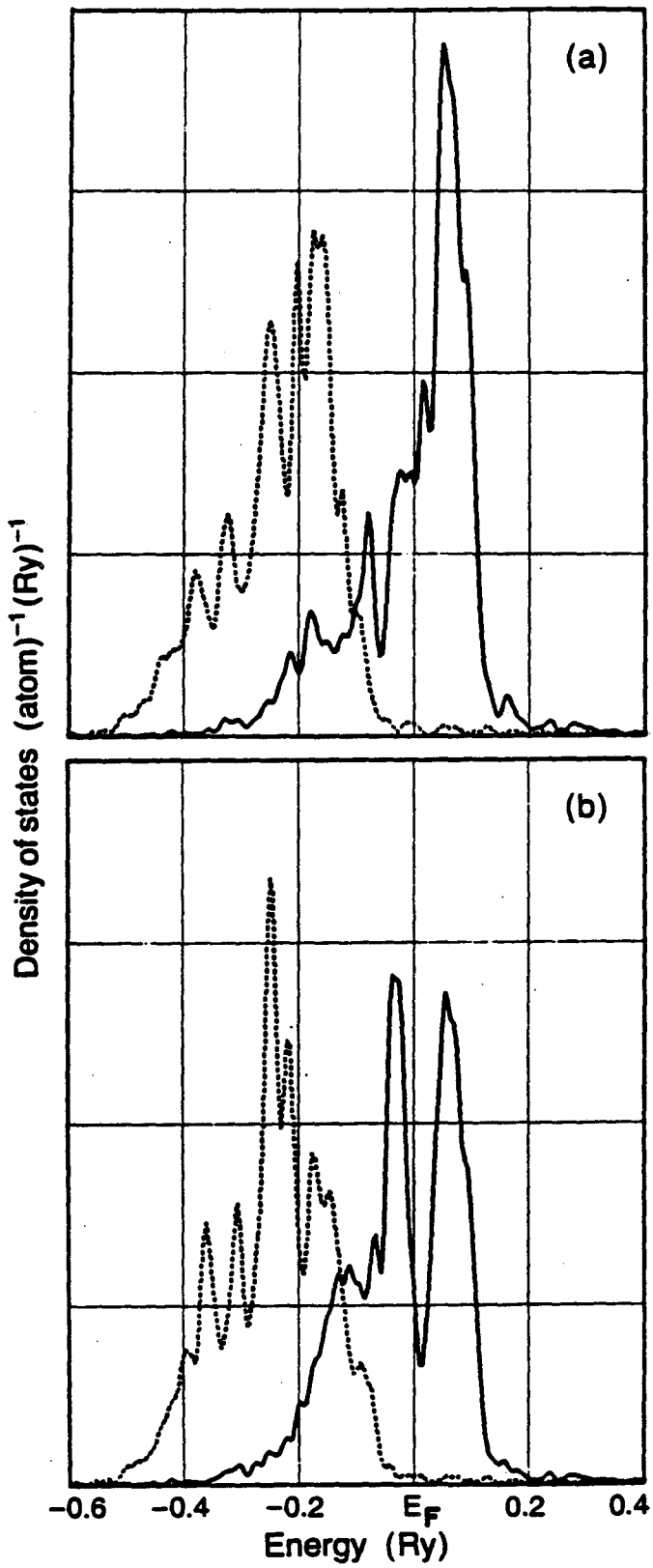

Figure 4

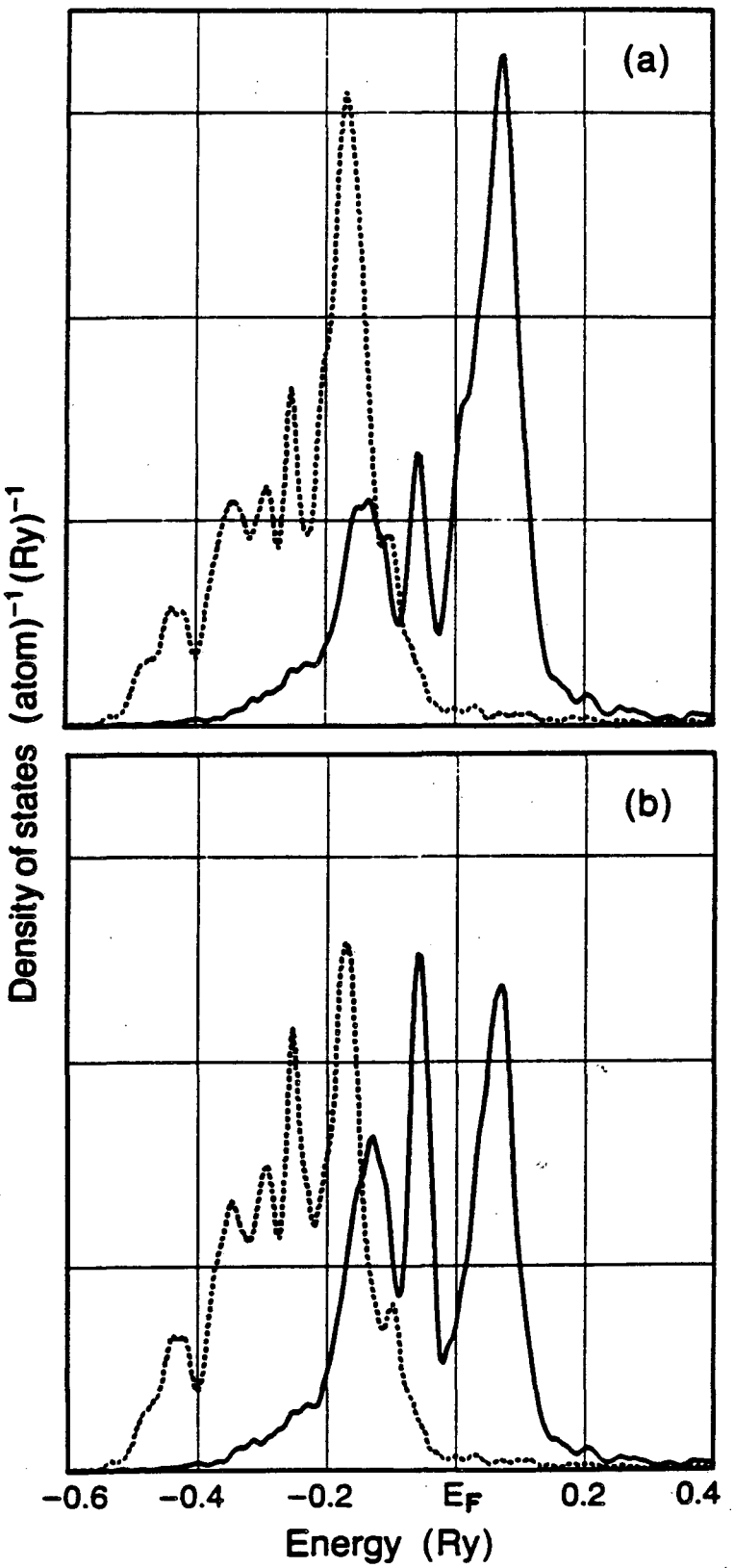

Figure 5

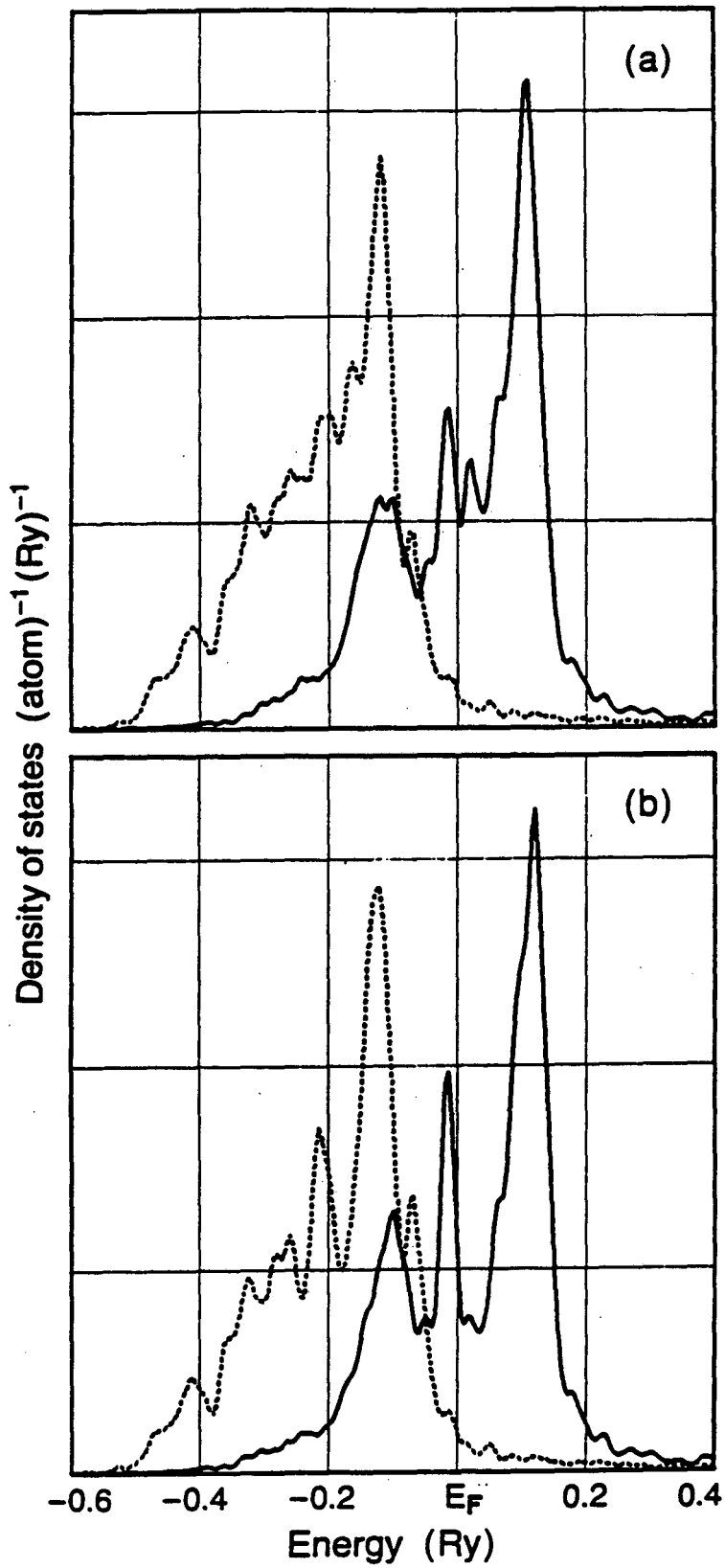

Figure 6

VII. ELECTRONIC STRUCTURE OF CHROMIUM SURFACES AND CHROMIUM MONOLAYERS ON IRON

A. Introduction

Bulk chromium occurs in the body-centered cubic structure with an antiferromagnetic (AF) ground state modulated by an incommensurable spin-density wave (SDW). The SDW is in one of the (100) directions with a wavelength of approximately 21 lattice spacings. The magnetization at the maximum is 0.59 Bohr magnetons.[2] Experimentally it is found that the addition of small amounts (approximately 1%) of group VII impurities such as Mn produces a simple AF structure[3] with a magnetic moment of approximately 0.67 Bohr magnetons. In this structure atoms in the body-centered positions of the bcc lattice have spins pointing only in one direction; atoms in the corner positions have spins in the opposite direction.

This simple AF structure demands that (100) planes contain atoms of only one spin direction. Consequently the (100) surface is expected to possess ferromagnetic order. Evidence of this planar ferromagnetism is found in the electron-capture spectroscopy results of Rau and Eichner.[4] Their sample, however, displayed a c(2x2) structure indicative of impurities, which may have affected their results. The (100) surface has been examined also by two angle-resolved photoemission experiments;[5-7] both find a surface state or resonance at an energy approximately 0.70 eV below the Fermi level. Unfortunately the experiments

disagree on the symmetry of this feature. Klebanoff *et al.*[6,7] also found a surface-related feature with a very small binding energy.

The (100) surface of chromium has also been examined theoretically[8-10] by means of a simple exchange interaction and a tight-binding approach which neglected the *sp* conduction electrons. Allan[8] finds that the surface magnetization is very large (2.8 Bohr magnetons) relative to the bulk and argues that this enhancement should penetrate into the bulk, decreasing by a factor (-0.5) per layer. (The negative sign refers to the AF). Grempel[10] finds a surface spin polarization of 2.6 Bohr magnetons and a very high surface Curie temperature.

Feibelman and Hamann,[11] in an effort to explain the superconducting properties of Au-Cr-Au sandwich films,[12] performed paramagnetic calculations within the local-density formalism for Cr (100) surface and overlayer systems. Near the Fermi level they find a large feature in the Cr surface layer which remains substantially unaffected by the application of, for example, a gold overlayer.

The (110) planes cut the simple AF bcc lattice so that an equal number of up and down spins are encountered. The (110) surface should therefore be an AF one. There have been two photoemission experiments on the Cr (110) surface. The experiment of Johansson *et al.*[13] found no evidence of surface states; the later experiment of Wincott *et al.*[14] measured the dispersion of a surface state (binding energy

of approximately 0.2 eV) along $\bar{\Delta}$. The periodicity of their spectra suggests an AF surface.

Stainless steel is the name given to a family of iron based alloys which contain at least 12% chromium. Auger electron spectroscopy[15] shows that when a 304 stainless steel sample (a common type) is heated, there is a strong enhancement of the Cr concentration at the surface. This is in agreement with chromium's lower heat of crystal formation.[16] It is this enhanced concentration of Cr at the surface which, when oxidized, is influential in preventing the rusting of the steel.

In this paper we present results of calculations for the magnetic and electronic properties of the (100) and (110) surfaces of Cr, and for the systems consisting of a monolayer of Cr deposited on the Fe (100) and (110) surfaces. We use the calculational method described in Chapter III.

B. Results

In this section we discuss the results of our calculations and compare them with experiments and with other relevant calculations. In Section 1 and 2 we discuss the Cr (100) and the Cr (110) surfaces, respectively. The Cr monolayer on Fe, which is a model for the stainless steel surface, is discussed in Section 3.

(1) Cr (100) Surface

Our calculation gives a surface spin polarization of 3.00 electrons. This enhancement relative to the bulk, a factor of 5.1 from the SDW maximum, is much larger than

that[17,18] found in Fe and Ni. The magnitude of the enhancement can be attributed to the large number of unpolarized d-holes present in the bulk. Consequently, the decreased bandwidth found at the Cr surface, which leads to a stronger effective magnetic interaction, can greatly increase the surface spin polarization. Elements like Fe or Ni, with fewer available unpolarized holes, experience smaller changes in the same local environment.

The narrowing of the Cr DOS at the (100) surface is shown in Figure 1. It is clear that most d-holes occur in the minority subband. This subband is essentially concentrated in a single peak structure entirely above the Fermi level. The surface DOS can be compared with the bulk DOS shown in Figure 2. Here the d-holes are almost evenly distributed between the two subbands. Furthermore it is clear that both subbands have sizeable strength on either side of the Fermi energy, which falls in a valley of the bcc DOS.

Figure 1(b) shows the DOS projected at the layer immediately below the surface. The width of each subband is approximately equal to the bulk value, which is consistent with the presence of all nearest, and most second-nearest neighbors. The spin polarization is opposite to that of the surface layer, which is consistent with the AF of chromium. However, it is clear that there is a substantial difference between the minority and the majority DOS, suggesting that the spin polarization is not bulklike.

The spin polarization of the second layer is (-1.56), substantially different from the bulk. The spin polarizations of the third through sixth layers are 1.00, (-0.93), 0.86, and (-0.85), respectively (see Fig. 3). A similar penetration of the enhanced surface magnetization was found in the Fe (100) surface,[17] although there the effect is much smaller. This penetration appears to be a direct consequence of the easy availability of unpolarized d-holes in bulk Cr. Each atom feels the larger exchange splitting of its neighbor towards the surface and responds by increasing its own; this is, in the case of Cr, an energetically very inexpensive process.

The (100) surface Brillouin zone is shown in Fig. 4(a). Several points have high symmetry. In particular $\bar{\Gamma}$ and $\bar{M}$ have symmetry C_{4v} (see Table I), whereas $\bar{X}$ has symmetry C_{2v} (see Table II). All symmetry lines have the symmetry of a single reflection plane. At all points of high symmetry it is possible to have symmetry gaps, i.e. areas of the energy spectrum where no states of a given symmetry occur. In these symmetry gaps surface states of that symmetry may exist: they are states entirely located in the surface layers and which make no connection with the bulk continuum. These surface states exist despite the absence of a true gap in the total density of states.

Figure 5 exhibits all states which are 60% localized within the two outermost layers on each side of our eleven-layer slab. Normally states are localized mostly on the

surface layer, but in this system the second layer is also unique; it is the layer with the highest polarization for spin direction opposite to that of the surface. It can therefore have its own localized states. The down-spin state[19] of symmetry $\bar{\Gamma}_5$ is one example of such state.

Table III lists those states at the symmetry points $\bar{\Gamma}$, $\bar{X}$, and $\bar{M}$ that are true surface states. The other states at these symmetry points are resonances, i.e., continuum states with a large amplitude at the surface.

One feature that may disturb the reader is that not all our surface states come in an exact two-fold degeneracy arising from the two surfaces of the slab (the peaks at $\bar{\Gamma}$ above the Fermi energy are a clear example). The splitting is a consequence of the finiteness of the slab: the surface states of one surface are able to interact with their counterparts at the other surface.

The theoretical surface-and second-layer Cr(001) electronic structures at $k_{||} = 0$ ($\bar{\Gamma}$) are shown in Figs. 6(a) and 6(b), respectively. Figure 6(a) shows a Δ_1-symmetry up-spin surface resonance at 0.249Ry binding energy. This is accompanied by a Δ_1-symmetry down-spin surface state at 0.210Ry binding energy that is localized on the second layer (Fig. 6(b)). Both of these initial states have primarily $\underline{d}_{z^2}$ orbital character with a small contribution from <u>sp</u> orbitals. Closer to E_F, we predict two very strong surface states of Δ_5 symmetry and $\underline{d}_{xz}$, $\underline{d}_{xy}$ orbital

character. These states exist in a Δ_5-symmetry gap of the surface-projected antiferromagnetic band structure. The up-spin state has binding energy 0.095Ry in Fig. 6(a) while the down-spin state is located 0.088Ry below (to the left of) E_F in Fig. 6(b). A small Δ_1-symmetry up-spin surface state of mostly $\underline{d}_{z^2}$ orbital character is also predicted with energy 0.050Ry above (to the right of) E_F in Fig. 6(a). This feature differs from the initial states predicted below E_F in that a companion Δ_1-symmetry down-spin surface state is not predicted for the second layer, Fig. 6(b).

We now evaluate the consistency of these theoretical predictions with the ARPES results of Klebanoff _et al._[6,7] The experimental Δ_1-symmetry photoelectron peak at ~0.24Ry binding energy has been previously attributed to a non-surface initial state because it shows negligible sensitivity to surface contamination.[20] Since this feature lies in the spectral region predicted for the Δ_1-symmetry surface resonance and its accompanying surface state, the ARPES experiment cannot determine the existence of these surface features at $\bar{\Gamma}$.

There is photoemission evidence for the theoretical Δ_5-symmetry surface states and the lower-energy Δ_1-symmetry state at $\bar{\Gamma}$. We believe that the up-spin and down-spin Δ_5-symmetry surface states in Fig. 6 correspond to the observed Δ_5-symmetry surface feature _2_. The nearly degenerate theoretical surface states have binding energies (0.09Ry) near that observed for the surface feature _2_

($E_{IN}(2)$ = 0.055Ry). The discrepany between the theoretical surface state binding energies and $E_{IN}(2)$ may be due in part to the influence of many-body processes on the spectroscopic binding energies E_{IN}. The calculations predict that as $k_{||}$ increases along the $\bar{\Gamma}$-$\bar{X}$ line in the surface Brillouin zone, the Δ_5-symmetry surface states disperse in the same manner toward larger binding energies. The dispersion observed for the surface feature 2 in P-polarization HeI_α ARPES measurements is presented in Fig. 7. The open circles are adjusted theoretical values for the binding energy of the even-symmetry component of the up-spin Δ_5 surface state. This component is symmetry allowed in P-polarization. The theoretical values were all reduced by 0.04Ry, so that the experimental and theoretical binding energies are equal at $\bar{\Gamma}$. Figure 7 demonstrates that the $k_{||}$-dependence of $E_{IN}(2)$ is similar to that predicted for the binding energy of the theoretical Δ_5-symmetry surface states.

The experimental surface feature 2 loses considerable spectroscopic intensity as $k_{||}$ increases along the $\bar{\Gamma}$-$\bar{X}$ line. This is consistent with the $k_{||}$-variation predicted for the even-symmetry component of the Δ_5 surface states. At $\bar{\Gamma}$, these theoretical surface features are surface states that are highly localized within the top two layers. As $k_{||}$ increases, these surface states broaden into surface resonances. Accompanying this broadening is a delocalization of surface resonance charge away from the surface. Since ARPES is intrinsically a surface-sensitive technique,

a charge delocalization would reduce the spectral intensity of the Δ_5-symmetry surface features. This expectation is in agreement with the variation of the experimental feature 2 intensity. However, a quantitative explanation of the experimental intensities would require the calculation of photoelectric transition matrix elements.

Since the symmetry, binding energy, and spectral variation with $k_{||}$ of the surface feature 2 are consistent with the theory, we assign the experimental surface feature 2 to nearly degenerate Δ_5-symmetry up-spin and down-spin surface states at $\bar{\Gamma}$. As such, feature 2 would have d_{xz} and d_{yz} orbital character. Note that this assignment predicts mixed spin polarization for the photoelectron peak 2.

The experimental surface feature 1 possesses Δ_1-symmetry. The only theoretical Δ_1-symmetry initial state near E_F is the unoccupied (+)-spin surface state located 0.050Ry above E_F in Fig. 6(a). The true energy position of this surface state may be closer to E_F than predicted. This possibility, combined with the very sharp onset of the feature 1 spectral intensity at E_F, leads us to assign the Δ_1-symmetry surface feature 1 to a peaked spectral profile produced by the truncation of a Δ_1-symmetry up-spin surface state by the Fermi level. As such, feature 1 would have mostly d_{z^2} orbital character. As $k_{||}$ increases along the $\bar{\Gamma}$-$\bar{X}$ line, the Δ_1-symmetry surface state is theoretically expected to lose less spectral intensity than the Δ_5-symmetry surface states (feature 2) because more of its charge

remains surface-localized. In addition, the Δ_1-symmetry surface state is predicted to disperse to lower energy with increasing $k_{||}$. This effect moves more of this state below the Fermi level, further enhancing the state's intensity, as $k_{||}$ increases. The persistent spectral intensity predicted for this Δ_1-symmetry surface state is consistent with the experimental $k_{||}$-dependence of feature 1.

Experimental surface feature 3 is observed over the $k^f_{||}$ range $1.0 \leq k^f_{||} \leq 2.0$ $\mathring{A}^{-1}$. This corresponds to a range of $k_{||}$ values $0.2 \leq k_{||} \leq 1.09$ $\mathring{A}^{-1}$ in the first surface Brillouin zone. The experiment finds that at $k_{||} = 0.85(8)$ $\mathring{A}^{-1}$, the surface feature 3 is composed of two nearly degenerate components that are even and odd with respect to reflection through the (100) mirror plane. The binding energies of the even and odd components were observed to be 0.053Ry and 0.059Ry, respectively. These properties are partially consistent with the theoretical results for the Cr(001) surface electronic structure along the $\overline{\Gamma}$-$\overline{X}$ line. At $k_{||} = 0.85$ $\mathring{A}^{-1}$, we predict the existence of an even-symmetry surface resonance at 0.050Ry. Several odd-symmetry surface resonances are also predicted from 0.07-0.11Ry below E_F. However these resonances are not strong features in the theory because they are broadened in energy and have much of their charge delocalized away from the surface. From a theoretical viewpoint, the large spectral intensity observed for each component of the surface feature 3 is surprising.

(2) Cr (110) Surface

Our calculation gives a two-atom unit surface cell with AF ordering as the ground-state configuration. This configuration is in agreement with the simple saw cut of the bulk along the (110) plane. We were unable to find a ferromagnetic locally stable minimum in the ground-state energy. The surface spin polarization in the AF configuration is 2.31 electrons. This value is smaller than that for the (100) surface as one would expect, since the (110) surface atom has six nearest neighbors, as opposed to four in the (100) surface. A larger bandwidth, suggested by the nearest neighbor argument, is shown in Figure 8(a). Figure 8(b) shows the DOS projected on one of the second-layer atoms, a nearest neighbor to the atom in Figure 8(a). As befits its nearest neighbor status in an AF structure, the spin polarization is opposite to that of the surface atom. The spin polarization of 1.00 electrons is considerably smaller than that of a second-layer (100) atom, 1.56. It is a consequence not only of the smaller (110) surface perturbation, but also of the larger interlayer distance in the (110) direction. In particular, (100) layers are separated by 0.5 $\underline{a}$ (where $\underline{a}$ is the lattice constant), whereas (110) layers are separated by 0.707 $\underline{a}$, with a consequent smaller coupling between layers.

The (110) surface Brillouin zone is shown in Figure 4(b). The special points $\bar{\Gamma}$, $\bar{X}'$, $\bar{M}$, and $\bar{X}$ all have symmetry C_{2v} (see Table II). The symmetry lines contain only a

single mirror plane. Figure 9 indicates all states that are over 50% localized within the outermost layer. Note that the up and down spin eigenvalues are identical because of the complete AF of bulk and surface. However, the up and down spin features show different symmetries at some wave-vectors. It is a consequence of the availability of two separate and distinct origins for the point group operations.

There also exists experimental disagreement on photoemission spectra taken at the (110) $\bar{\Gamma}$ point. The data of Johansson et al.[13] show no surface features; those of Wincott et al.[14] show a state of presumed symmetry $\bar{\Gamma}_3$ which was measured from $\bar{\Gamma}$ to $\bar{X}$. The binding energy of this state, 0.011Ry to 0.022Ry, is smaller than the one we find, but the dispersion is similar. In particular, we find the lowest binding energy, 0.053Ry, to occur at approximately three quarters of the distance from $\bar{\Gamma}$ to $\bar{X}$, and for a local maximum to occur at the middle point. We find this state to be a resonance, not a surface state, because the $\bar{\Sigma}_3$ gap does not extend below the Fermi energy. Wincott et al.[13] find an AF periodicity equal to ours. We believe that their experimental inability to find our surface feature of symmetry 1 is caused by the use of s-polarized light. (Symmetry 2 features at $\bar{\Gamma}$ are undetectable in photoemission.) In their paper, however, they do not state the precise polarization of their beam.

(3) Cr Monolayers on Fe

We have calculated the spin polarization of a Cr monolayer atop the Fe (100) surface to be 3.63 electrons, with a ferromagnetic arrangement pointing oppositely to the underlying Fe substrate. This value is the largest spin polarization we have ever calculated, or found in the literature, for a transition-metal system. It is interesting that it occurs for a system as important as the pre-oxidized stainless-steel surface. We were unable to obtain a local stable minimum for a Cr ferromagnetic layer, ferromagnetically ordered with respect to the iron.

Insight into this result may be gained by comparing it with the dilute FeCr alloy. Neutron scattering[21] results show that the isolated Cr atoms point oppositely to the surrounding Fe bulk and have a spin polarization of 1.2 electrons, twice the maximum bulk value of the SDW. This latter result presumably stems from the stronger electron-electron interaction in Fe, and a consequent stronger exchange splitting which helps Cr increase its own splitting and magnetization. This is the same argument explored in great detail for the iron-cobalt alloy,[17] where Co has the stronger electron-electron interaction. The combined effect of diminished number of neighbors and stronger Fe exchange results in the calculated large Cr moment. We may understand the AF coupling by noting that Mn is the element intermediate between Fe and Cr, which suggests that the Fe-Cr interaction may be similar to the Mn-Mn interaction.

Manganese exhibits localized moments but no ferromagnetism, implying that Fe and Cr would not couple ferromagnetically either.

Figure 10 shows the DOS projected on the Cr monolayer and on the underlying Fe layer. The most obvious feature is the enormous minority DOS at the Cr monolayer (peak value of approximately 60 / atom-Ry). It is a consequence not only of the surface band narrowing, but also of the absence of Fe majority holes to which the Cr minority holes (same spin) may be coupled. These two facts leave a subband with essentially no effective nearest neighbors, and therefore very narrow. The underlying Fe atoms are slightly affected by the Cr layer, and lower their spin polarization to 1.95 electrons.

Consideration of a Cr monolayer atop the Fe (110) surface suggests several alternative configurations. One might expect the monolayer to be AF because of the AF interaction of each Cr atom with its four Cr neighbors. This arrangement forces half the Cr atoms to have a ferromagnetic interaction with the four underlying nearest Fe atoms. As already discussed, Fe has a very strong effect on the Cr spin polarization (it doubles the value of the Cr polarization in the dilute alloy). The Fe substrate therefore would favor a ferromagnetic Cr monolayer, with AF order with respect to the bulk. Clearly there are two competing effects, and the nature of the ground state can be determined only after a detailed calculation.

We find that the ground state consists of a ferromagnetic Cr monolayer with its spins oriented in the direction opposite to the Fe substrate, similar to the Cr on Fe (100) arrangement. The spin polarization of the Cr is 2.25 electrons, smaller than the pure Cr surface. There is, as in the (100) monolayer, a small decrease in the spin polarization of the underlying Fe layer to a value of 2.03 electrons. The projected DOS at the Cr layer and at the underlying Fe layer is shown in Figure 11. Changes from the bulk DOS are not spectacular and mostly they reflect just the increased spin polarization.

We find that a structure consisting of an AF chromium layer is metastable: it produces a local minimum in the total energy curve, 0.05 Ry / surface atom above the ground state. The spin polarization of the two different Cr atoms are 3.03 and (-3.31) electrons, with the larger magnitude corresponding to the atom with AF arrangement to both its Cr and Fe nearest neighbors. It is clear that because of the different magnitudes of the spin polarizations the Cr monolayer is not truly AF, but rather ferrimagnetic. One finds in the projected DOS (Figure 12) a narrow and tall minority-hole peak on the second atom, for much the same reasons given for the (100) monolayer results.

(C) Conclusions

The (100) surface of Cr is found to be ferromagnetic with a spin polarization of 3.00 electrons, whereas the (110) surface is found to be AF. Both magnetic

configurations are in agreement with experiment and constitute the configuration of the (100) and (110) planes in the commensurable AF bulk structure. At both surfaces there is considerable penetration of the greatly enhanced surface magnetization into the bulk. Both the large surface spin polarization and the penetration may be understood as consequences of the large number of d-holes available for spin polarization. A very strong surface state of symmetry $\bar{\Gamma}_5$ is found at the center of the (100) surface Brillouin zone. This is in agreement with a recent photoemission experiment in Cr.

Chromium monolayers on Fe are found to be ferromagnetic, with the Cr spins aligned in the opposite direction to the Fe spins. At the (110) surface this arrangement forces Cr nearest neighbors to have the same spin direction, a result which indicates the strength of the Fe-Cr interaction. The (100) Cr monolayer possesses the largest spin polarization for a transition-metal system known to the authors. This polarization, 3.63 electrons, is caused by the combination of (100) surface band narrowing and the strong antiferromagnetic Fe-Cr interaction.

Many predictions made here regarding magnetic configurations could be easily tested by photoemission experiments. In particular X-ray spin polarized photoemission could easily check the anti-parallel arrangement of the Cr and Fe spins, since the Cr core levels should order their excitation energies oppositely to those of Fe. Enhanced

magnetization of the Cr surfaces could be deduced from the increased differences between the up and the down spin excitation energies relative to those in the bulk. We hope that our results will stimulate additional experimental work aimed at determining the behavior of these extremely magnetic systems.

References

1. S.A. Werner, A.S. Arrott and H. Kendrick, Phys. Rev. 155, 528 (1967).

2. G. Shirane and W.J. Takei, J. Phys. Soc. Japan Suppl. 17, BIII, 35 (1962).

3. W.C. Koehler, R.M. Moon, A.L. Trego and A.R. MacKintosh, Phys. Rev. 151, 405 (1966).

4. C. Rau and S. Eichner, Phys. Rev. Lett. 47, 939 (1981).

5. G. Gewinner, J.C. Peruchetti, A. Jaéglé and R. Pinchaux, Phys. Rev. B 27, 3358 (1983).

6. L.E. Klebanoff, S.W. Robey, G. Liu and D.A. Shirley, Phys. Rev. B 30, 1048 (1984).

7. L.E. Klebanoff, R.H. Victora, L.M. Falicov, and D.A. Shirley, submitted to Phys. Rev. B.

8. G. Allen, Surface Sci. 74, 79 (1978).

9. G. Allan, Phys. Rev. B 19, 4774 (1979).

10. D.R. Grempel, Phys. Rev. B 24, 3928 (1981).

11. P.J. Feibelman and D.R. Hamnann, Phys. Rev. B 31, 1154 (1985).

12. M.B. Brodsky, P. Marikar, R.J. Friddle, L. Singer and C.H. Sowers, Solid State Commun. 42, 675 (1982).

13. L.I. Johansson, L.G. Petersson, K.F. Berggren and J.W. Allen, Phys. Rev. B 22, 3294 (1980).

14. P.L. Wincott, N.B. Brookes, D.S. Law, G. Thornton and H.A. Padmore, Vacuum 33, 815 (1983).

15. G. Betz, G.K. Wehner, L. Toth and A. Joshi, J. Appl. Phys. 45, 5312 (1974).

16. "CRC Handbook of Chemistry and Physics," 53rd. edition (CRC Press, Cleveland, 1972), p. F-188.

17. R.H. Victora, L.M. Falicov and S. Ishida, Phys. Rev. B 30, 3896 (1984).

18. J. Tersoff and L.M. Falicov, Phys. Rev. B 26, 6186 (1982).

19. Up-spin states are those states with the same spin direction as the majority spin states of the surface layer; down-spin states have opposite spin direction.

20. L.E. Klebanoff, S.W. Robey, G. Liu, and D.A. Shirley, submitted to Phys. Rev. B.

21. A.T. Alfred, B.D. Rainford, J.S. Kouvel and T.J. Hicks, Phys. Rev. B14, 228 (1976).

TABLE I

Character Table for the Point Group C_{4v}

Representation	E	C_2	$2C_4$	$2\sigma_v$	$2\sigma_d$
1	1	1	1	1	1
2	1	1	1	-1	-1
3	1	1	-1	1	-1
4	1	1	-1	-1	1
5	2	-2	0	0	0

TABLE II

Character Table for the Point Group C_{2v}

Representation	E	C_2	σ_v	σ_v'
1	1	1	1	1
2	1	1	-1	-1
3	1	-1	1	-1
4	1	-1	-1	1

The operation σ_v' is the reflection through the line perpendicular to $\vec{k}_{\bar{x}}$ in the (100) surface, and perpendicular to $\vec{k}_{\bar{x}'}$ in the (110) surface.

TABLE III

Surface States at Special Points of the

(100) Surface Brillouin Zone

Label	Energy (Ry)
$\bar{\Gamma}(1\uparrow)$	+0.050
$\bar{\Gamma}(5\downarrow)$	-0.088
$\bar{\Gamma}(5\uparrow)$	-0.095
$\bar{\Gamma}(1\downarrow)$	-0.210
$\bar{M}(2\downarrow)$	+0.064
$\bar{M}(3\uparrow)$	+0.021
$\bar{M}(1\uparrow)$	-0.002
$\bar{M}(4\downarrow)$	-0.074
$\bar{M}(4\uparrow)$	-0.201
$\bar{M}(5\downarrow)$	-0.235
$\bar{M}(5\uparrow)$	-0.237

Figure Captions

FIGURE 1 The d-orbital component of the projected density of states. (a) The chromium (100) surface layer. (b) The chromium (100) second layer. Solid lines are states with the spin orientation of the surface minority states; dashed lines correspond to the majority states.

FIGURE 2 The d-orbital component of the bulk chromium density of states projected on one atom. Solid and dashed lines differentiate the two spin directions.

FIGURE 3 Our prediction for Cr(001) surface and near-surface magnetism. Atoms whose magnetic moments point to the right are indicated by darkened spheres. Atoms whose magnetic moments point to the left are symbolized by open spheres. The diameter of the sphere representing an atom is drawn proportional to the magnitude of the atom's theoretical spin polarization. The surface spin polarization is predicted to be 3.00 electrons. (Figure courtesy of L.E. Klebanoff.)

FIGURE 4 Surface Brillouin zones.

FIGURE 5 Surface states and resonances at the Cr (100) surface. States shown to the right of a particular k-vector are states with the spin orientation of the surface atom majority states; those shown to the left correspond to the

minority states. The presence of two or four degenerate states is shown by the increased length of the marker.

FIGURE 6 The d orbital component of the projected density of states at $\bar{\Gamma}$. (a) The chromium (100) surface layer. (b) The chromium (100) second layer. (c) The chromium (100) fifth layer. Solid lines are states with the spin orientation of the surface minority states; dashed lines correspond to the majority states.

FIGURE 7 The dispersion of the surface feature 2 along the $\bar{\Gamma}$-$\bar{X}$ line of the surface Brillouin zone observed using P-polarized HeI_{α} radiation. The open circles are adjusted theoretical values for the dispersion of the even-symmetry component of the Δ_5-symmetry up-spin surface state. The theoretical binding energies were reduced by 0.049Ry so that experiment and theory agree at the $\bar{\Gamma}$ point. (Figure courtesy of L.E. Klebanoff.)

FIGURE 8 The d-orbital component of the density of states projected on one atom. (a) The chromium (110) surface layer. (b) The chromium (110) second layer. Solid and dashed lines differentiate the two spin directions.

FIGURE 9 Surface states and resonanaces at the Cr (110) surface. States shown to the immediate right of a particular k-vector are states with one spin orientation; those to the left have the opposite spin. The presence of two degenerate states is shown by an increased length of the marker.

FIGURE 10 The d-orbital component of the projected density of states. (a) The chromium (100) monolayer. (b) The iron (100) interface layer. Solid lines are states with the spin orientation of minority bulk iron states; dashed lines correspond to the majority states.

FIGURE 11 The d-orbital component of the projected density of states. (a) Ground state, the Cr (110) monolayer. (b) Ground state, the Fe (110) interface layer. Solid lines are states with the spin orientation of the minority bulk iron states; dashed lines correspond to the majority states.

FIGURE 12 The d-orbital component of the projected density of states for the antiferromagnetic chromium monolayer on iron (110). (a) Chromium atom with the iron spin orientation. (b) Chromium atom with spin pointing oppositely to the iron spin direction. Solid lines are states with

the spin orientation of the minority bulk iron states; dashed lines correspond to the majority states.

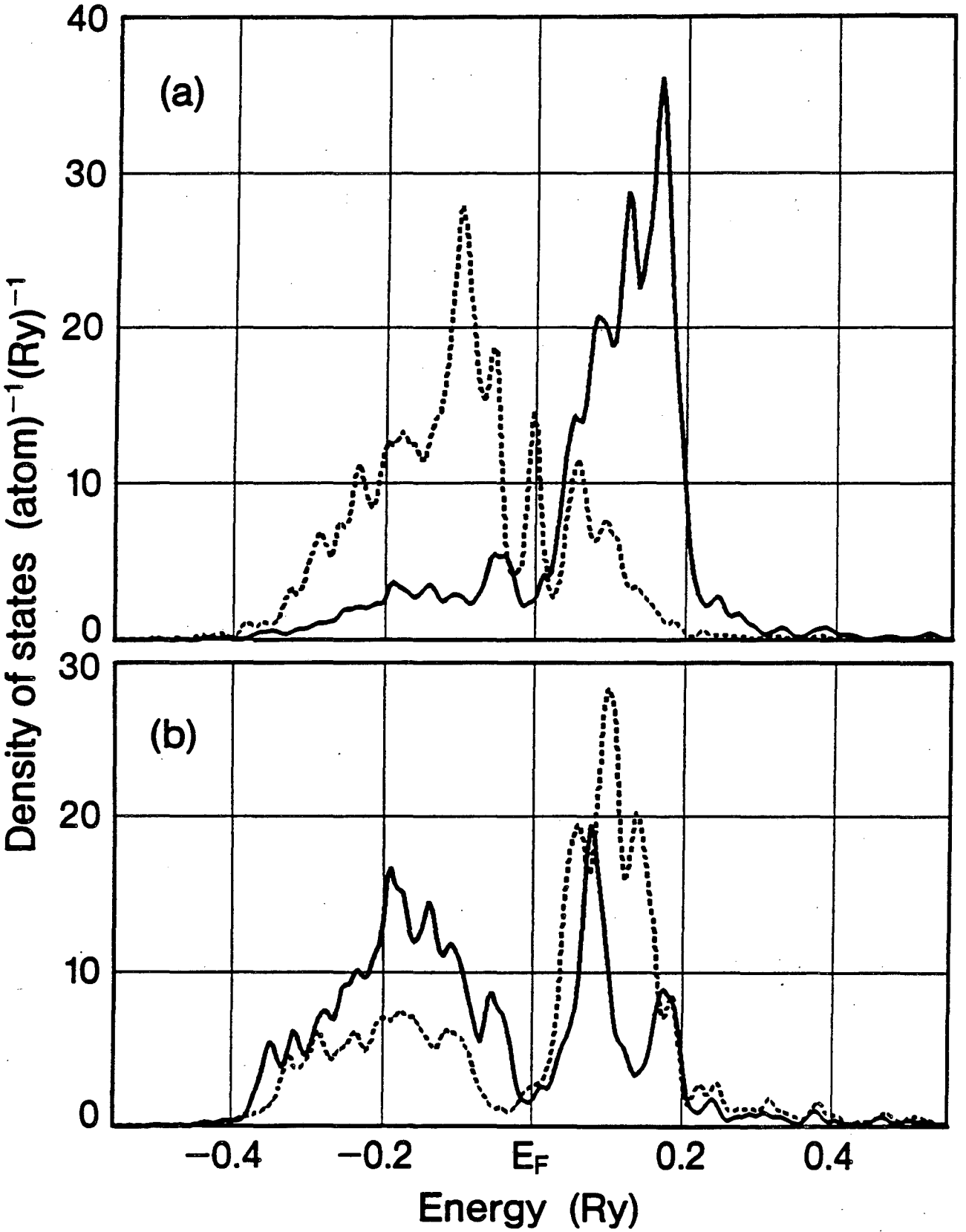
(a)
(b)
Density of states (atom)$^{-1}$(Ry)$^{-1}$
40
30
20
10
0
30
20
10
0
−0.4
−0.2
E_F
0.2
0.4
Energy (Ry)

Figure 1

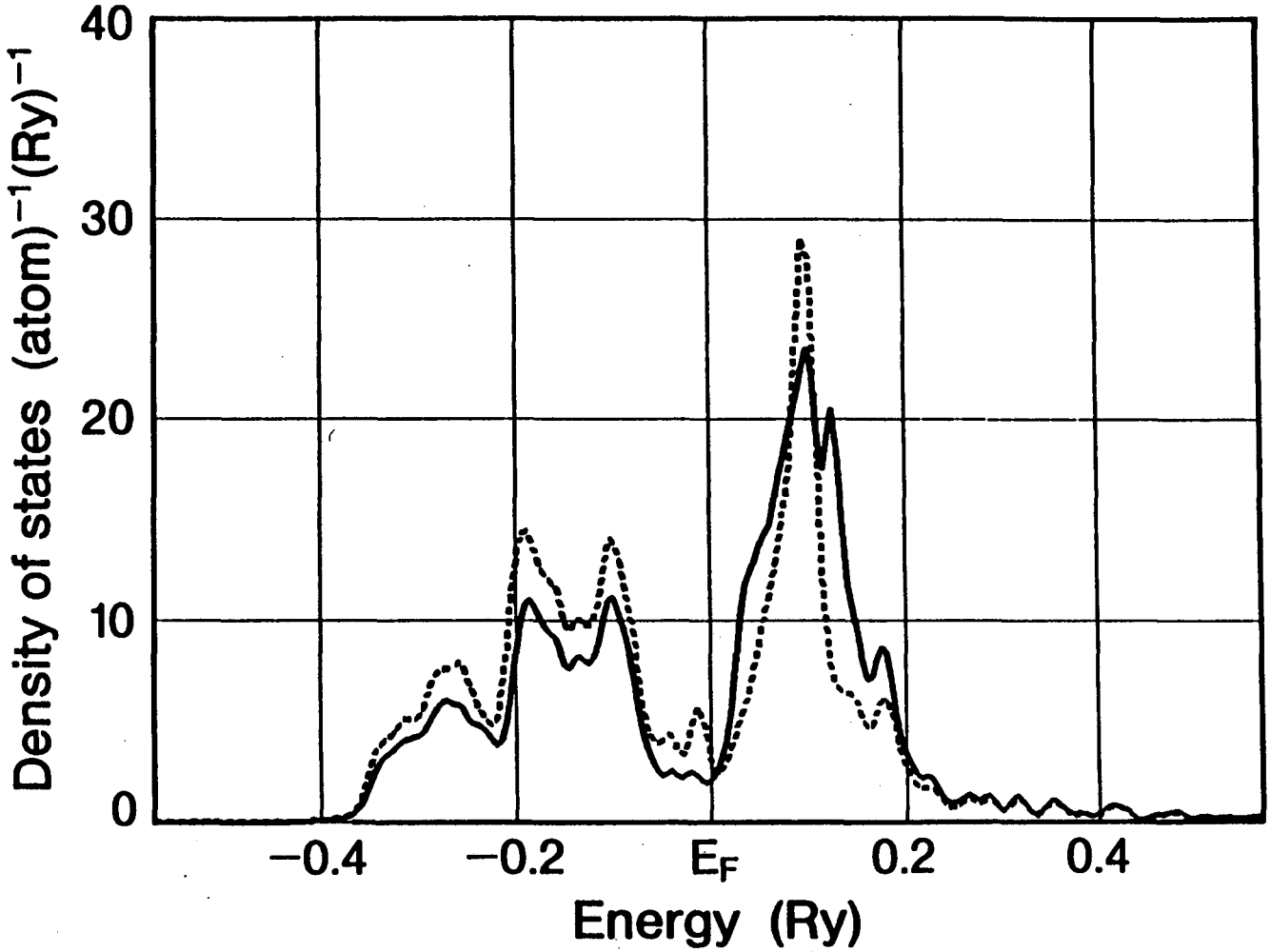
40
30
20
10
0
Density of states (atom)$^{-1}$(Ry)$^{-1}$
−0.4
−0.2
E_F
0.2
0.4
Energy (Ry)

Figure 2

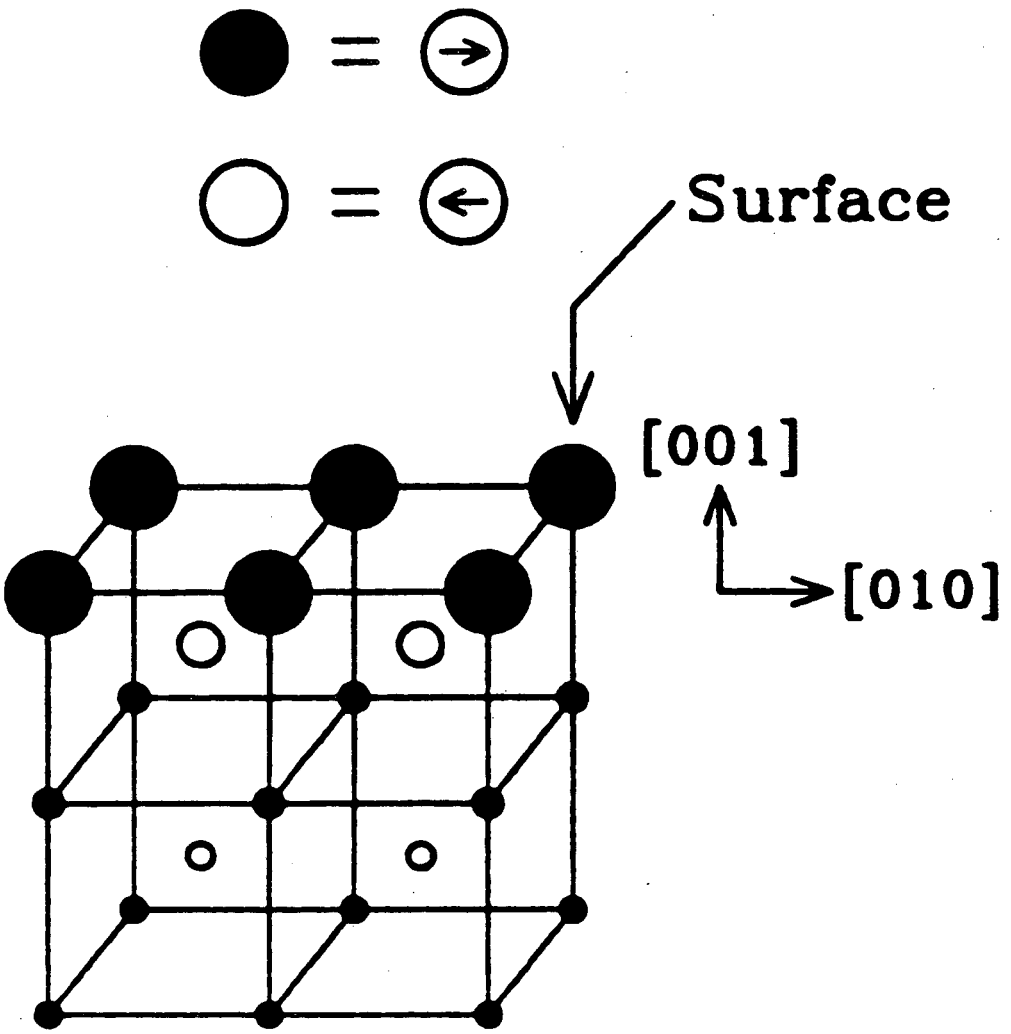

Figure 3

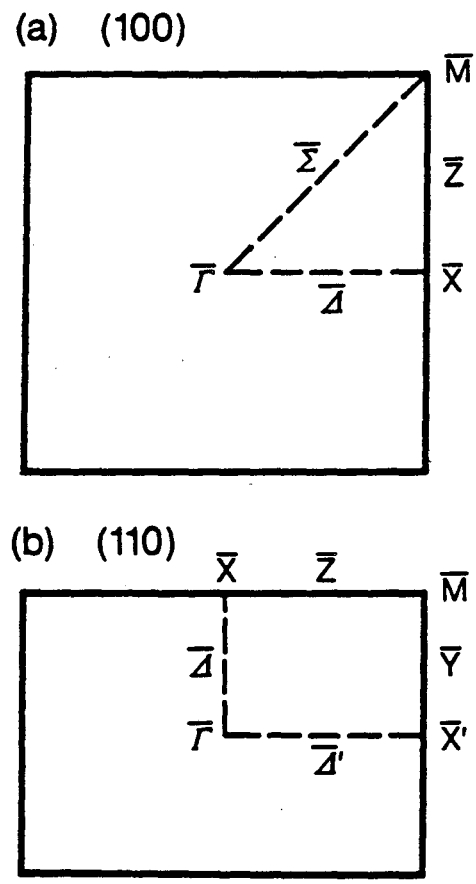

Figure 4

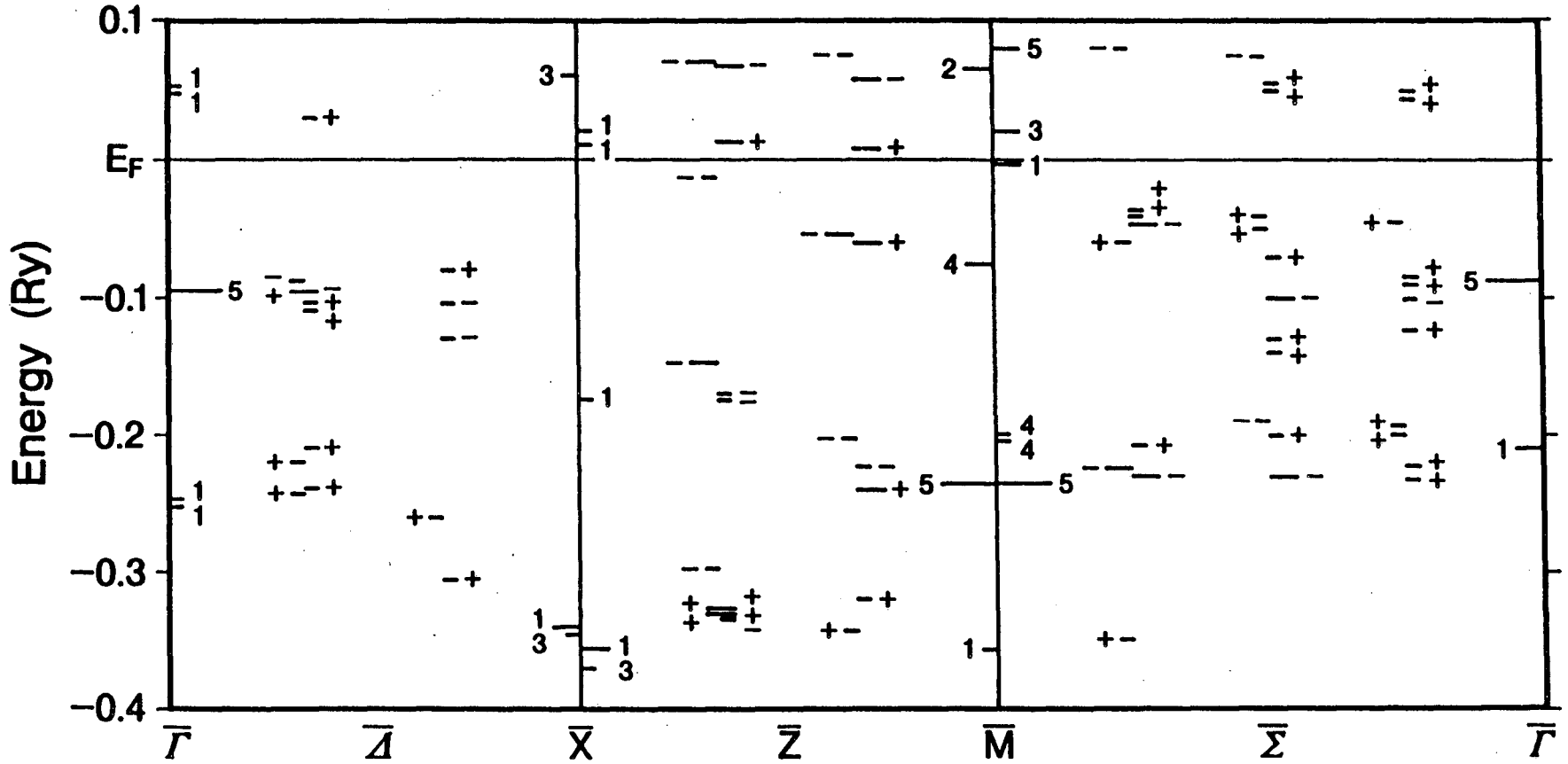
Energy (Ry)
0.1
E_F
−0.1
−0.2
−0.3
−0.4
$\bar{\Gamma}$
$\bar{\Delta}$
$\bar{X}$
$\bar{Z}$
$\bar{M}$
$\bar{\Sigma}$
$\bar{\Gamma}$

Figure 5

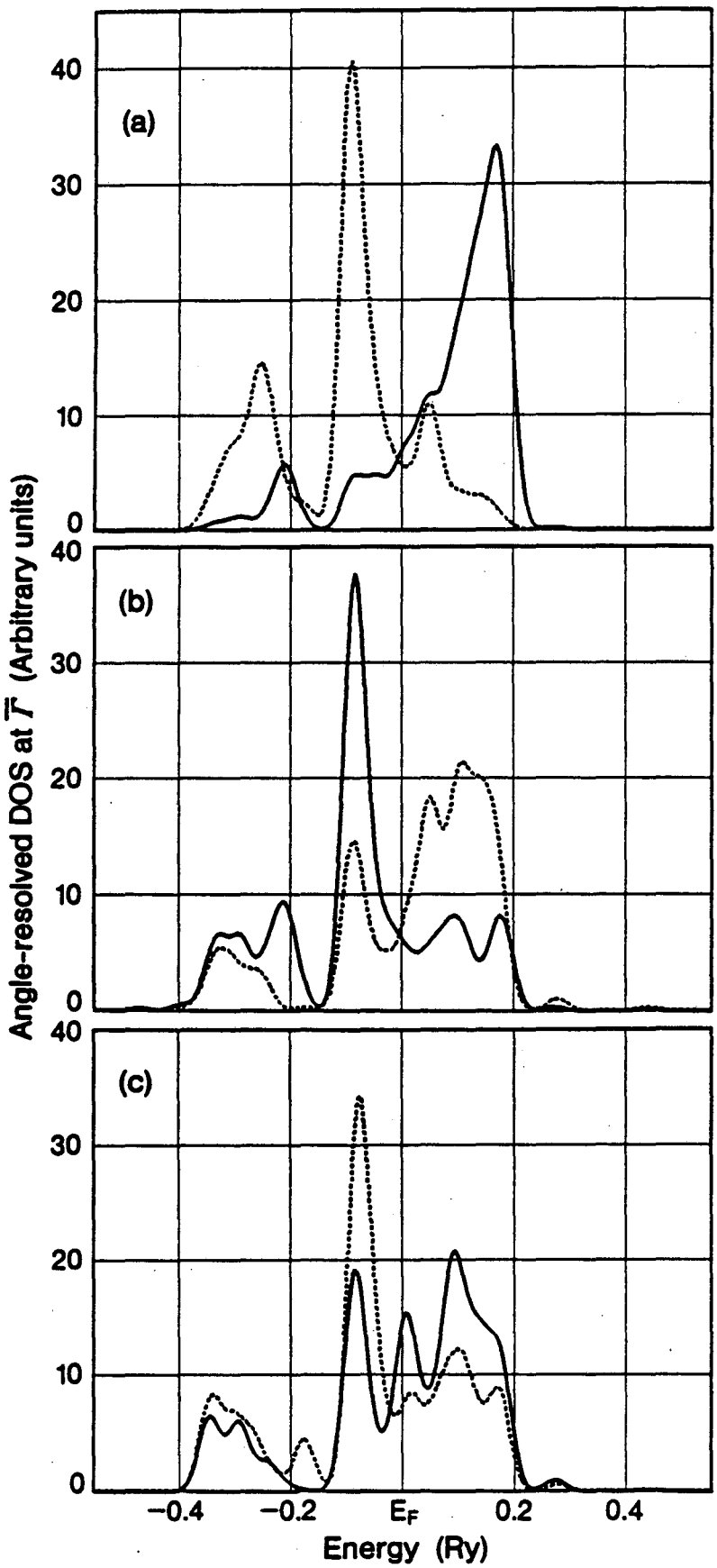
(a)
(b)
(c)
40
30
20
10
0
Angle-resolved DOS at $\bar{\Gamma}$ (Arbitrary units)
−0.4
−0.2
E_F
0.2
0.4
Energy (Ry)

Figure 6

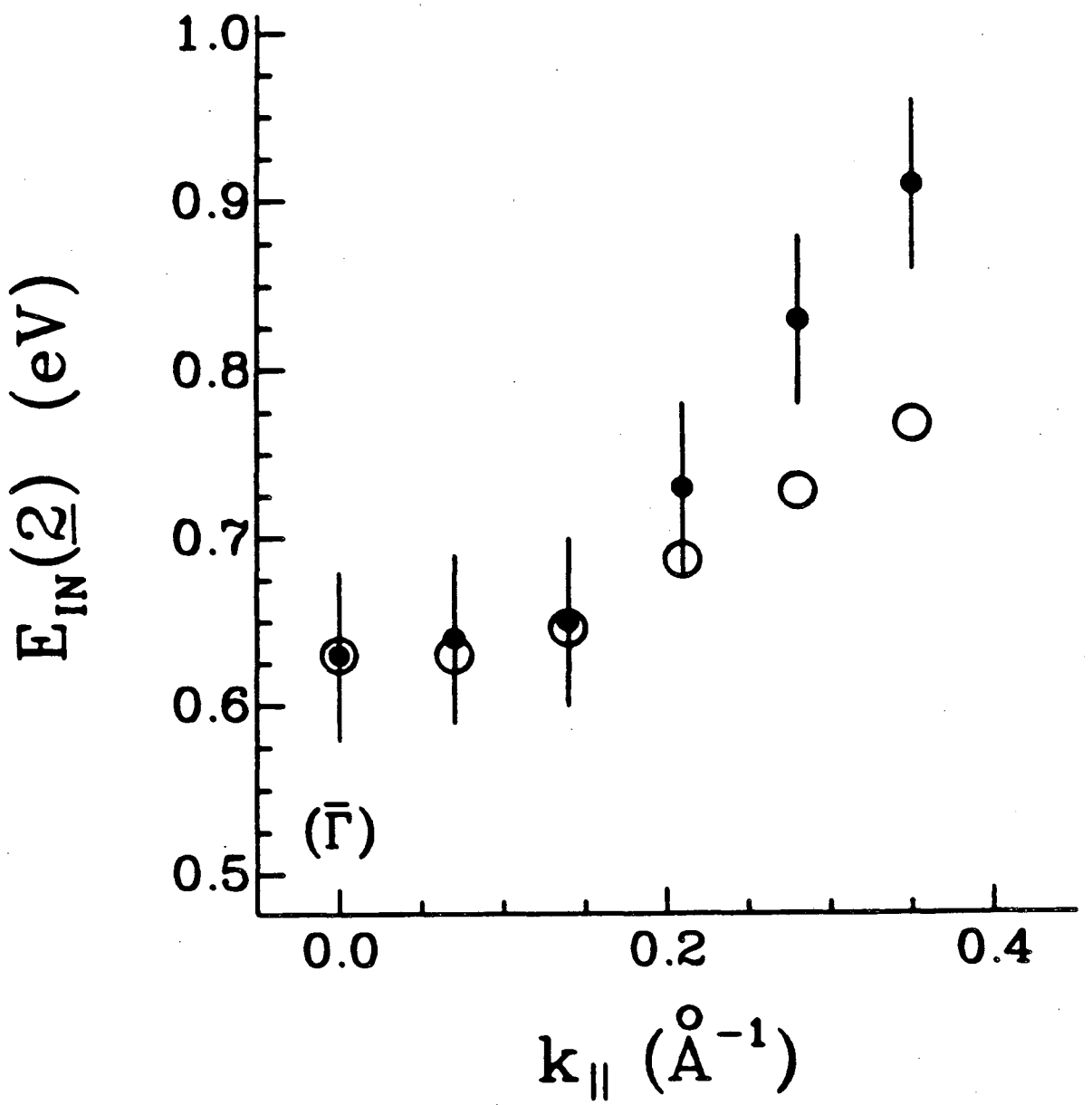
1.0
0.9
0.8
0.7
0.6
0.5
$E_{IN}(\bar{2})$ (eV)
($\bar{\Gamma}$)
0.0
0.2
0.4
$k_{\parallel}$ ($\mathring{A}^{-1}$)

Figure 7

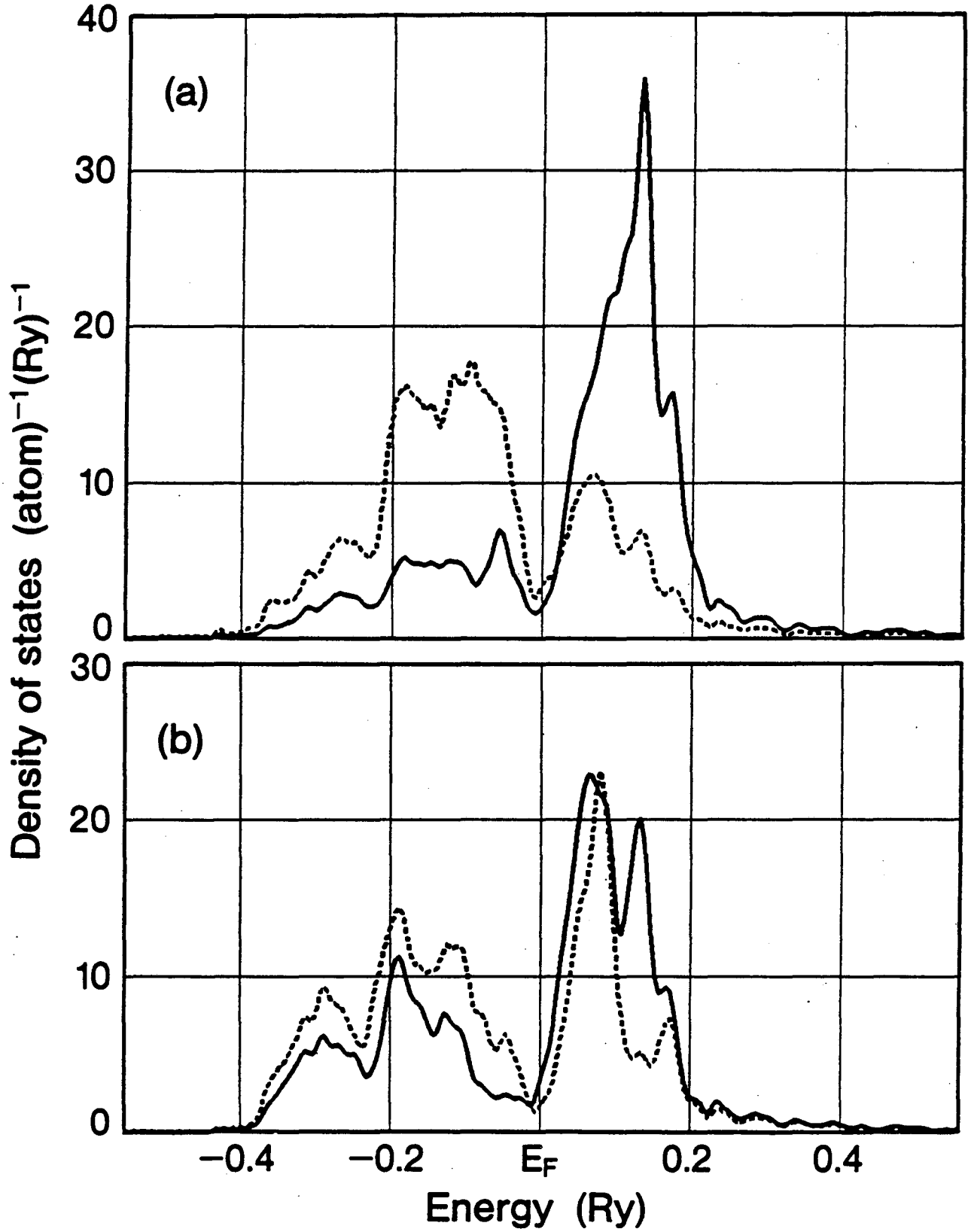
(a)
(b)
40
30
20
10
0
30
20
10
0
Density of states (atom)$^{-1}$(Ry)$^{-1}$
−0.4
−0.2
E_F
0.2
0.4
Energy (Ry)

Figure 8

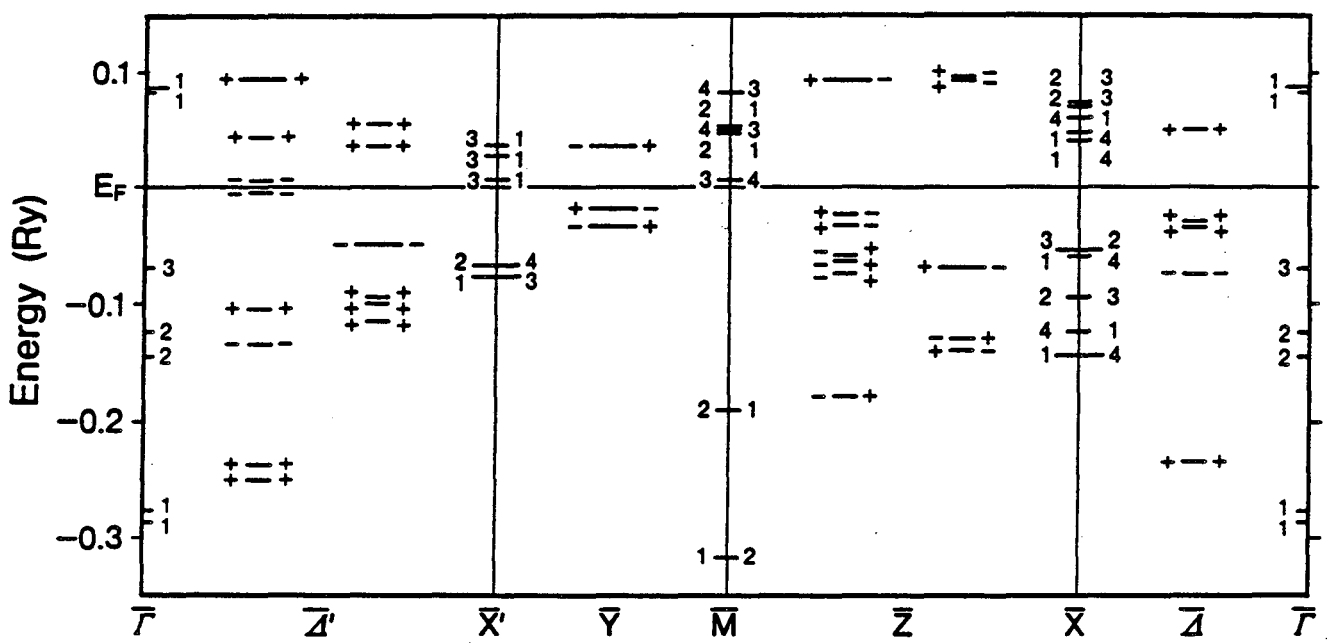
Energy (Ry)
0.1
E_F
−0.1
−0.2
−0.3
$\bar{\Gamma}$
$\bar{\Delta}'$
$\bar{X}'$
$\bar{Y}$
$\bar{M}$
$\bar{Z}$
$\bar{X}$
$\bar{\Delta}$
$\bar{\Gamma}$

Figure 9

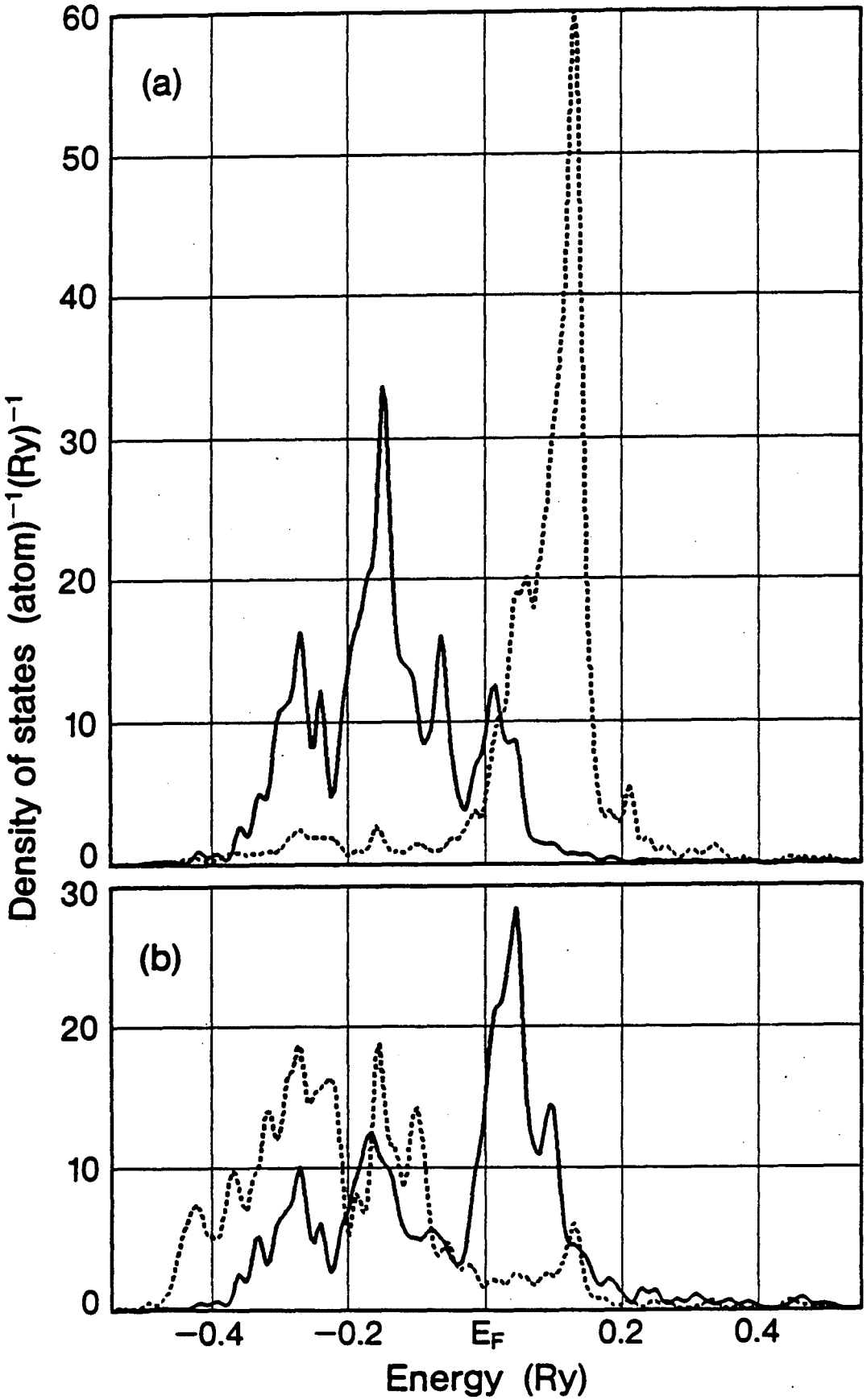
(a)
(b)
Density of states (atom)$^{-1}$(Ry)$^{-1}$
60
50
40
30
20
10
0
30
20
10
0
−0.4
−0.2
E_F
0.2
0.4
Energy (Ry)

Figure 10

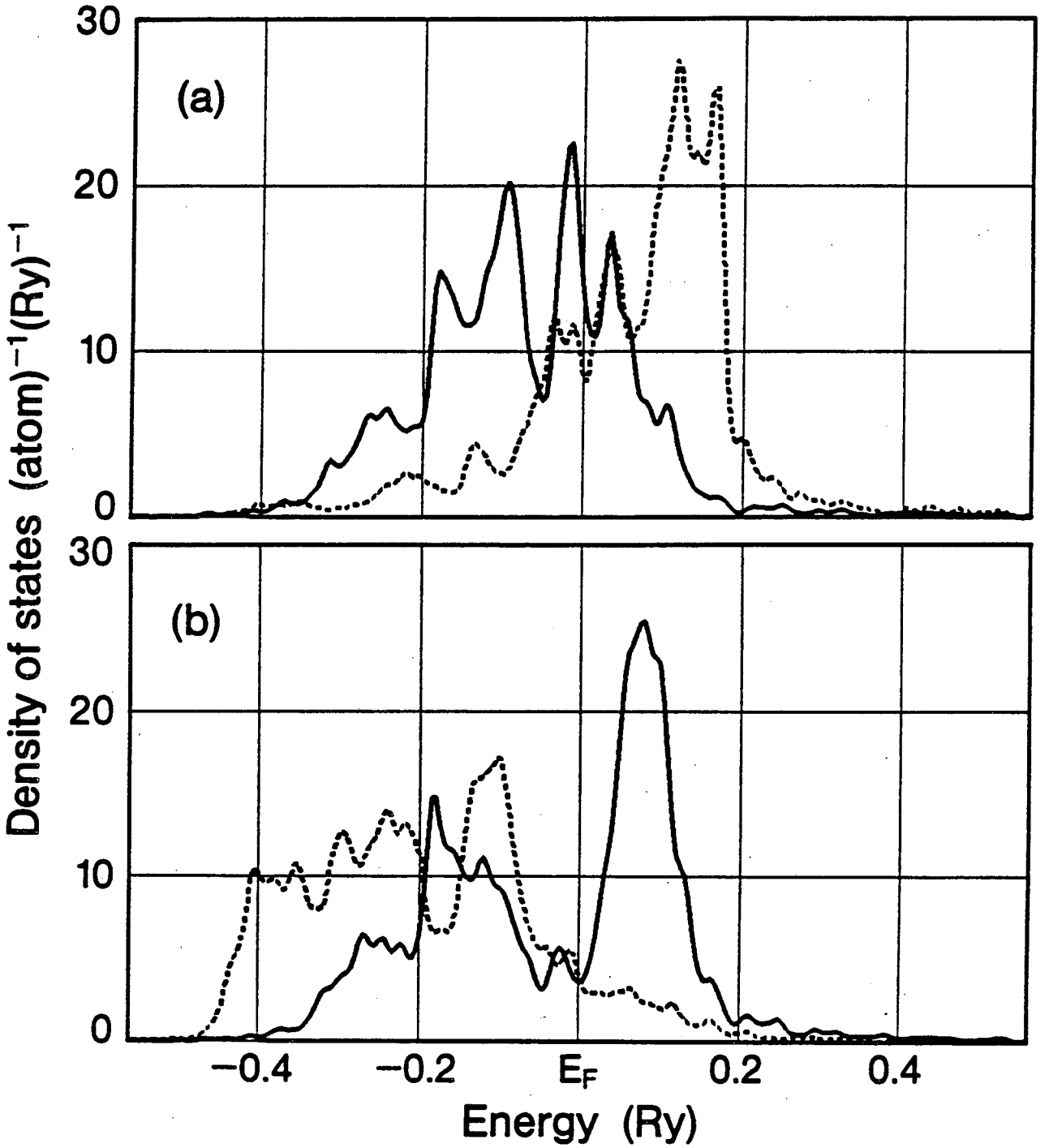
30
20
10
0
(a)
30
20
10
0
(b)
Density of states (atom)$^{-1}$(Ry)$^{-1}$
−0.4
−0.2
E_F
0.2
0.4
Energy (Ry)

Figure 11

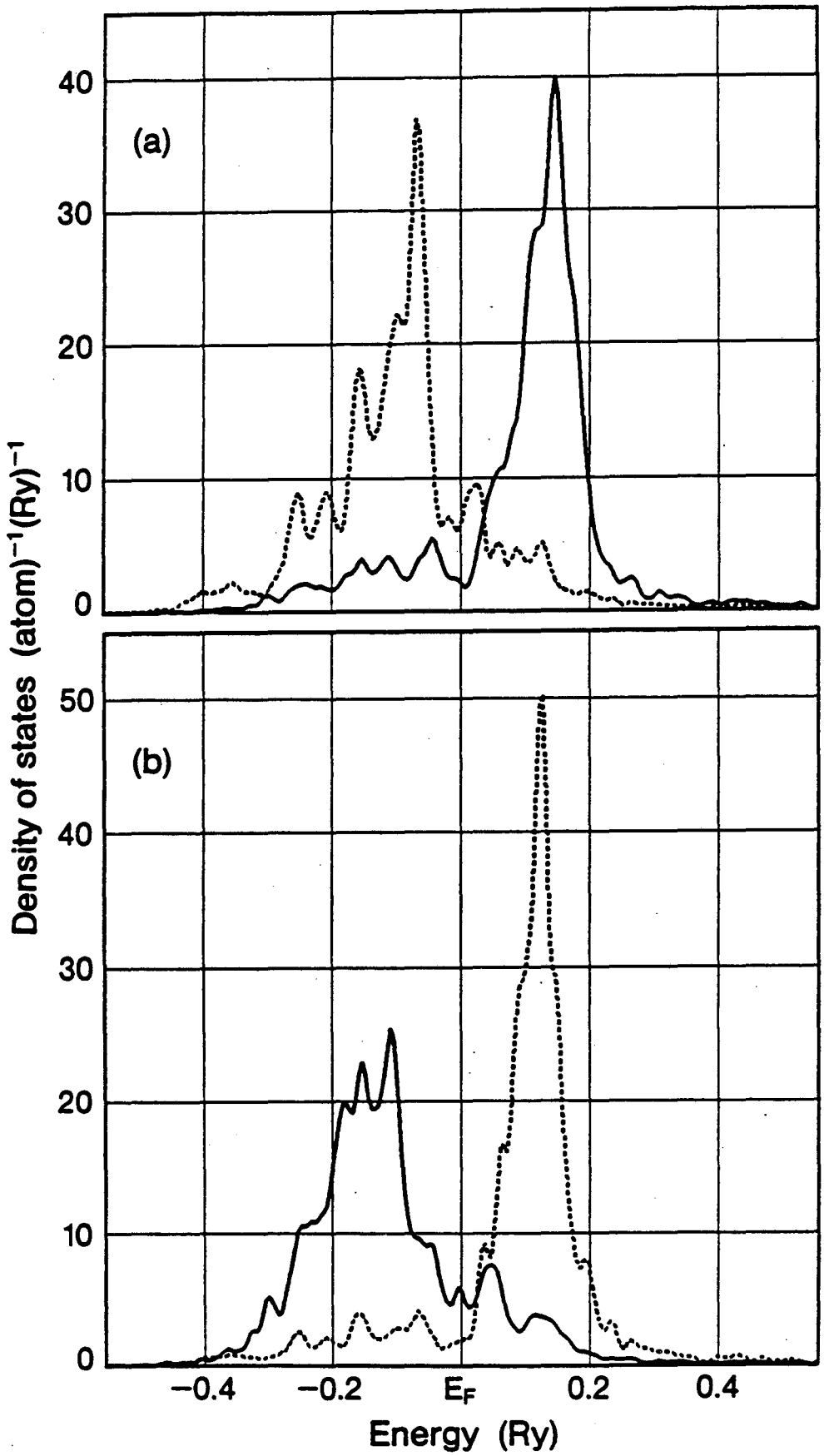
(a)
(b)
Density of states (atom)$^{-1}$(Ry)$^{-1}$
0
10
20
30
40
50
−0.4
−0.2
E_F
0.2
0.4
Energy (Ry)

Figure 12

VIII. CONCLUSION

Itinerant magnetism is clearly a complicated phenomenon. Even the presence or absence of a magnetic ground state can be difficult to predict. This is exemplified in our Hubbard model of Chapter II in which the four-electron ground state has zero spin, but the five-electron ground state has maximum spin. This is in contradiction to expectations based on simple rules, such as those of Hund, which would have predicted magnetic ground states for both electronic fillings. Realistic systems provide similar difficulties; the five-fold increase in spin polarization at the Cr(100) surface relative to the bulk would be difficult to foresee without a comprehensive calculation or experiment.

The bulk of this thesis has described calculations, using the technique described in Chapter III, for the electronic and magnetic properties of a variety of transition metal systems. (See Table I) Many of these calculations produced unusual or unexpected results. The Cr monolayer on the Fe(100) surface was found, for example, to be ferromagnetic with a spin polarization of 3.63 electrons: a value considerably larger than any other known transition metal system. Another very interesting result was the presence of an excited state in the Co monolayer on Cu possessing a new kind of magnetic order, which we called "spatially modulated." Our analysis of the unusually shaped Fe-Co section of the Slater-Pauling curve

demonstrated the inadequacy of the widely regarded Pauling explanation.

There are also general considerations elucidated by Table I. It is clear that our calculational scheme can systematically examine a variety of systems. It is equally clear that the number of available systems, e.g., all combinations of overlayers on substrates or all alloys, is enormously larger than the large number of systems we did investigate. The latter consideration suggests the need for a study of the systematics: the former consideration suggests that we are in a position to do so. Consequently, the final contribution of this thesis will be to use the results calculated in Chapters IV-VII to construct a set of qualitative rules governing the magnetic properties of heterogeneous transition metal systems.

Four of the calculations have been made for pure transition metal surfaces. These calculations [Cr(100), Cr(110), Fe(100), and Fe(110)] all demonstrate that the removal of neighboring atoms decreases the projected bandwidth on the surface. Consequently, the electron-electron interaction to bandwidth ratio increases and so does the magnetism. In short, <u>removal of nearest neighbor atoms of its own kind tends to enhance magnetism</u>.

These four surface calculations also help justify the next rule. It is recalled that the Cr surface enhancement of the magnetization is enormous; four to five times over bulk values. The enhancement at the Fe surface is smaller

(20% to 40%) but still significant. The enhancement at the FeCo surfaces is quite small: less than 15%. The relevant difference between these systems is the number of available unpolarized d holes. FeCo has very few; Fe has approximately 0.7 per atom, and Cr has more than 4 per atom. (The concept of d-holes is not entirely concrete due to the presence of sp-d hybridization; it is the qualitative idea that is important.) Consequently, magnetization enhancement is most pronounced in those elements where the bulk magnetization is not close to saturation.

Bulk FeCo displays an interesting principle in itself. Chapters V and VI demonstrated that the strongly exchange split Co can help increase the Fe magnetization. This same effect occurs in the Cr near surface region where the strongly exchange split surface Cr atoms help increase the spin polarization of the lower Cr layers. In general, we conclude that the presence of a strongly magnetized atom with a large exchange splitting near a weakly magnetic but polarizable atom with a smaller splitting, considerably enhances the magnetization of the latter.

The final rule is exemplified by the calculations for the Co overlayers on Cu, in which it is found that a Co surface layer in contact with Cu has a lower spin polarization than a surface layer only in contact with Co. This suppression of magnetization by a nonmagnetic substrate has been explored in a number of experimental and

theoretical studies as described in the introduction to Chapter IV. Examination of all these results suggests that <u>the presence of a nonmagnetic unpolarizable atom next to - and coupled to - a magnetic transition metal element tends to decrease the magnetization of the latter</u>.

These four rules are only qualitative, and yet it is very clear that they bring some order to the complicated systematics of heterogeneous systems displaying itinerant magnetism. It is to be hoped that the results and analysis presented in this thesis will help guide future investigators in their searches through the beautiful, but problematical, subject that is itinerant magnetism.

TABLE I

Spin-polarization Results for all Ordered Systems

System	Spin Polarization
fcc Co	1.56
bcc Co	1.80
bcc Fe	2.12
bcc Cr	0.67
sc FeCo - Fe atom	2.66
sc FeCo - Co atom	1.78
(100) Fe surface	2.90
(110) Fe surface	2.55
(100) Cr surface - surface layer	3.00
(100) Cr surface - second layer	-1.56
(110) Cr surface	2.31
(100) FeCo surfaces - Fe surface layer	2.95
(100) FeCo surfaces - Co surface layer	2.03
(110) FeCo surface - Fe atom	2.75
(110) FeCo surface - Co atom	1.86
(110) Fe monolayer on FeCo - Co position	2.63
(110) Fe monolayer on FeCo - Fe position	2.67
(100) Cr monolayer on Fe	3.63
(110) Cr monolayer on Fe	2.25
(111) Co monolayer on Cu	1.63
(111) Co dilayer on Cu - surface layer	1.65
(111) Co dilayer on Cu - interface layer	1.58

This report was done with support from the Department of Energy. Any conclusions or opinions expressed in this report represent solely those of the author(s) and not necessarily those of The Regents of the University of California, the Lawrence Berkeley Laboratory or the Department of Energy.

Reference to a company or product name does not imply approval or recommendation of the product by the University of California or the U.S. Department of Energy to the exclusion of others that may be suitable.

TECHNICAL INFORMATION DEPARTMENT
LAWRENCE BERKELEY LABORATORY
UNIVERSITY OF CALIFORNIA
BERKELEY, CALIFORNIA 94720